MOLECULAR MECHANISM OF THE INTERACTION BETWEEN LGL/TOMOSYN HOMOLOG, SRO7, AND THE RAB GTPASE SEC4 IN POLARIZED EXOCYTOSIS

Kelly Ann Watson

A dissertation submitted to the faculty of the University of North Carolina at Chapel Hill in partial fulfillment of the requirements for the degree of Doctor of Philosophy in the Department of Cell Biology and Physiology in the School of Medicine

Chapel Hill
2015

Approved by:

Patrick Brennwald

Jean Cook

Douglas Cyr

Robert Duronio

Stephanie Gupton

Brenda Temple

ABSTRACT

Kelly Ann Watson: Molecular mechanism of the interaction between Lgl/Tomosyn homolog, Sro7, and the Rab GTPase Sec4 in Polarized Exocytosis
(Under the direction of Patrick Brennwald)

Polarized exocytosis requires the proper localized delivery, docking and fusion of secretory vesicles with sites of active growth on the plasma membrane. Members of the Tomosyn/Lgl/Sro7 family play important roles in vesicle trafficking and cell polarity in eukaryotic cells. The yeast homolog, Sro7, is thought to act as a downstream effector of the Sec4 Rab GTPase to promote SNARE assembly during Golgi to cell surface vesicle transport. Here we report the identification of a Sec4 binding site on the surface of Sro7 that is contained within a cleft created by the junction of two adjacent β-propellers which form the core structure of Sro7. We combined *in vitro* results with *in vivo* suppression studies and *in silico* modeling to validate the Sro7-Sec4 docking interaction interface. Close examination of this docking model suggests a structural basis for the high substrate and nucleotide selectivity in effector binding by Sro7. Analysis of the surface variation within the homologous interaction site on Tomosyn-1 and Lgl-1 structural models suggests a possible conserved Rab GTPase effector function in Tomosyn vertebrate homologs. Additionally, overexpression of either Sro7 or the Exocyst complex component Rab effector, Sec15, results in the formation of a cluster of post-Golgi vesicles within the cell. We describe a novel assay that recapitulates post-Golgi vesicle clustering *in vitro* utilizing purified Sro7 and vesicles isolated from late secretory mutants. We made use of this assay to analyze the effects of Sro7 mutants in which conserved charged patches on Sro7 were mutated to the reverse charge and found that one of the charge reversal mutant proteins, Sro7-

R189D,R222D, had a specific defect in clustering vesicles both *in vivo* and *in vitro*. We show that this mutation acts by effecting a conformational change in Sro7 from a "closed" to "open" structure, suggesting a novel function for this conformational switch in Sro7 to coordinate Rab-dependent membrane tethering with regulation of SNARE assembly prior to membrane fusion.

Dedicated to my parents, Joseph and Cathleen Watson, and my grandfather, Charles Whitehead.

ACKNOWLEDGEMENTS

I would first like to thank my advisor, Dr. Patrick Brennwald, for his guidance these past six years. He has trained me how to think critically and ask exciting, but fruitful questions. He has challenged me to improve both my speaking and writing abilities. Most importantly, he inspires in us excitement and curiosity to attack the many unsolved scientific questions of cell biology.

I was very fortunate to be in a lab environment with extremely engaging, helpful and supportive scientists throughout my time in graduate school. Dr. Guendalina Rossi, thank you for being a mentor and dear friend. The impact you have had on my growth as both a scientist and person is incalculable. Dr. Leah Watson, the advice you have given these past 6 years is priceless. Thank you for all of the laughter the three of us shared during my time at UNC.

I would like to thank my committee, Dr. Brenda Temple, Dr. Doug Cyr, Dr. Bob Duronio, Dr. Stephanie Gupton and Dr. Jean Cook, for asking constructive questions and encouraging me during my study.

I am thankful for my family. My parents, Joseph and Cathleen Watson, brother, Ryan Watson, and partner, Richard Strakosch, have always been supportive of me in every aspect of my life. Thank you for your advice, motivation and belief in me.

Finally, graduate school would not have been a success without the support of my friends. Thank you to everyone who has been a part of this process.

PREFACE

The following is a compilation of my primary and secondary author publications. Chapter one will be revised and submitted as a review article and chapter two is a published primary research article. Chapter three is a published research article that I contributed significantly to as second author, specifically as follows: I characterized the biochemical interaction between the Sro7 clustering mutant (Sro7-D189,D222) and both Myo2 and Exo84 (Figure 6), I collaborated to design, construct, purify and characterize the Sro7 C-terminal tail mutant (Sro7-K914,F942) (Figure 7), and I generated the structural images for Figures 5 and 7. Together, these works comprise my dissertation.

TABLE OF CONTENTS

LIST OF TABLES

LIST OF FIGURES

LIST OF ABBREVIATIONS

aPKC	atypical protein kinase C
ER	endoplasmic reticulum
GDI	GDP dissociation inhibitor
GDP	guanosine 5’-diphosphate
GST	glutathione S-transferase
GTPases	guanosine triphosphatases
GTPγS	guanosine 5’-3-O-(thio)triphosphate
HSP	high speed pellet
Lgl	Lethal giant larvae
SNARE	soluble N-ethylmaleimide-sensitive factor adaptor protein receptor
t-SNARE	target membrane SNARE
TRITC	tetramethylrhodamine isothiocyanate
YPD	yeast peptone dextrose

CHAPTER 1

Introduction

1.1 Polarized Exocytosis

The establishment of cell polarity is essential for all eukaryotic cells to perform numerous diverse cellular processes, such as cell movement, axonal outgrowth, secretion of hormones and cell differentiation. Maintaining cell polarity requires the proper transport of lipids, proteins and other materials to the correct cellular compartment. Much of this trafficking process is mediated by small, fluid-filled organelles enclosed by lipid bilayers, or secretory vesicles, that bud from the Golgi apparatus and fuse with the plasma membrane. This membrane trafficking pathway is called polarized exocytosis and requires the precise localized delivery, docking and fusion of secretory vesicles with specific sites of active growth on the plasma membrane. In the last three decades, researchers have made significant progress exploring the details of this elegant pathway, however the precise mechanisms that regulate the spatial and temporal transport of secretory vesicles and their cargo to the correct cellular destinations remain to be fully elucidated.

One of the most pivotal moments in the trafficking field came in 1980, when Randy Schekman and his student, Peter Novick, conducted a density-based screen for mutants that were conditionally defective for secretion in the budding yeast, *Saccharomyces cerevisiae*, identifying 23 essential genes involved at various stages of the secretory pathway [1]. Developing conditional mutants was particularly useful because blocking each major step in the secretory pathway essentially sorted out the order of secretory events in cells: ER to Golgi, intraGolgi, and

Golgi to plasma membrane [2]. In 2013, Schekman, along with Thomas Südhof and James Rothman, won the Nobel Prize for their work in budding yeast, neurons and *in vitro* systems, respectively, that was collectively responsible for discovering the intracellular exocytic trafficking machinery which regulates protein and membrane transport within all eukaryotic cells [3].

The identification of a near complete collection of genes critical for vesicle transport in budding yeast and mammalian cells has reinforced the belief that secretion is a conserved process, as almost every yeast member has a clear ortholog present in mammalian cells performing analogous functions. Therefore, what is understood in one system is likely to have implications in the other. Additionally, because of its well-defined genetic and biochemical tools available, budding yeast is a particularly good model system for studying vesicle transport and exocytosis.

1.2 Yeast Exocytic Machinery

Polarized exocytosis can be organized into three basic steps. In yeast, the first step involves budding of vesicles from the Golgi, followed by transport of vesicles along actin cables by the type V myosin motor, Myo2, [4] and delivery to the correct plasma membrane site. Next, secretory vesicles are tethered to the target membrane, which is coordinated by the interaction between the Rab GTPase protein, Sec4, on vesicles and the Exocyst tethering complex on the plasma membrane [5-7], (Figure 1.1). Following tethering, a trans-SNARE complex forms, which drives vesicle fusion with the plasma membrane.

From yeast to humans, Rabs, SNAREs and tethering proteins collaborate to ensure that vesicles are delivered and fuse at the correct time and place.

1.2.1 Rab GTPases

Rab proteins are a large family of small GTPases that direct and regulate vesicular trafficking events in the cell at all steps in the secretory pathway. The Rab family is part of the Ras superfamily of small GTPases. There are at least 66 Rab proteins present in mammalian cells and 11 yeast Rab proteins. Rab GTPases function like molecular switches, cycling from an inactive, GDP-bound state, to an active, GTP-bound state [8]. Several upstream regulators catalyze Rab cycling between active and inactive nucleotide states: Guanine nucleotide Exchange Factors (GEFs) initiate the GDP- to-GTP activating switch, while GTPase Activating Proteins (GAPs) stimulate GTP-hydrolysis and the return to an inactive, GDP-bound state. Activated Rab proteins bind to numerous effector proteins that regulate many different membrane transport pathways and processes.

The founding member of the Rab family is the yeast Rab GTPase, Sec4 [1]. Sec4 is required for transport of post-Golgi vesicles to the plasma membrane [9], and therefore localizes to post-Golgi vesicles and sites of polarized growth on the plasma membrane [9]. The nucleotide state of Sec4 is regulated by its GEF, Sec2. Mutants of *SEC2* show an accumulation of vesicles with random distribution throughout the cell, confirming that the activation of Sec4 by Sec2 directs polarized transport of secretory vesicles [10-11]. Sec4 is thought to mediate vesicle tethering at least in part through interaction with its effector, the Exocyst tethering complex subunit, Sec15 [12].

1.2.2 SNAREs

SNAREs (soluble N-ethylmaleimide sensitive factor attachment protein receptors) are the primary machinery responsible for vesicle fusion at the target membrane [13]. SNARE protein structure generally consists of a C-terminal membrane-anchored tail domain and membrane-

proximal helical SNARE motifs [14]. Biochemical reconstitution studies via *in vitro* transport systems pioneered by James Rothman and colleagues led to the SNARE hypothesis, suggesting that SNARE proteins on the surface of vesicles, or v-SNAREs, bind specifically with SNARE proteins on the target membrane, or t-SNAREs, to form an active trans-SNARE complex which cinches opposing membranes close together [15].

Alternatively, SNARE proteins are referred to as Q-SNAREs or R-SNAREs based on the presence of highly conserved glutamine or arginine residues in the polar "zero layer" of the SNARE motif [16]. The coiled-coil interactions in helical SNARE motifs drive pairing of 3 Q-SNARE domains with 1 R-SNARE domain into a tight bundle [17-20]. The energy that is released during the formation of this stable 4-helical SNARE bundle is the major driving force behind vesicle fusion [21]. In general, there is correlation of R-SNAREs with v-SNAREs and of Q-SNAREs with t-SNAREs, however, the 3Q:1R SNARE motif ratio is not required within the yeast exocytic SNARE complex, as complexes containing four glutamine residues are fully functional [22].

The most extensively studied SNARE proteins reside in neurons and provoke synaptic vesicle fusion. The neuronal SNARE machinery includes: the membrane v-SNARE protein, synaptobrevin (R-SNARE, also known as VAMP), the plasma membrane-anchored t-SNARE, syntaxin (Qa-SNARE), and the soluble t-SNARE, SNAP-25 (comprising both Qb- and Qc-SNARE motifs) [17]. While not exactly structurally similar based on sequences, yeast form a similar SNARE complex at the plasma membrane. In yeast, the v-SNAREs are two redundant proteins, Snc1 and Snc2, while the t-SNAREs are soluble Sec9 and Sso1 / Sso2 [23-25]. Like SNAP-25, Sec9 contributes the Qb- and Qc- SNARE helices to one each from Sso and Snc to drive fusion of docked secretory vesicles [26].

While different sets of SNARE proteins function at distinct steps throughout trafficking pathways, aiding in vesicle transport specificity, individual SNARE proteins localize to unspecific areas on their respective membranes. For example, in yeast, Sso1 / Sso2 distributes across the entire plasma membrane, yet secretory vesicles find a way to specifically dock and fuse with sites of active growth [26]. Biochemical and genetic studies have identified several proteins that function in membrane transport after vesicle formation, but prior to vesicle fusion. This intermediate step, where an initial connection is formed between a vesicle and its target membrane, is known as vesicle tethering and may be responsible for the earliest stages of fusion specificity [1-2].

1.2.3 Tethering Factors

Tethering factors are thought to mediate the initial attachment between a vesicle and its membrane target. There are two general classes of tethering factors: large homodimeric coiled-coil tethering proteins and multi-subunit tethering complexes (MTCs). Coiled-coil tethers are mostly long, rod-like proteins, while MTCs are hetero-oligomers containing 3-10 protein subunits. This section will focus primarily on MTCs.

Perhaps the most extensively studied multi-subunit tethering complex is the Exocyst, a conserved octameric protein complex consisting of late secretory proteins: Sec3, Sec5, Sec6, Sec8, Sec10, Sec15, Exo70, and Exo84. The Exocyst is required for post-Golgi vesicle trafficking to the plasma membrane [27]. Structures of the eight Exocyst subunits consist of conserved alpha-helical rod bundles, suggesting they evolved from a common ancestor. The Exocyst, along with the conserved oligomeric Golgi (COG), Dsl1 and the Golgi-associated retrograde protein (GARP) MTC complexes are grouped together based on this similar subunit sequence homology into the Complex Associated with Tethering Containing Helical Rods, or

CATCHR family, the largest class of tethering proteins [28-30]. Tethering factors both physically and functionally interact with a multitude of trafficking proteins—namely Rab GTPases and SNAREs—to orchestrate the poorly understood linkage between vesicle docking and vesicle fusion.

Three of the four CATCHR family tethering proteins have been shown to act as direct effectors for Rab GTPases. In yeast, the Exocyst subunit, Sec15, is a downstream effector of the Rab GTPase Sec4 [7]. This Rab effector role is conserved for the Exocyst in higher eukaryotes where, for example, Sec15 is a downstream effector of Rab11, the Rab GTPase that mediates vesicle transport between endosomes and the plasma membrane [30-31]. The COG complex interacts with activated Ypt1 and Ypt6 during retrograde intra-Golgi trafficking in yeast, essential for proper glycosylation of secretory proteins [32-36]. Furthermore, of the 66 identified mammalian Rabs, 12 of them have been shown to interact with different COG subunits [32, 36-38]. The GARP complex facilitates fusion of endosome-derived vesicles to the trans-Golgi network [39-40]. GARP interacts with GTP-bound Ypt6 in yeast (ortholog to mammalian Rab6) [41]. While diverse Rab GTPases mediate vesicle docking and tethering in the multitude of membrane trafficking pathways, it is their interactions with distinct tethering effectors, however, that imparts specificity to vesicle targeting.

Likewise, vesicle tethering factors interact with SNARE proteins, possibly by directly activating specific SNARE complex assembly, providing a final layer of specificity at the last stage of exocytosis: vesicle fusion. For example, in yeast the Exocyst subunit, Sec6, has been shown to bind the t-SNARE Sec9 both *in vitro* and *in vivo*, and this interaction inhibits the assembly of Sec9-containing SNARE complexes *in vitro* [42-43]. The Sec6-Sec9 interaction is perhaps a critical regulatory stage that proceeds assembly of the Exocyst complex, and the

release of Sec9 by Sec6, triggered by Exocyst assembly, promotes SNARE complex assembly at the plasma membrane. Of the remaining CATCHR family complexes, the Dsl1 complex interacts with the endoplasmic reticulum-localized STX18 SNARE complex [44-45], the COG complex has been shown to interact with numerous intra-Golgi and trans-Golgi SNARE complexes [36, 46] and the GARP complex interacts with the trans-Golgi STX16 SNARE complex [40-41].

1.3 Lethal Giant Larvae Family and Trafficking

Genetic screens in yeast to detect additional exocytic machinery associated with the SNARE complex identified a novel Sec9 (t-SNARE)-binding protein, Sro7 [47]. Sro7 is a member of the Lethal Giant Larvae (Lgl) / Tomosyn family of proteins that function in maintenance of cell polarity. *Lgl* proteins are highly structurally conserved, containing multiple WD40 domain repeats and sequence similarity within many elements of the domain interface [48] (Figure 1.2). Lgl homologs are present in vertebrates (*Lgl1* and *Lgl2*—also known as *Hugl-1* and *Hugl-2*—and neuronal *Tomosyn-1* and *Tomosyn-2)*, in *Drosophila melanogaster* (*Lgl* and *Tomosyn*), in *Caenorhabditis elegans* (*Lgl* and *Tomosyn*), and in budding yeast (*SRO7* and *SRO77)* (Figure 1.3).

The mechanisms of Lgl function in cell polarity remain controversial. Two different, yet not mutually exclusive hypotheses have been suggested to explain the function of the Lgl family in cell polarity: regulation of polarization of the actomyosin cytoskeleton and regulation of polarized exocytosis.

1.3.1 Lgl

Lethal (2) giant larvae (*lgl*), discovered by Bridges in *Drosophila*, was the first tumor suppressor gene to be documented [49]. *lgl* mutant larvae suffer from imaginal disc outgrowth

resulting from a loss of cell polarity and die before entering metamorphosis [50]. Additionally, *lgl* mutant flies share many of the properties of human tumors, such as loss of tissue architecture, cell shape and failure of cells to differentiate [51-56]. There is a strong correlation between loss of human Lgl1 and pancreatic carcinoma, malignant melanoma and colorectal cancer [57].

Lgl proteins play a crucial role in regulating cell polarity. *Lgl*, along with *dlg* and *scrib*, comprise a class of functionally related neoplastic tumor suppressors termed the Scribble complex, where mutations in any of these genes cause overproliferating cells to lose the ability to organize an epithelial monolayer and differentiate [56, 58-62]. Lgl localizes to the basolateral membrane and regulates apical-basal polarity in epithelial cells through interactions with the Par6-atypical protein kinase C (aPKC) polarity complex [56, 61-62]. Par6 binds to mislocalized Lgl, where aPKC-mediated phosphorylation of Lgl at a conserved phosphorylation site prevents it from associating with the apical membrane [63-66]. Lgl also inhibits aPKC from localizing to the baso-lateral membrane [61, 67-68]. This antagonistic interaction maintains the identities of the apical and basolateral membranes.

Numerous studies suggest that the role of Lgl in cell polarity is as a regulator of the actin cytoskeleton. Experiments in *Drosophila* demonstrate that *lgl* physically associates with the nonmuscle myosin II [69-70]. This interaction, regulated by phosphorylation of Lgl by aPKC, localizes myosin II to the apical cortex of metaphase neuroblasts to modify the actin cytoskeleton [70]. Additionally, myosin II is mislocalized in the neural progenitor cells of $Lgl1^{-/-}$ mice [71]. The cell polarity defects in the $Lgl1^{-/-}$ brain are very similar to the brain phenotype of myosin II-B mutant mice [72].

Conversely, there is significant evidence that Lgl functions in polarized exocytosis by regulating pathways that mediate vesicle fusion and exocytosis. In Madin-Darby canine kidney

(MDCK) epithelial cells, Lgl associates with the basolateral specific t-SNARE, Syntaxin4, as well as in complex with Syntaxin4/Snap-23 [63]. The interaction with t-SNAREs is a structurally conserved and functionally important feature of the Lgl family, as chimeric Lgl proteins in which large regions of yeast Sro7 and mammalian Lgl were exchanged could functionally rescue growth and secretion defects associated with loss of Sro7 when chimeras retained the ability to bind the yeast t-SNARE, Sec9 [74]. In neurons, Lgl was also shown to interact with the Rab GTPase, Rab10 at a common state of axonal membrane protrusion [75]. Additionally, *Drosophila lgl* is required for signaling and secretion of Decapentaplegic (DPP)—a member of the transforming growth factor beta (TGFbeta) family [73].

1.3.2 Tomosyn

Tomosyn was initially discovered in a pulldown assay for proteins that bind to the neuronal t-SNARE, syntaxin1 [76]. In mammalian brain, two distinct genes drive the expression of seven closely related isoforms with distinct patterns of localization, sharing a conserved structure: b-tomosyn-1, m-tomosyn-1, s-tomosyn-1, xb-tomosyn-2, b-tomosyn-2, m-tomosyn-2 and s-tomosyn-2[77-78]. The m-tomosyn and s-tomosyn isoforms are brain specific, while b-tomosyn is ubiquitously expressed and has a role in non-neuronal cell exocytosis. All tomosyn isoforms possess three structural domains: a C-terminal region containing an R-SNARE-like coiled-coil domain, an N-terminal region enriched with WD40 repeats that are predicted to fold into a propeller-like structure, and a hypervariable linker domain that differs between the spliced variants [79]. The tomosyn coiled-coil SNARE domain associates with syntaxin1 to form a four-protein complex including the t-SNARE, SNAP-25, and the calcium sensor, synaptotagmin [76, 80]. Formation of this tomosyn-syntaxin complex prevents association with the v-SNARE, synaptobrevin (VAMP) [81].

Tomosyn-1 has been suggested to act as a negative regulator of exocytosis based on studies in PC12 and chromaffin cells, and in several neurosecretory cells and neurons [80, 82-85]. In neuronal-like PC12 cells, overexpression of tomosyn-1 leads to a reduction in calcium-dependent human growth hormone secretion [76, 85]. When overexpressed in 3T3-L1 adipocytes, tomosyn interacts with the adipocyte t-SNARE complex, syntaxin-4 and SNAP-23, inhibiting VAMP-2 association and blocking insulin-stimulated fusion of GLUT4 vesicles [86]. In mouse pancreatic β-cells, overexpression of m-tomosyn significantly decreases insulin secretion and siRNA knockdown of tomosyn expression was associated with an increase in growth hormone exocytosis [87]. Taken together, these results combined with numerous other studies suggest a function for tomosyn in polarized exocytosis and regulation of neurotransmitter release by affecting the formation of trans-SNARE complexes.

1.3.3 Sro7

Whereas both Lgl and Tomosyn demonstrate the ability to bind SNARE proteins, the yeast Lgl family member, Sro7, was the first family member to suggest an *in vivo* functional role for the Lgl family in polarized exocytosis. *SRO7* and its redundant protein homolog, *SRO77*, were isolated from a multicopy screen for suppressors of Rho3, a small GTPase critical for maintenance of cell polarity[88]. The following year, our lab identified Sro7 in a screen for binding partners of the SNAP25-like yeast t-SNARE, Sec9 (Figure 1.1) [47]. This interaction is regulated by the C-terminal autoinhibitory tail of Sro7 in that when it binds to Sro7, the SNARE domain of Sec9 is precluded from binding [48]. This conformational switch between an "open" form, with an unbound tail, and "closed" form with the tail bound, likely plays a role in triggering SNARE complex assembly—perhaps in a spatially-defined fashion.

Upon deletion of *SRO7* and *SRO77*, secretory vesicles accumulate in the cell, specifically in the polarized bud, while the actin cytoskeleton and its polarized distribution remains unperturbed [47]. This phenotype is similar to that of late secretory mutants and suggests that the Lgl family functions in polarized exocytosis rather than in cytoskeletal regulation. Consistent with the exocytic defect being due to a role in SNARE assembly, Sro7 was also found associated with ternary SNARE complexes of Sec9/Sso/Snc.

Sro7 is the only Lgl / Tomosyn family member whose crystal structure has been determined [48] (Figure 1.2A), however structural sequence alignment of Sro7 with Lgl and Tomosyn suggests significant structural conservation (Figure 1.2B). This structure consists of two, 7-bladed WD40 beta-propeller domains followed by a 60-residue-long C-terminal tail that binds back to the protein. Structural conservation among the Lgl family members is especially clear within the 14 WD40 repeats and in many elements of the domain interface (Figure 1.2B). The beta-propeller domains are arranged in a way that resembles an open clamshell structure. Both Lgl and Tomosyn have insertions in the 10D-11A loop containing conserved sites for phosphorylation by aPKC and cAMP-dependent protein kinase (PKA), respectively. Interestingly, many residues in the C-terminal regulatory tail of Sro7 are conserved in Tomosyn, but not in Lgl.

Recent evidence suggests that Sro7 could also act as a direct effector of the Rab GTPase, Sec4 [89] (Figure 1.1). Sro7 was shown to bind preferentially to Sec4 *in vitro* in the presence of GTP and has genetic properties consistent with it functioning downstream of Sec4. More recently, the Lu group showed that there is a requirement *in vivo* for Rab10 and Lgl at a common state of axonal membrane protrusion [75]. Their biochemical data suggest that these proteins may interact, but distinct from the Sec4-Sro7 interaction in that it is a GDP-, not GTP-

dependent interaction and in this case Lgl has been suggested to function upstream of Rab10 to activate it, instead of act as its effector.

1.4 Thesis Contributions

The goal of my thesis was to understand the molecular details and functional significance of the interaction between Sro7 and the Rab GTPase Sec4. Chapter 2 details studies directed at identifying the interaction interface between Sro7 and the Rab GTPase, Sec4. Biochemical results combined with *in vivo* suppression studies and computational modeling pinpointed the Sro7-Sec4 docking interface. Specifically, we found that mutations in Sro7 which disrupt the Sro7-Sec4 interaction also demonstrate a clear deficiency *in vivo* to overcome defects in Exocyst complex function. Chapter 3 describes the development of a novel *in vitro* assay that recapitulates post-Golgi vesicle tethering by Sro7-induced clustering of vesicles. These studies establish that the presence of Rab GTPase Sec4 on the surface of the post-Golgi vesicle is critical for vesicle clustering in the *in vitro* system. Additionally, Sro7 point mutations designed to destabilize the Sro7 C-terminal autoregulatory tail demonstrate that the conformational status of the tail ("closed" vs "open" as previously described) plays an important role in regulating the activity of Sro7-induced vesicle clustering.

1.5 Figures

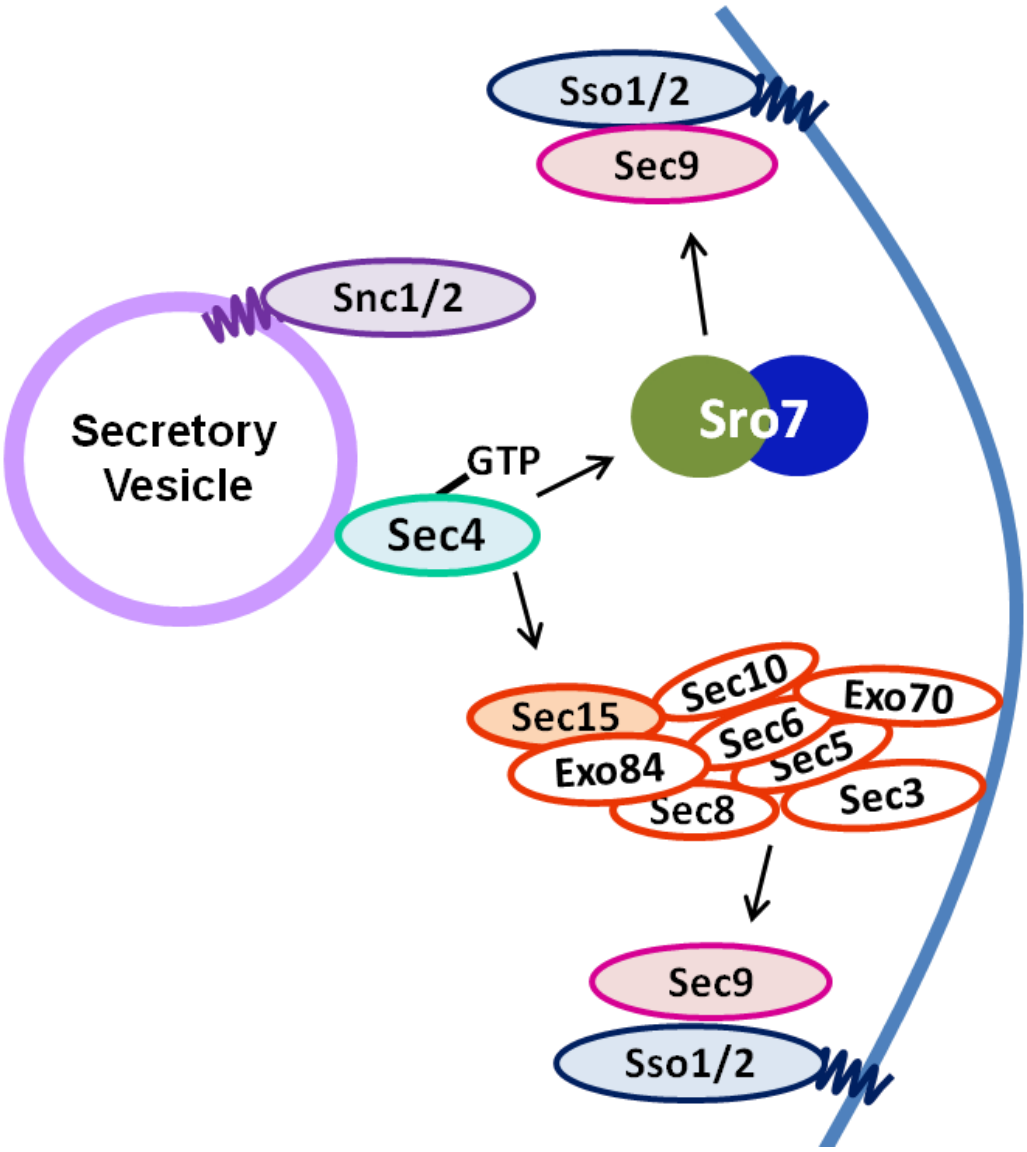

Figure 1.1 - Schematic of *S. cerevisiae* post-Golgi secretory machinery.
The Rab GTPase Sec4 (cyan) on post-Golgi vesicles (light purple) interacts with the Sec15 component of the Exocyst complex (orange) to tether vesicles to the plasma membrane (blue). The Sec6 component of the Exocyst complex can also interact with the t-SNARE, Sec9 (pink). The v-SNAREs on the vesicle, Snc1 and Snc2, are shown in purple. The t-SNAREs on the plasma membrane, Sso1 and Sso2, are shown in dark blue. A second downstream effector of Sec4 is Sro7 (green and blue). Like the Exocyst, Sro7 also interacts with the t-SNARE, Sec9.

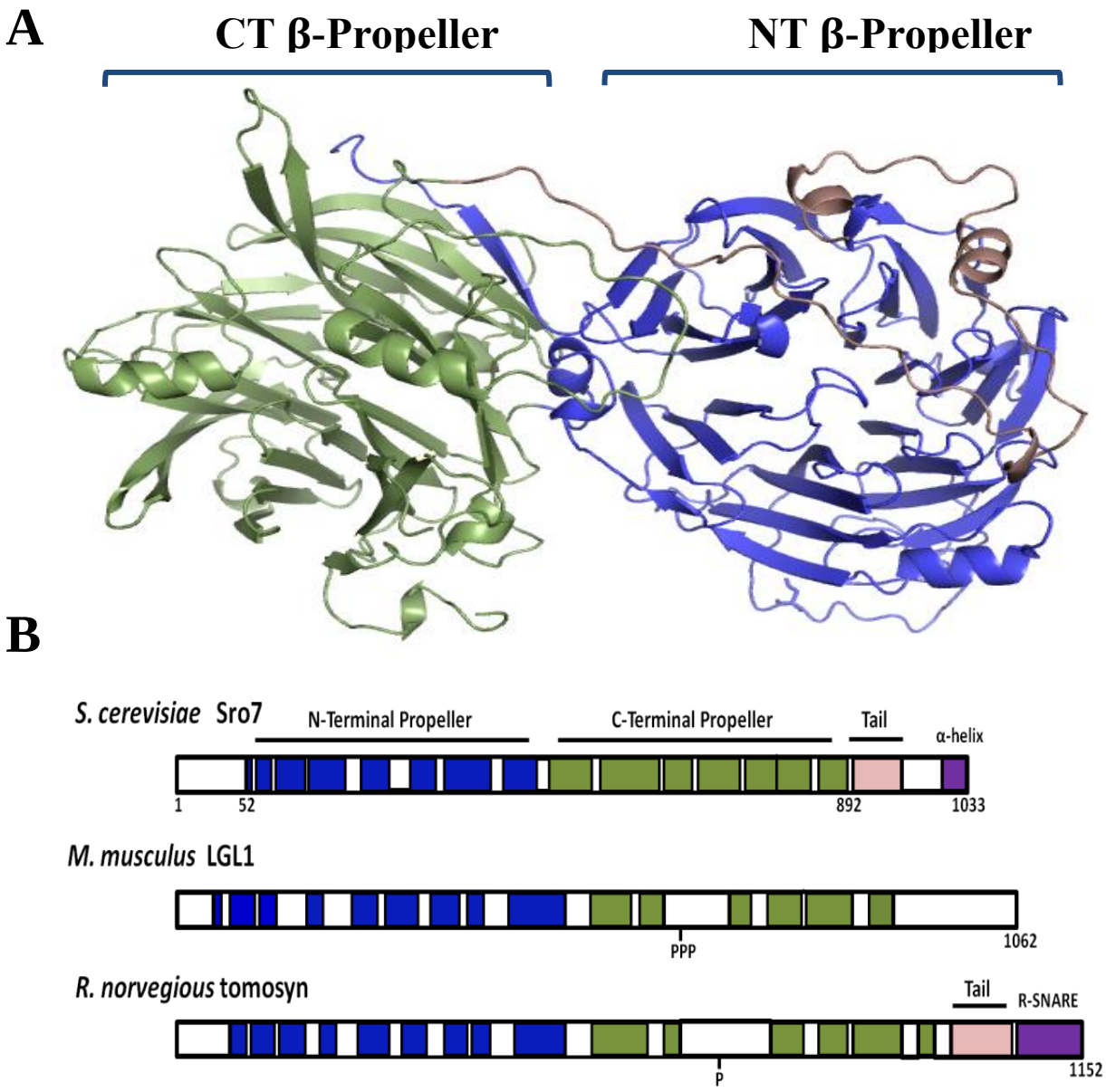

Figure 1.2 – Structural conservation within the lethal giant larvae family.
A, Crystal structure of Sro7 showing the N-terminal propeller in blue, the C-terminal propeller in green and the autoinhibitory tail in light pink. B, Schematic illustrating the structural alignments between Sro7 and the Lgl and Tomosyn family members. Phosphorylation sites are indicated on Lgl1 and tomosyn.

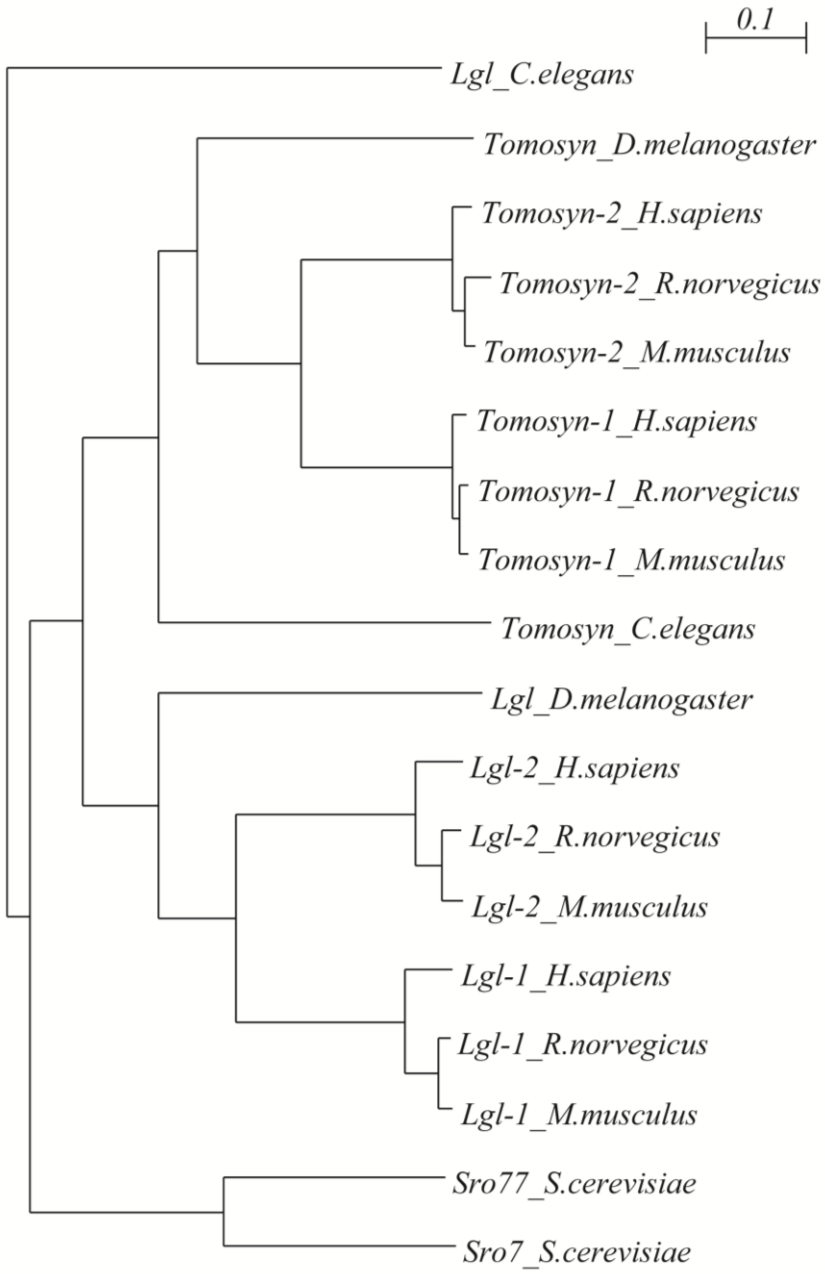

Figure 1.3 – Phylogenetic tree of Lgl/Tomosyn family of proteins.
Lgl/Tomosyn homologs are present in humans, *Mus musculus* mice, and *Rattus norvegicus* rats (*Lgl1* and *Lgl2*—also known as *Hugl-1* and *Hugl-2*—and neuronal *Tomosyn-1* and *Tomosyn-2)*, in *Drosophila melanogaster* fuit flies (*Lgl* and *Tomosyn*), in *Caenorhabditis elegans* worms (*Lgl* and *Tomosyn*), and in *Saccharomyces cerevisiae* budding yeast (*SRO7* and *SRO77).*

CHAPTER 2

Structural Basis for Recognition of the Sec4 Rab GTPase by its Effector, the Lgl/Tomosyn Homolog, Sro7[1]

2.1 Overview

Members of the Tomosyn/Lgl/Sro7 family play important roles in vesicle trafficking and cell polarity in eukaryotic cells. The yeast homolog, Sro7, is thought to act as a downstream effector of the Sec4 Rab GTPase to promote SNARE assembly during Golgi to cell surface vesicle transport. In this paper, we describe the identification of a Sec4 binding site on the surface of Sro7 that is contained within a cleft created by the junction of two adjacent β-propellers which form the core structure of Sro7. Computational docking experiments suggested four models for interaction of GTP-Sec4 with the Sro7 binding cleft. Further mutational and biochemical analyses confirmed that only one of the four docking arrangements is perfectly consistent with our genetic and biochemical interaction data. Close examination of this docking model suggests a structural basis for the high substrate and nucleotide selectivity in effector binding by Sro7. Finally, analysis of the surface variation within the homologous interaction site on Tomosyn-1 and Lgl-1 structural models suggests a possible conserved Rab GTPase effector function in Tomosyn vertebrate homologs.

[1] Reproduced from *Molec Biology of the Cell*, 2015 Jul 22.E15-04-0228.[Epub ahead of print]

2.2 Introduction

Polarized exocytosis requires the proper localized delivery, docking and fusion of secretory vesicles with sites of active growth on the plasma membrane. In the budding yeast, *Saccharomyces cerevisiae*, secretory vesicles are delivered to specific plasma membrane sites where the Rab GTPase Sec4 mediates vesicle tethering through its interaction with the Exocyst complex subunit, Sec15 [7, 10]. Following vesicle tethering, a trans-SNARE complex forms between the vesicle SNARE proteins Snc1/2 and the plasma membrane SNARE proteins Sec9 and Sso1/2, which drives vesicle fusion [23-25].

Genetic screens in yeast identified a Sec9-binding protein, Sro7, as an important regulator of Golgi to cell surface trafficking [47, 88]. Sro7 is a member of the structurally conserved Lethal Giant Larvae (Lgl) / Tomosyn family of proteins involved in polarity. Lgl was first discovered in *Drosophila melanogaster*, where mutant Lgl larvae suffer from imaginal disc outgrowth and show many of the properties of human tumor behavior, such as loss of tissue architecture, cell shape and failure to differentiate[50]. The exact mechanism of function for this family of proteins in cell polarity is controversial [90]. Studies on *Drosophila* Lgl suggest that it functions in regulating actin polarity by interacting with myosin II [69]. Mammalian Lgl is also known to antagonistically interact with the Cdc42-Par6-atypical Protein Kinase C (aPKC) polarity complex to maintain the identity of the apical and basolateral membranes in epithelial cells [91]. The neuronal family member, Tomosyn-1 (or Stxbp5) forms a complex with syntaxin-1, SNAP25 and synaptotagmin, directly competing with VAMP (synaptobrevin) for forming an active SNARE complex [76, 81]. This suggests that Tomosyn functions in polarity by regulating neurotransmitter release by affecting the formation of trans-SNARE complexes in exocytosis. In yeast, deletion of Sro7 and its redundant homolog Sro77 causes secretory vesicles to accumulate

in the emerging bud while the actin cytoskeleton is unperturbed [47]. This is phenotype is similar to that of late secretory mutants and implicates that the Lgl / Tomosyn family functions in polarized exocytosis rather than cytoskeletal regulation.

Recent evidence suggests that Sro7 could also act as a direct effector of Sec4 [89]. Sro7 was shown to bind to Sec4 in the presence of GTP and has genetic properties consistent with it functioning downstream of Sec4. However, there has not been rigorous testing that proves the physical interaction with Sec4 is required for Sro7 function *in vivo*, so the mechanism of this interaction and if it plays a role in exocytosis still remains unknown.

Sro7 is the only Lgl / Tomosyn family member whose X-ray structure has been determined [48]. In this study, we utilized the crystal structure of Sro7 to identify charged surface patches on Sro7 and screened for their involvement in the Sro7-Sec4 interaction. We combined these *in vitro* results with *in vivo* suppression studies and *in silico* modeling to validate the Sro7-Sec4 docking interaction interface. We found that disruption of the Sro7-Sec4 interaction results in a reduction of Sro7 function *in vivo*. Moreover, bioinformatic analysis suggests the possibility that the Sro7-Sec4 Rab-binding interface may be conserved in vertebrate Tomosyn-1.

2.3 Results

2.3.1 The interaction between Sro7 and the yeast Rab GTPase Sec4 is specific and GTP-dependent.

We have shown previously that Sro7 binds preferentially *in vitro* to the GTP-locked conformation of the yeast Rab GTPase Sec4 [89]. More recently, Wang *et al.* [75] reported an interaction between Lgl—the mammalian homolog of Sro7—and the Rab10 GTPase that may play a role during axonal membrane protrusion. However, the biochemical analysis of this

interaction suggests that Lgl and Rab10 interact in a GDP- rather than GTP-dependent manner. This further suggests that Lgl1 may act as a GDI displacement factor (GDF) facilitating the activation of Rab10, instead of as a Rab GTPase effector transducing the GTP-Rab function.

This prompted us to further examine nucleotide and Rab-binding specificity of Sro7 with the yeast Rab GTPases. We therefore examined binding properties of Sro7 with representatives of each subgroup of the well-characterized yeast Rab GTPase family [92-94]. Representatives of each of the 8 yeast Rab subfamilies—Sec4, Ypt1, Ypt32, Ypt51, Ypt6, Ypt7, Ypt10 and Ypt11—were purified from E.coli as N-terminally-tagged GST fusions, immobilized on glutathione sepharose beads and exchanged with GTPγS, GDP or no nucleotide (Figure 2.1). As seen in Figure 2.1, purified full-length Sro7 binds specifically to GTPγS-Sec4 and fails to show significant binding to any of the other 7 Rab proteins tested (Figure 2.1). Importantly, Sro7 binding is completely dependent on Sec4 being in a GTP-bound, activated state and no detectable binding was seen to GDP or nucleotide-free forms of any of the 8 Rab GTPases in yeast. Taken together, these results indicate that the interaction between Sro7 and the yeast Rabome is highly specific to Sec4 in its active or GTP-bound state.

2.3.2 Biochemical screen identifies two Sro7 mutants deficient in binding to Sec4-GTP.

To begin to explore the molecular mechanism by which the Sec4 GTPase regulates Sro7, we set out to identify the site(s) of interaction between these proteins. Currently, Sro7 is the only member of the lethal giant larvae/tomosyn protein family for which a high-resolution crystal structure has been determined [48]. Sequence analysis based on close relatives of Sro7 combined with structural analysis identified a number of conserved surface patches as potential candidate sites on Sro7 for interaction with upstream regulators (i.e. the Rab Sec4) or downstream targets of its function (i.e. the t-SNARE Sec9). We focused our interrogation within each conserved

patch on charged residues by creating charge-reversal mutations because of their high likelihood to disrupt protein-protein interactions. We therefore generated a collection of 12 different charge-reversal mutations that span both β-propeller domains of Sro7 and exclude known sites of interaction with the Sec9 N-terminus and with the regulatory tail of Sro7 (Figure 2.2A, B) [48]. Wildtype Sro7 and the Sro7 mutants were purified to homogeneity from yeast using a multi-step procedure we have previously described [95] and all proteins were subjected to SDS-PAGE and Coomassie staining to assess both purity and quantity of each preparation (Figure 2.2C).

As a first examination of overall protein integrity, we compared wildtype Sro7 and the Sro7 mutant proteins for binding to a known Sro7 ligand, the t-SNARE Sec9[47]. All twelve charge-reversal mutants bind GST-Sec9 comparably to wildtype Sro7 and statistical analysis of the binding data demonstrates that differences are not significant (Figure 2.2C).

To determine if any of the 12 surface patches on Sro7 were involved in mediating specific binding to Sec4-GTP, we subjected each of the purified mutant proteins to binding assays with Sec4 that had been exchanged with GTPγS or GDP. Of the 12 Sro7 mutant proteins, two—Sro7-K395E and Sro7-R599E, R600E—no longer bind to Sec4-GTP, while the remaining 10 bind Sec4-GTP at levels statistically similar ($p > 0.05$) to wildtype Sro7 (Figure 2.2C). None of the mutations have any detectable effect on the nucleotide-specificity of the interaction with Sec4.

In parallel to the biochemical analysis of the surface patch mutants, we examined the effect of each mutation on *in vivo* function, utilizing two distinct genetic assays. First, we examined the ability of the Sro7 mutants to function as the sole source of Sro7 in the cell. A double deletion in Sro7 and its redundant homolog, Sro77, (*sro7*Δ*, sro77*Δ) is cold-sensitive and sensitive to salt, but one extra-chromosomal copy of wildtype Sro7 complements this phenotype

[47, 96]. As the sole source of Sro7, all twelve of the charge-reversal mutants complement the cold and salt sensitivity of *sro7*Δ*, sro77*Δ like wildtype *SRO7* (Table 2.1). To determine if the lack of any detectable growth phenotype for the two Sec4-binding deficient mutants was related to the presence of the mutants on an extra-chromosomal plasmid, we integrated each defective allele (*sro7-K395E* and *sro7-R600E*), as well as an allele with both mutations (*sro7-K395E,R600E*) into the native *SRO7* locus by gene replacement (see Figure 2.8 for details on the integration). The results of this analysis, shown in Figure 2.2E and Figure 2.8, demonstrate that each of the single mutants are able to fully restore growth as the sole source of *SRO7* at all temperatures and media conditions examined, including 17 ^{o}C and 0.7M NaCl. Furthermore, the absence of a growth phenotype is unlikely due to residual binding present in each mutant as the phenotype is identical to wildtype even when both mutations are combined in a single allele (*sro7-K395E,R600E).*

The second genetic assay makes use of our previous observation that Sro7 plays a role as an effector of Sec4 that is parallel to the Exocyst complex, as overexpression of Sro7 strongly suppresses growth defects associated with deletions or temperature-sensitive mutations in subunits of the Exocyst complex[47, 87, 89]. Temperature-sensitive alleles of the Sec15 component of the Exocyst (*sec15-1)* are particularly sensitive to small increases in *SRO7* dosage, as just a single additional copy (*CEN* plasmid) is sufficient to suppress temperature-sensitivity of *sec15-1* at 37^{o}C (Figure 2.2D). When the *sec15-1* suppression analysis was extended to the collection of surface patch mutants, we found that only the *sro7-K395E* and *sro7-R599E, R600E* alleles demonstrated loss of suppression. The other 10 surface patch alleles suppress *sec15-1* temperature sensitivity at levels comparable to wildtype *SRO7*. Taken together with the binding

data in Figure 2.2C, these results identify a potential surface(s) on Sro7 involved in the interaction with Sec4 both *in vitro* and *in vivo*.

2.3.3 Computational docking studies extracted interacting elements from the best scoring complexes of Sro7 and Sec4-GTP to produce four models.

To examine the structural implications of the *in vitro* and *in vivo* effects of the Rab binding mutants described above, we mapped the sites of the Sro7-K395 and Sro7-R599, R600 residues on the crystal structure of Sro7. Interestingly, these sites suggest that both the N-terminal and C-terminal β-propeller domains contribute to Sec4 binding and implicate a cleft formed by the intersection of the two propeller domains of Sro7 (Figure 2.3B). The identification of these novel Sro7 mutants peaked our interest in understanding the engagement between Sro7 and Sec4 in more detail. However, the relative low affinity of the interaction between Sro7 and Sec4-GTP make it unsuitable for analysis by co-crystallization experiments. Therefore, we took an alternative approach that involved the combination of *in silico* docking studies with *in vitro* binding assays and *in vivo* suppression data to generate models for Sro7-Sec4 interaction. Like Sro7, the crystal structure of Sec4-GTP has previously been determined [97]. We utilized the ClusPro 2.0 docking program to perform docking simulations between Sro7 and Sec4. The simulations filtered conformations for low desolvation and electrostatic energies and ranked poses by cluster size for the best scoring protein-protein complexes. The results revealed that four of the high-scoring models include the involvement of Sro7 residues K395 and R599 or R600 in the *in silico* interaction with Sec4-GTP (shown in red, Figure 2.3B) which is consistent with the *in vitro* binding data described above. Additionally, all of these four models implicate one or both of the switch I and II regions of Sec4, which are the structural elements of

Ras GTPases that change in response to the nucleotide state and are therefore strongly predicted to be involved in the interaction with a Sec4 effector protein such as Sro7.

All four Sro7-Sec4 docking models included the same Sro7 interface for Sec4 binding (Figure 2.3A). This region is in a pocket on the opposing side of the protein from where the Sro7 regulatory tail and the t-SNARE, Sec9 bind. To confirm that this Sro7 interface is involved in binding to Sec4, as predicted by these four docking models, and to further delineate the site of Sec4 binding on Sro7, we created a second set of Sro7 mutants at this interface (shown in orange, Figure 2.3B). We characterized the Sro7 mutants both *in vitro* by binding to Sec4-GTP and *in vivo* by analysis of their ability to suppress the growth defect of *sec15-1* at 37^{o}C. The results, shown in Figure 2.3C, demonstrate that two of the three mutant proteins—Sro7-D326R and Sro7-S327A, T329E—are deficient in binding to Sec4-GTP, while Sro7-D361K binds Sec4-GTP comparably to wildtype Sro7. Likewise, when we examined the Sro7 mutants *in vivo* by testing their ability to suppress the temperature sensitivity of *sec15-1* we found that the same two mutants that are deficient in binding to Sec4-GTP—*sro7-D326R* and *sro7-S327A, T329E*—are also unable to suppress growth at the restrictive temperature (Figure 2.3C). Also consistent with the binding data, we see that *sro7-D361K* suppresses *sec15-1* at 37^{o}C similarly to wild-type *SRO7* suppression (Figure 2.3C). As with our previous Sec4-binding mutants, these alleles show no obvious growth defects as the sole source in complementation of the severe cold-sensitive growth defect present in the *sro7*Δ, *sro77*Δ double deletion strain (Table 2.1). The results of this characterization support the prediction that the Sro7 interface incorporated in the 4 docking models is highly likely to be a component of the binding site for Sec4-GTP. Moreover, these results are consistent with the previous finding in Figure 2.2 that Sro7 mutants unable to bind

Sec4-GTP also demonstrate a clear defect *in vivo* to overcome the loss in Exocyst complex function present in *sec15-1*.

2.3.4 Novel mutations in Sec4 were designed to discriminate between predicted *in silico* docking models.

While the same binding interface of Sro7 is involved in all four docking models, the orientation of Sec4 with respect to Sro7 is substantially different in each model (Figure 2.4A). We therefore generated a second set of mutations in surface-exposed, charged Sec4 residues with the aim of distinguishing between the four models. To accomplish this, we chose six residues to mutate with high predictive value in distinguishing between the four models based on differences in their predicted distance from Sro7 in the four models. Residues were scored for high interaction potential when the distance was less than 4Å and low interaction potential when the distance was greater than 4Å (Figure 2.5A). For example, the Sec4-D56R mutant is predicted to be involved in Sec4-Sro7 docking in Models A, C and D, but not in Model B. Therefore, this particular mutation will discriminate Model B from the other models. The locations of the novel set of Sec4 mutations tabulated in Figure 2.5A are shown by a ribbon diagram in Figure 2.4B.

Wildtype Sec4 and the discriminatory Sec4 mutants were purified as GST fusion proteins, exchanged with either GTPγS or GDP and tested for binding to wildtype Sro7. The binding data shown in Figure 2.4C demonstrates that 4 of the 6 mutant proteins tested exhibit a significant defect in binding to Sro7, while 2 of the mutant Sec4 proteins bind to Sro7 at levels similar to wildtype Sec4. In order to analyze the *in vivo* consequences of Sec4 mutations resulting in a loss of binding to Sro7, we utilized the fact that, like *SRO7*, one additional copy of *SEC4* (on *CEN*) strongly suppresses the temperature-sensitivity of a *sec15-1* strain [98]. As can be seen in Figure 2.4C, all four of the mutant alleles of *SEC4* which encode proteins defective in

binding to Sro7 *in vitro* also have completely lost the ability to suppress the *sec15-1* mutant temperature-sensitivity. Likewise, the two mutant *SEC4* alleles which encode proteins that bind to Sro7 at levels similar to that of wildtype Sec4, also demonstrate suppression of *sec15-1* temperature-sensitivity in a manner indistinguishable from wildtype *SEC4*. The strong correlation between the biochemical and genetic analyses strongly supports the notion that the interaction between Sec4 and Sro7 observed *in vitro* is also important for the function of both proteins within the cell.

We next examined whether the binding and suppression data would allow us to discriminate between the four docking arrangements described above. We compiled the tabulated predicted effects of the Sec4 mutations on Sro7-Sec4 binding for each of the four models based on the distance of the mutated residue from the Sro7 binding interface (Figure 2.5A). As previously stated, low interaction potential (marked as – in Figure 2.5A) corresponds with mutated Sec4 residues at a distance greater than 4 Å from Sro7, while high interaction potential (marked as + in Figure 2.5A) corresponds with mutated Sec4 residues at a distance of less than 4 Å from Sro7. Based on the *in vitro* and *in vivo* studies described above, mutations that blocked both Sro7 binding and *sec15-1* suppression are indicated with an asterisk—while those mutations that had no effect on binding and suppression are unmarked (Figure 2.5A). In interpreting these results it is important to note that it is possible for a residue to be predicted within 4 Å of the interface and still not affect binding when mutated. However, when a mutated residue is greater than 4 Å from the binding interface in a particular docking model there is a strong prediction that the mutated residue will have no effect on the observed *in vitro* interaction and *in vivo* suppression analyses. For example, in docking Models A and B, Sec4-E80K is predicted to be greater than 4 Å from the binding interface on Sro7, yet this mutant dramatically

affected the Sro7-Sec4 interaction both *in vitro* and *in vivo*. Therefore, it is unlikely that Models A and B are the correct docking arrangement between Sro7 and Sec4 and this is scored as an inconsistency (in red) in Figure 5A. As can be seen, Models A, B and C all contain several inconsistencies when comparing the predicted effects of the mutations with the effects observed *in vitro* and *in vivo*. In contrast, Model D (shown in Figure 2.5B) is the sole model with perfect correlation between its interaction predictions and the actual *in vitro* and *in vivo* data (Figure 2.5A). Additionally, 4 of the 5 mutated Sec4 residues in Model D are predicted to be within 4 Å of the Sro7-Sec4 binding interface and demonstrate a strong effect on both binding and suppression.

Three distinct patches of mutations on both proteins affecting the Sro7-Sec4 interaction correspond nicely between Sro7 (orange residues) and Sec4 (purple residues)—Sro7-R599E, Sro7-R600E and Sec4-D136R on the C-terminal β-propeller front side of the binding cleft (Figure 2.5, Inset Below), Sro7-K395E and Sec4-D56R on the N-terminal β-propeller front side of the binding cleft (Figure 2.5, Inset Below), and Sro7-D326R, Sro7-T329K, Sec4-E80K and Sec4-R83D on the N-terminal β-propeller back side of the binding cleft (Figure 2.5, Inset Right). Based on this extensive analysis, we invalidated 3 of the 4 docking models and have substantial evidence that Model D is the native docking arrangement for interaction between Sro7 and Sec4-GTP.

2.3.6 How does Sro7 selectively bind GTP-bound Sec4?

The results shown in Figure 2.1 demonstrate that Sro7 has the biochemical properties of a Rab effector with high substrate-specificity for Sec4—as we do not detect Sro7 interaction with any other Rab GTPase in yeast. In addition, the Sro7-Sec4 interaction is highly specific to the GTP-bound or activated form of Sec4. Our determination of a well-validated, high-resolution

model for Sro7-Sec4 docking allows us to identify elements of the binding interaction that are likely responsible for these two effector specificity aspects of Sro7 with Sec4. Close examination of the model illustrates four regions within Sec4 that are in most intimate contact with Sro7 (Figure 2.6). Two of the regions in close contact with Sro7 are the switch I and switch II domains of Sec4—the two regions that undergo the most conformational change when comparing GDP and GTP-bound structures and are therefore critical to nucleotide-specific recognition of small GTPases by effectors and accessory proteins [99]. The four Sro7 contact regions within Sec4 are: residues 46-58 (the entire switch I domain), residues 79-84 (within the switch II domain), Sec4-135-140 and Sec4-162-167. The first two regions make contact with the Sro7 N-terminal β-propeller domain, while the latter two interact with the Sro7 C-terminal β-propeller domain.

To determine which of these four regions is likely used by Sro7 to distinguish Sec4 from other Rab GTPases in yeast, we examined sequence alignments of the 8 yeast Rab family members used in Figure 2.1—Sec4, Ypt1, Ypt31, Vps21, Ypt10, Ypt6, Ypt7 and Ypt11. We found that the Sro7 interacting region within the Sec4 switch II domain is highly conserved within the yeast Rabome (Figure 2.6). Therefore, the interaction of Sro7 with the switch II domain of Sec4 is unlikely to be involved in mediating Rab specificity, but rather likely plays a role in determining the nucleotide binding state specificity of the protein. Like the switch II domain, the C-terminal half of the Sec4 switch I domain (residues 52-58) is also highly conserved amongst the yeast Rab GTPases (Figure 2.6). In contrast, the first 6 residues of the switch I domain (residues 46-51) of Sec4 are quite distinct from those of the homologous switch I domains in the other yeast Rabs (Figure 2.6—dark Blue residues boxed in Yellow). In fact, of the four contact sites in our model utilized by Sro7 to bind Sec4, only this segment of the Sec4

switch I domain demonstrates the kind of variability that one would expect of a site responsible for the Sro7 substrate specificity. Taken together, we conclude that while Sro7 contact with both the switch I and switch II domains is likely responsible for recognition of the GTP-bound state of Sec4, it is the specific interaction with the N-terminal segment of the switch I domain that provides the high degree of Rab specificity for recognition of Sec4-GTP by the Sro7 effector protein.

2.3.7 Conservation of the Sro7-Sec4 binding interface within the Lgl family of proteins.

Structural and evolutionary examination of surface residue variation has demonstrated that protein-protein interfaces are significantly more constrained in their variability when compared to non-interaction surfaces [100-101]. Structural alignments of Sro7 with its closest vertebrate homologs Tomosyn and Lgl demonstrate that the overall dual β-propeller domain structure of Sro7 is likely shared between all three members of this family [48]. Since the SNARE regulatory function is shared between yeast and vertebrate homologs [102], it is possible that the Rab effector function is also shared with one or more of the vertebrate homologs. If so, one might expect to see a reduced surface variability within the region predicted to form the homologous Sro7-Sec4 binding cleft. We therefore used a combined structural and phylogenetic approach to examine the surface variability of vertebrate members of Tomosyn and Lgl, especially within the region homologous to where Sec4 interacts with Sro7. We used the MODELLER program to build structural models of Tomosyn-1 and Lgl-1 using the crystal structure of Sro7 as a template. The Tomosyn-1 model is similar to that made by Williams *et al*. [103]. We then mapped onto the models invariant residues identified from multiple sequence alignments. A multiple sequence alignment of 16 Sro7 homologs from the Saccharomycetaceae family, one family of budding yeast, was used for comparison (Figure 2.7 Left Panels). Invariant

residues were also identified from an alignment of 47 Tomosyn-1 vertebrate (fish, frog, bird, and mammal) homologs (Figure 2.7 Middle Panels) and from 34 Lgl-1 vertebrate homologs (Figure 2.7 Right Panels). Conserved invariant residues are indicated in pink on the Sro7 crystal structure and the Tomosyn and Lgl structural models, respectively (Figure 2.7). While rates of surface change are overall much greater in the yeasts compared to vertebrates (presumably due to both functional redundancy with the Exocyst complex and much shorter generation time), specific sites of low variability are apparent in all three family members.

There are three areas on the surface of Sro7 with decreased variability within the yeast family—regions homologous to where the Sro7 regulatory tail binds back to the N-terminal β-propeller, the binding site for the N-terminus of the t-SNARE Sec9 [48], and residues within the Sro7-Sec4 binding pocket (Figure 2.7). When we focus specifically on the Sec4 binding cleft on Sro7, the variability among the yeast members reveals two conserved sites in the Sro7-Sec4 binding pocket—one on the C-terminal β-propeller including the Sro7-R600 residue and one on the N-terminal β-propeller including the Sro7-K395 residue (Sro7 Inset, Figure 2.7). Residues Sro7-R600 and Sro7-K395 were previously shown to be directly involved in the Sro7-Sec4 interaction (Figure 2.2). The conserved Sro7-K395 area in the docked Sro7-Sec4 structure interacts with the Sec4 switch I domain (yellow), the region of Sec4 responsible for effector specificity, consistent with the correlation between decreased protein surface variability and functional importance (Sro7 Inset, Figure 2.7).

Human Tomosyn-1 and Lgl-1 protein sequences were used to build structural models based on the Sro7 crystal structure template. As with the yeast family members, invariant surface residues within Tomosyn and Lgl vertebrate homologs were mapped onto the structural models of Tomosyn-1 and Lgl-1. In contrast to yeast, Tomosyn family members have several

conserved regions spanning both faces of its dual propeller structure, likely attributed to increased surface fixation from acquired functionality (Figure 2.7). Like Tomosyn, Lgl vertebrates also developed greater surface residue conservation, however, the invariant residues are located primarily on one protein face—the same face as where the aPKC phosphorylation sites reside (Figure 2.7). A focused examination of the region of Tomosyn that is homologous to the Sro7-Sec4 binding pocket reveals that vertebrate Tomosyn-1 family members maintain significant conservation within the interaction interface. Notably, there is a cluster of invariant residues in Tomosyn-1 that correspond with the part of the binding cleft in Sro7 containing the critical K395 residue (Tomosyn Inset, Figure 2.7).

Interestingly, the surface conservation in vertebrate Lgl-1 members is quite distinct from the conservation observed in vertebrate Tomosyn-1 proteins. While there is a significant increase in overall Lgl surface residue conservation when compared to Sro7 and Tomosyn-1, the region corresponding to the Sec4 binding pocket in Sro7 is significantly more variable in Lgl-1 (Lgl Inset, Figure 2.7). This suggests that of the two vertebrate branches of the Sro7/Lgl/Tomosyn family, Tomosyn is the most likely to have a conserved role as an effector for a vertebrate Rab GTPase.

2.4 Discussion

This study describes for the first time the structural details of the Sec4 GTPase interaction with a direct downstream effector, Sro7. While previous work detailed the interaction between Sro7 and its downstream t-SNARE target, Sec9, this study gives us our first structural clues as to how a member of the Lgl/Tomosyn/Sro7 family of proteins is engaged by a Rab GTPase. One of the defining characteristics of the Lgl/Tomosyn/Sro7 family is the central structure composed of two adjacent 7-bladed beta-propellers having extensive interactions between the N- and C-

terminal propellers [48]. Here we map the binding site utilized by the Sec4 GTPase in its interaction with Sro7 to a cleft formed at the intersection of these two propellers—an interaction which is highly specific to the yeast Rab family member Sec4 in its activated, GTP-bound form.

Our bioinformatic analysis of the sequence variation found in vertebrate members of the Tomosyn1/2 family suggests that this cleft may also be important for the interaction between Tomosyn and a related small GTPase—perhaps as part of an ancestral function for this family of proteins that predates the divergence of the family members [104-105]. Interestingly, there is significantly less conservation in the homologous Sro7-Sec4 binding interface for members of the Lgl1/2 family when compared to Tomosyn1/2. We can only speculate about the precise significance of this difference, but it could be attributed to divergence or loss of the ancestral Rab effector function as the Lgl family evolved distinct functions from Tomosyn in metazoans. This functional separation between family members could have occurred in parallel to the loss of the C-terminal R-SNARE motif in members of the Lgl family in metazoans [104]. Interestingly, Wang *et al*. [75] have reported a direct interaction between Lgl1 and the Rab10 GTPase. However, unlike the GTP-dependent Sro7-Sec4 interaction, Lgl1 appears to interact specifically with the GDP- rather than GTP-bound form of Rab10.

A surprising aspect of this study arose when investigating the importance of interaction with the Sec4 GTPase to the *in vivo* function of Sro7 within the cell. While there is an absolute requirement for Sro7-Sec4 interaction to rescue the late secretory mutant *sec15-1*, mutant forms of Sro7 that are unable to bind Sec4-GTP, however, show no detectable growth or secretion defect when present as the sole source of *sro7* and *sro77* in the cell (Table 2.1). The simplest explanation for this behavior is that Sro7 function overlaps significantly with the function of the Exocyst complex as part of a dual or parallel effector pathway. The Exocyst and Sro7 were both

shown to bind directly to Sec4-GTP and have SNARE regulatory properties [48, 89, 106]. In fact, overexpression of Sro7 suppresses a number of mutations and deletions in components of the Exocyst and has genetic properties consistent with a parallel function [47, 89]. Further work will allow us to determine more precisely which aspects of the Sec4/Sro7 effector pathway (I.e. vesicle tethering vs SNARE assembly) represent elements functioning in parallel to those of the Exocyst complex, and which aspects are unique to Sro7 or the Exocyst in carrying out Sec4's essential functions in exocytosis [89, 95].

2.5 Materials and Methods

2.5.1 Media and Reagents

Yeast growth media used in this study includes: YPD (1% bacto-yeast extract, 2% bacto-peptone, 2% dextrose [Difco, Sparks, MD]), S minimal (0.67% yeast nitrogen base without amino acids and 2% dextrose [Difco, Sparks, MD]), agar [Fisher Scientific, Pittsburgh, PA], and dropout media (0.67% yeast nitrogen base without amino acids, synthetic complete amino acid supplement minus appropriate amino acid(s) and 2% dextrose [US Biological, Swampscott, MA]).

Bacteria growth media used in this study includes: Terrific Broth (TB; 4.7% bacto-TB, 1% glycerol [Fisher Scientific, Pittsburgh, PA]), Super Optimal Broth (SOB; 2% tryptone [Difco, Sparks, MD], 0.5% bacto-yeast extract, 2.5mM KCl [Sigma Aldrich, St. Louis, MO], 1M NaCl, 10mM MgCl2, 10mM MgSO4 [Fisher Scientific, Pittsburgh, PA]), Super Optimal Broth with Catabolite Repression (SOC; SOB + 2.5% glucose), and Lysogeny Broth (LB; 1% bacto-tryptone, 0.5% bacto-yeast extract, and 1% NaCl).

Reagents used in this study: GTPγS, Triton X-100, GDP, sodium azide, sodium fluoride, dithiothreitol (DTT), β-mercaptoethanol, Pepstatin A and LAA components (Leupeptin 1 mg/mL, Aprotinin 2 mg/mL, Antipain 1 mg/mL) were obtained from Sigma Aldrich [St. Louis, MO]. Ampicillin and AEBSF (4-(2-aminoethyl) benzenesulfonyl fluoride) was obtained from US Biological [Swampscott, MA]. Tween20 and Broad Range Protein Standard was obtained from BioRad [Hercules, CA]. Glutathione Sepharose 4B, Protein A Sepharose and Precision Protease was obtained from GE Healthcare [Milwaukee, WI]. Secondary antibodies for the Odyssey Imaging System are from LI-COR Biosciences [Lincoln, NE] and Molecular Probes [Eugene, OR]. 5-fluoroorotic acid (5-FOA) was obtained from Thermo Scientific [Waltham,

MA]. IgG Sepharose 6 Fast Flow beads were obtained from Amersham Biosciences [Piscataway, NJ].

2.5.2 Yeast Strains and Genetic Analysis

The yeast strains that were constructed and used for this study are listed in Table 2.2. Yeast transformations were performed using the lithium acetate method [107]. For genetic analysis, at least three different spores were analyzed per experiment.

2.5.3 Plasmids and Molecular Biology

The plasmids that were constructed and used for this study are listed in Table 2.3. Sro7 charge reversal mutants were generated by site-directed mutagenesis on pB2129 (Sro7, *CEN, HIS3* plasmid). Protein A-tagged Sro7 constructs were generated as BamHI/HindIII subclones in pB966 (Protein A, 2 µ plasmid) as previously described [95]. Sro7 charge-reversal mutants were generated by site-directed mutagenesis on pB1931 (Sec4, *CEN*, *LEU2* plasmid). GST-tagged Sec4 constructs were generated as BamHI-SalI fragments in pB 2173 (pGEX-6P1 plasmid). GST-tagged Rab protein constructs were generated using genomic DNA as BamHI-SalI fragments (Ypt32, Ypt51, Ypt1, Ypt6, Ypt7, Ypt10) or BglII-SalI (Ypt11) fragments and subcloned into pB 2173 (pGEX-6P1 plasmid). Constructs were confirmed by sequencing.

2.5.4 Protein Purification

Wildtype Sro7 and Sro7 charge reversal mutant proteins were purified as previously described [95]. GST fusion proteins (Sec4, Sec4 charge reversal mutants, Ypt32, Ypt51, Ypt1, Ypt6, Ypt7, Ypt10, and Ypt11) were transformed into BL21 *Escherichia coli* and expressed as previously described [89]. Sec9 with a C-terminal His_6 tag was purified from *E. coli* as previously described [74].

2.5.5 *In Vitro* Binding Assays

In vitro binding of wildtype Sro7 and Sro7 charge reversal mutants to GST fusions of Sec9, Sec4, Sec4 mutants and the 7 Rab family proteins were performed using previously described conditions [89] with the following modifications: During nucleotide exchange, beads were incubated with 100 μM GTPγS, GDP or nucleotide free for 30 minutes at 25 degrees Celsius. Following this incubation, $MgCl_2$ was added to a final concentration of 30 mM and incubated for 1 hour at 25 degrees Celsius. Binding buffer consisted of 20 mM Tris-HCl, pH 7.4, 140 mM NaCl, 10 mM $McCl_2$, 1mM DTT and 0.5% Triton X-100. *In vitro* binding of wildtype Sro7 and Sro7 charge reversal mutants to GST-Sec9 (Full length) was performed using previously described conditions [74]. Binding percentages for all *in vitro* binding experiments were expressed as percent binding relative to wildtype Sro7 binding. P values were determined using Student's *t* test from three separate binding experiments for each protein.

2.5.6 Protein-Protein Docking Analysis

Docking simulations between Sro7 and Sec4 were performed with the automated docking server ClusPro 2.0 [108] using solved crystal structures for Sro7 [48; PDB Code 2OAJ] and for GTP-Sec4[97; PDB Code 1G17]. We did not utilize the advanced option of attractive residues to drive the complex toward the regions of interest on Sro7 and Sec4 during the ClusPro docking calculations. ClusPro results were refined complex structures based on the largest clusters of poses that represent the most likely protein-protein interactions. We analyzed the top 10 clusters for each of 4 scoring functions provided, including (1) Balanced, (2) Electrostatic-favored, (3) Hydrophobic-favored, and (4) VdW+Electrostatic. The 40 ClusPro complexes were analyzed for docking poses that placed D56 of switch I and/or E80 of switch II of GTP-Sec4 near to Sro7 residues R599/R600 and/or K395. From the 40 docking poses, the top 10 poses for each of the 4

scoring functions included 9 poses which involved both the Sec4 and Sro7 residues of interest. These 9 poses could be separated into 4 unique poses, as some poses were identified as large clusters for more than 1 scoring function. A contact analysis for residues in Sec4 within 4Å of Sro7 interface residues was calculated using PyMOL tools.

2.5.7 Tomosyn-1 and Lgl-1 Model Building

The sequences for human Tomosyn-1 and Lgl-1 were submitted to the HHpred fold recognition server (http://toolkit.tuebingen.mpg.de/hhpred). The 14 WD-repeat structure of yeast Sro7 was identified as a top hit. The models of Tomosyn-1 and Lgl-1 were built using MODELLER [109] based on the yeast Sro7 (PDB ID 2OAJ) template.

2.5.8 Sequence Analysis

Sequences for vertebrate Tomosyn-1 and for Tomosyn homologs in the Hemichordate acorn worm (*Saccoglossus kowalevskii*) and the Echinoderm purple sea urchin (*Strongylocentrotus purpuratus*) were identified using BLAST [110] and aligned in ClustalX [111-112]. A similar procedure was followed for Lgl-1 homologs in vertebrates and the higher metazoans.

2.6 Tables and Figures

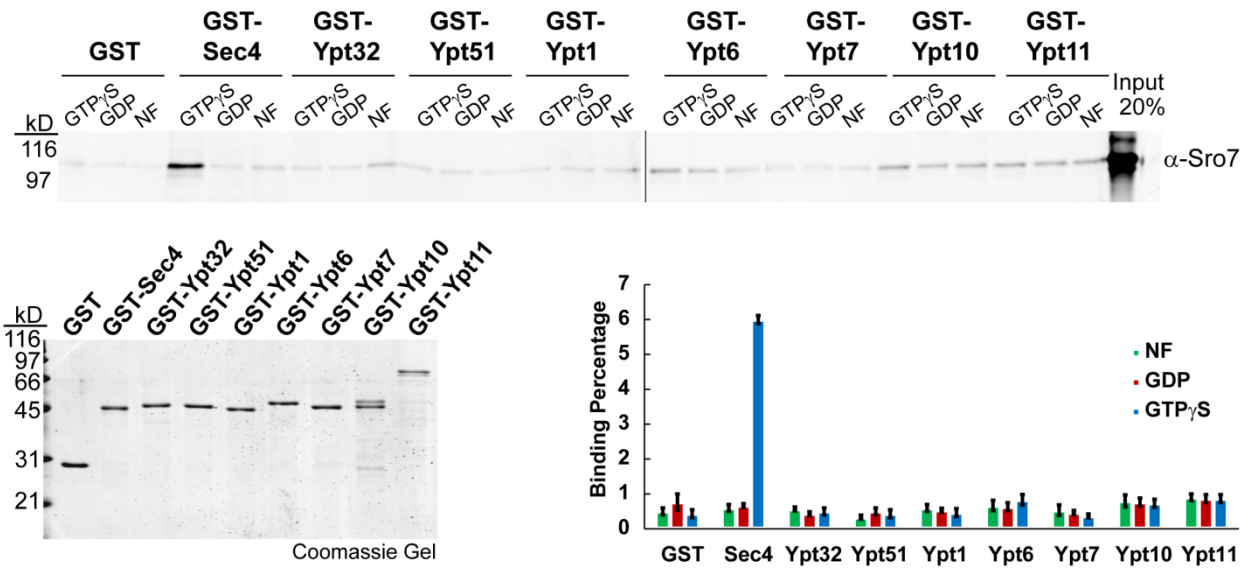

Figure 2.1 - The interaction between Sro7 and the yeast Rab GTPase Sec4 is specific and GTP-dependent.
Soluble Sro7 was tested for binding to 8 representatives of the yeast Rab GTPase family immobilized on glutathione Sepharose beads following exchange with GTPγS, GDP or no nucleotide. Coomassie gel compares the amounts of Rab GTPases used in the in vitro binding. Quantitation is based on 3 independent experiments.

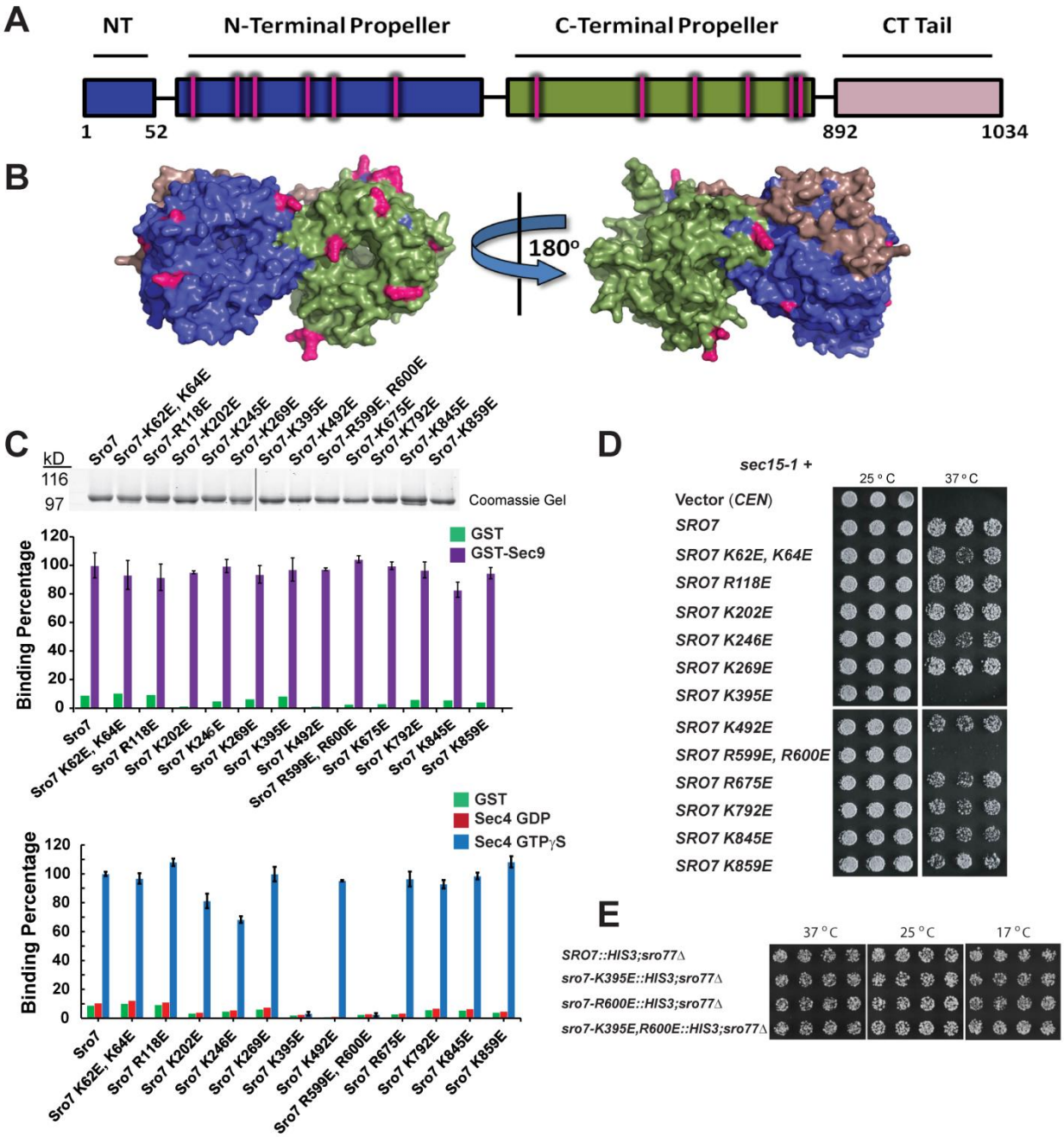

Figure 2.2 - Biochemical screen identifies two Sro7 mutants deficient in binding to Sec4-GTP.

(A) Schematic of Sro7 showing the N-terminal propeller in blue, the C-terminal propeller in green and the autoinhibitory tail in light pink. Sites of charge-reversal mutations are indicated in fuschia. (B) Surface-filling models of Sro7 showing the 12 residues subjected to mutation in fuschia. (C) Coomassie gel of purified Sro7 and the Sro7 charge-reversal mutant proteins. Quantitation of Sro7 and Sro7 mutant protein binding to GST, GST-Sec9 or GST-Sec4 previously loaded with either GTPγS or GDP. Binding was expressed as a percentage with

wildtype Sro7 binding set to 100%. Quantitation in each graph was based on 4 independent experiments. (D) The mutant strain *sec15-1* was transformed with a plasmid (*CEN*) expressing *SRO7*, the charge-reversal mutants or vector only. Three independent transformants were picked into microtiter wells and transferred to YPD media at 25 and 37 degrees Celsius. (E) Wildtype and *SRO7* mutants unable to bind Sec4 were integrated as the sole source at the *SRO7* locus. Four independent colonies were picked into microtiter wells and transferred to YPD media at 37, 25 and 17 degrees Celsius.

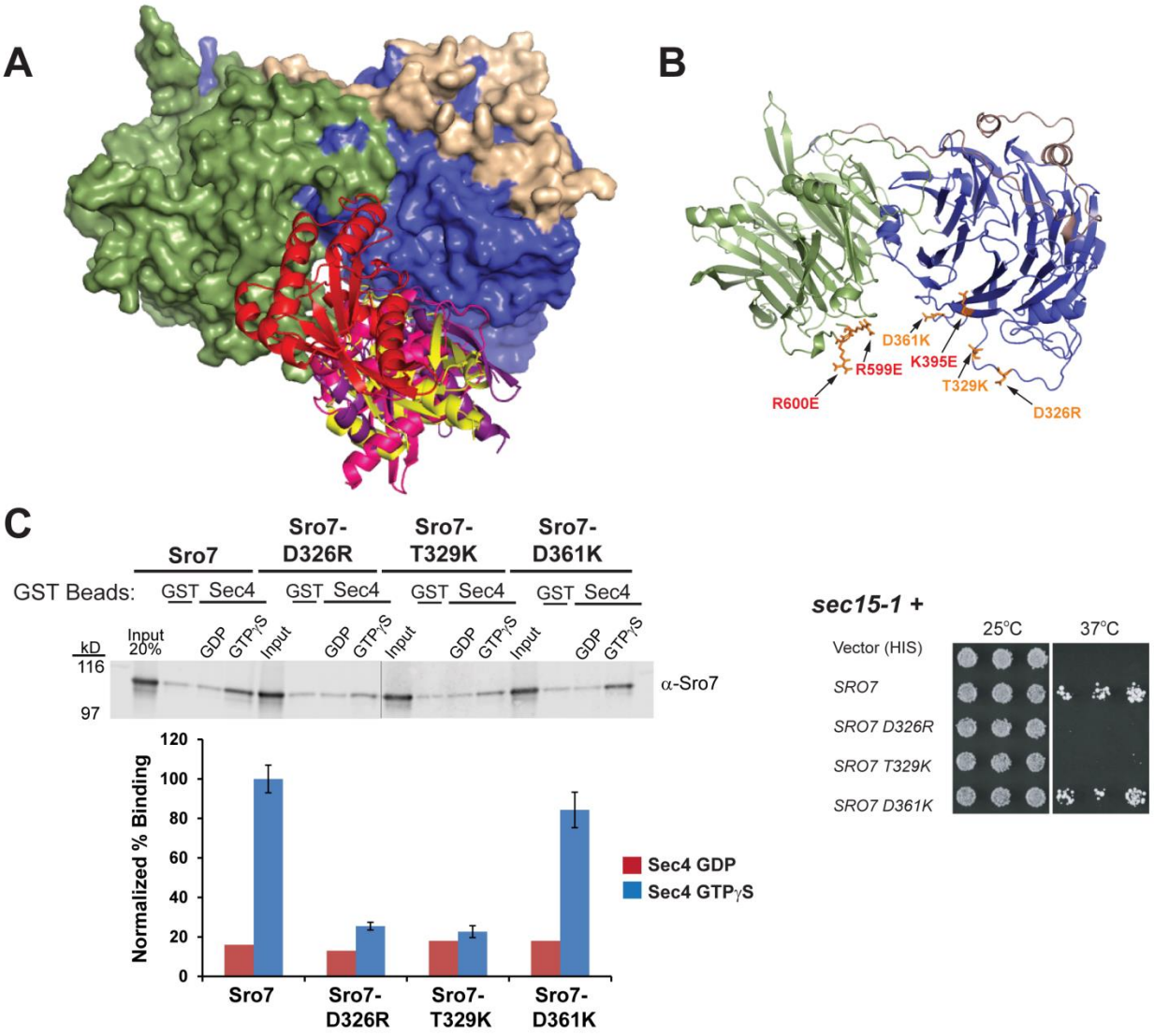

Figure 2.3 - Computational docking studies extracted interacting elements from the best scoring complexes of Sro7 and Sec4-GTP to produce four models.
(A) Surface-filling model of Sro7 with an overlay of the four Sec4 docking arrangements. The Sro7 N-terminal propeller is shown in blue, the C-terminal propeller is in green and the C-terminal tail is in light pink. The Sec4 ribbon diagrams (Models A-D) are colored in yellow, pink, red and purple, respectively. (B) Ribbon diagram of Sro7 is shown with new mutations at the Sro7-Sec4 interface marked in orange. Original mutations are marked in red. (C) Purified wildtype Sro7 or Sro7 mutants were tested for binding to GST-Sec4 following exchange with either GTPγS or GDP. Western blot and quantitation from 4 independent experiments is shown. The mutant strain *sec15-1* was transformed with a plasmid (*CEN*) expressing *SRO7*, the novel discriminatory mutants or vector only. Three independent transformants were picked into microtiter wells and transferred to YPD media at 25 and 37 degrees Celsius.

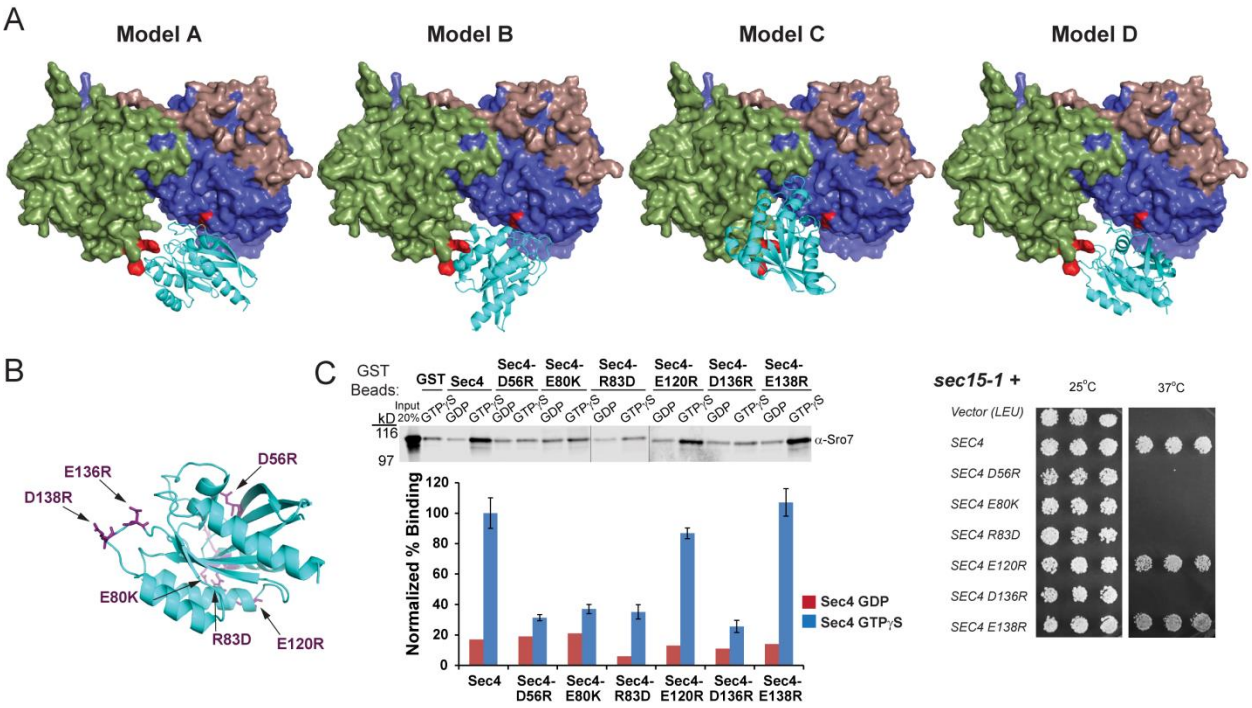

Figure 2.4 - Novel mutations in Sec4 were designed to discriminate between predicted *in silico* docking models.
(A) In the surface-filling models (A-D) of Sro7, the N-terminal propeller is shown in blue, the C-terminal propeller in green, and the C-terminal tail in light pink. The Sro7 mutations defective in binding Sec4-GTP (cyan) are shown in red. (B) Ribbon diagram of Sec4-GTP shown with discriminatory mutations in purple. (C) Wildtype Sec4 or Sec4 mutants were purified as GST fusion proteins and bound to Sro7 as previously described. Western blot of binding and quantitation from 4 independent experiments is shown. *Sec15-1* was transformed with a plasmid (*CEN*) expressing *SEC4*, the discriminatory mutants or vector only. Three independent transformants were picked into microtiter wells and transferred to YPD media at 25 and 37 degrees Celsius.

A

	Docking Model Interaction Prediction				
	Sec4 Mutants	Model A	Model B	Model C	Model D
*	D56R	+	-	+	+
*	E80K	-	-	+	+
*	R83D	-	+	-	+
	E120R	-	+	-	-
*	D136R	+	-	-	+
	E138R	+	-	+	+
	Inconsistencies:	2	3	2	0

B

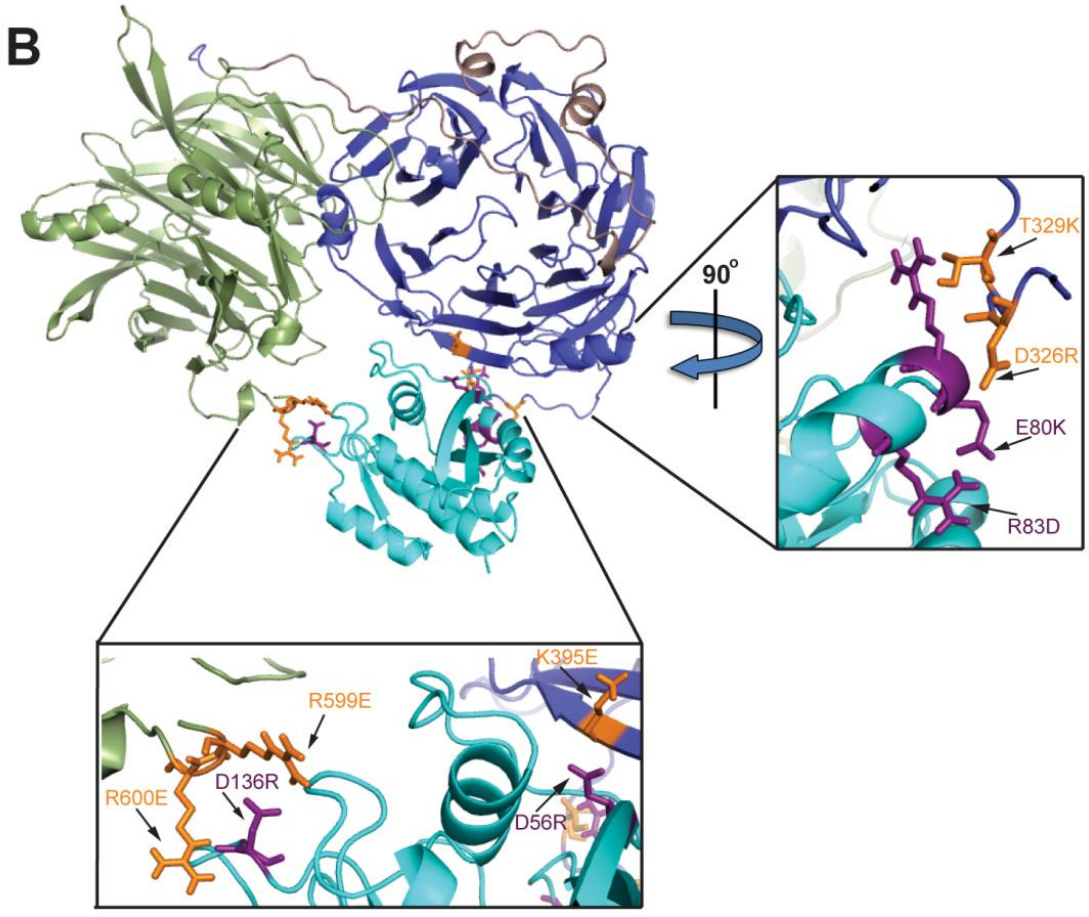

Figure 2.5 - Mutations in Sec4 predict a precise model for the docking of Sec4 onto the binding cleft of Sro7.
(A) Table of interaction predictions for Sec4 discriminatory mutations specific to each docking model based on their distance from Sro7. Distances greater than 4 Angstroms were scored as a low interaction prediction (-), while distances less than 4 Angstroms were scored as a high interaction prediction (+). Based on *in vitro* and *in vivo* characterization, mutations that affected the interaction are indicated with an asterisk. Results inconsistent with the initial interaction prediction are indicated in red. (B) Validated docking interaction between Sro7 and Sec4-GTP.

Sro7 residues involved in the interaction are shown in orange. Sec4 residues involved in the interaction are shown in purple. Insets are enlargements of docking site straight on (Inset Below) and at a 90 degree rotation (Inset Right).

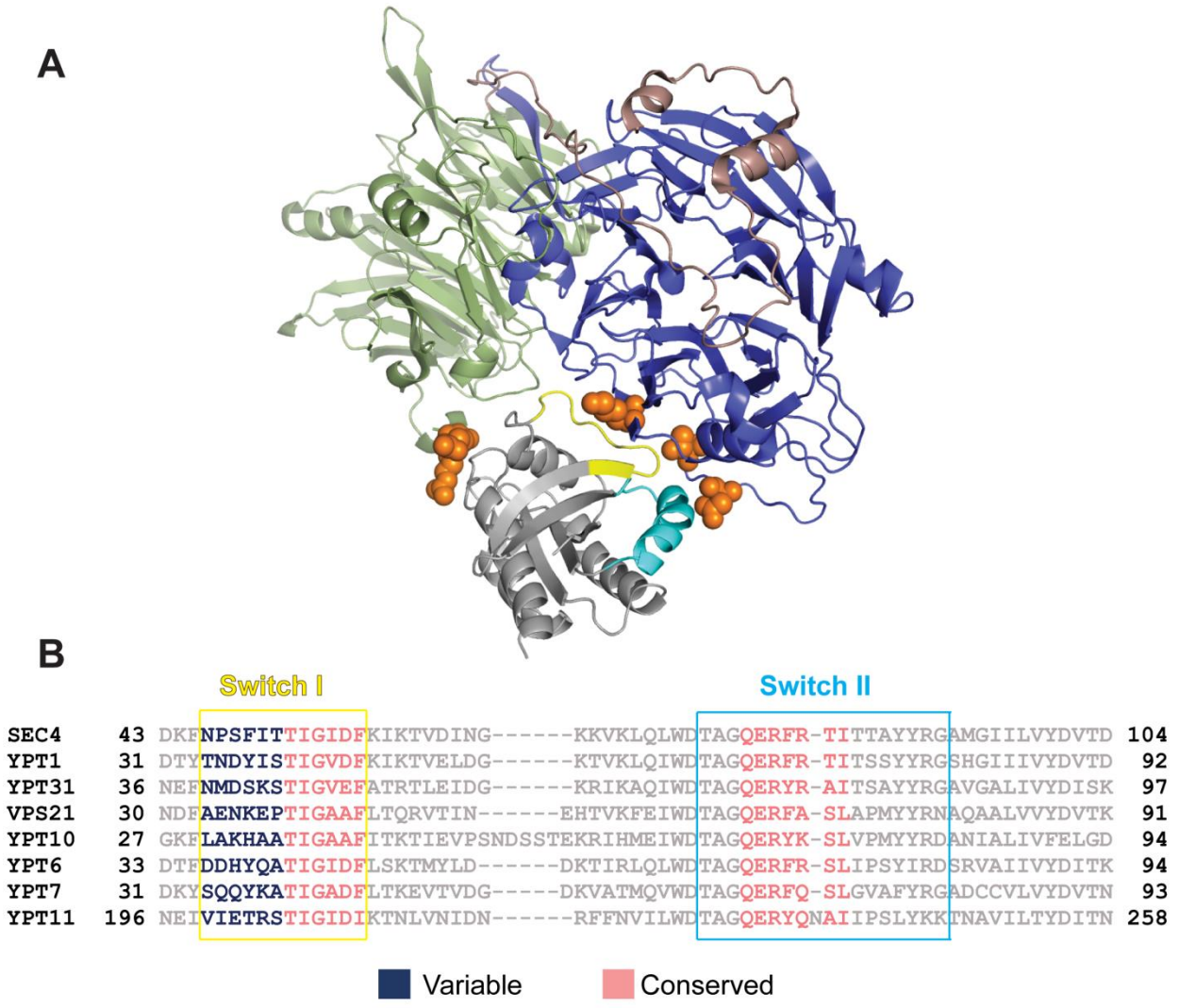

Figure 2.6 - Sec4 effector specificity for Sro7 interaction is attributed to the Sec4 N-terminal half of the Switch I domain.
(A) Crystal structure of Sro7 docked with Sec4-GTP (grey). The N-terminal propeller is blue, the C-terminal propeller is green and the autoinhibitory tail is light pink. Ribbon diagram of Sec4 is shown with the Switch I domain in yellow (residues 48-56) and the Switch II domain in cyan (residues 76-93). Sro7 residues involved in the interaction are shown in orange. (B) Multiple sequence alignments were performed using ClustalX with each of the 8 yeast Rab family member representative proteins (Ypt1, Ypt31, Vps21, Ypt10, Ypt6, Ypt7 and Ypt11). The Sec4 Switch I sequence is boxed in yellow and the Sec4 Switch II sequence is boxed in cyan. Switch domain residues within 4 Angstroms of Sro7 are highlighted as either highly variable (dark blue) or highly conserved (light red) for the 8 yeast Rab proteins.

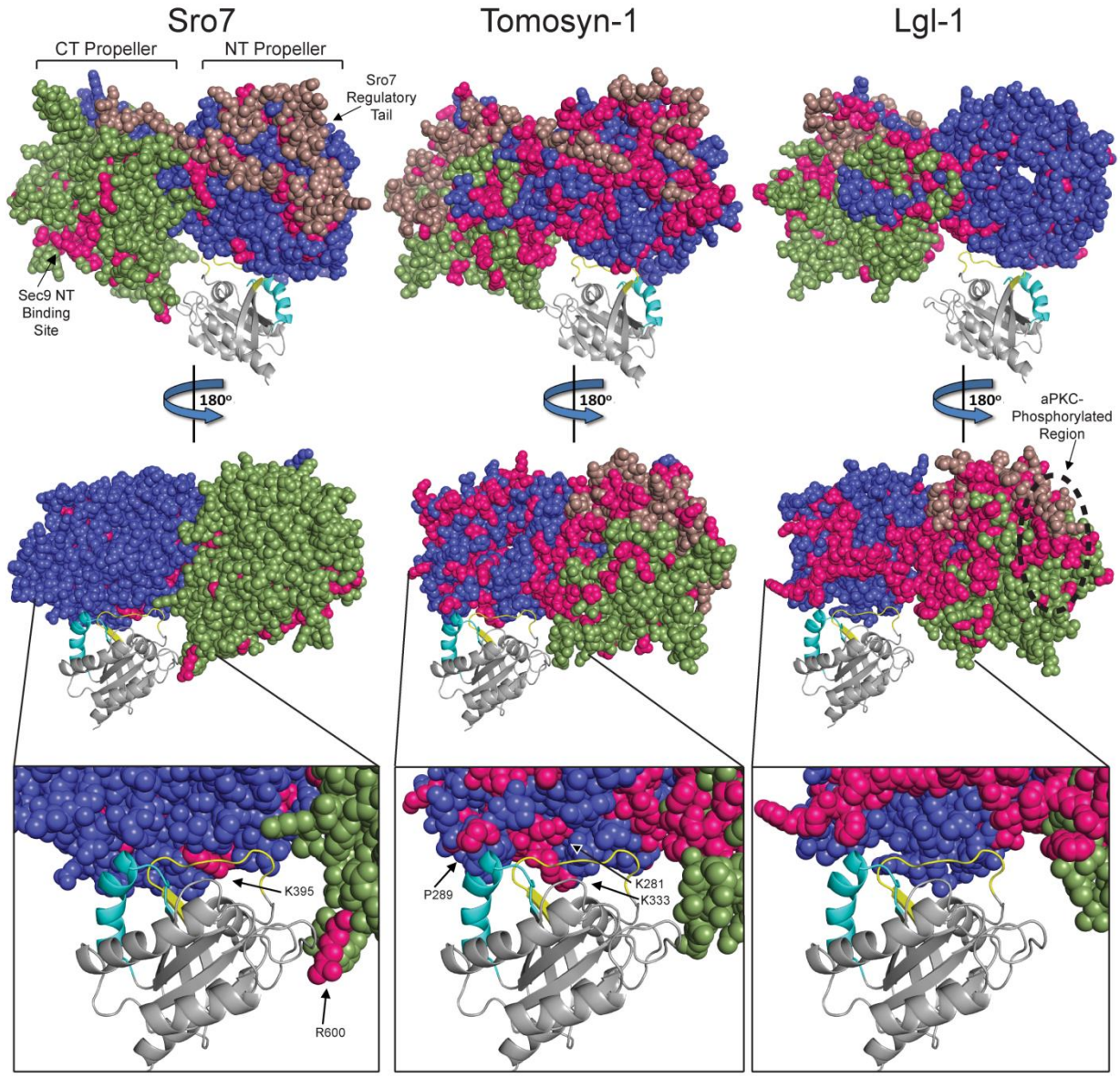

Figure 2.7 - Conservation of the Sro7-Sec4 binding interface within the Lgl family of proteins.

Crystal structure of Sro7 (left) and structural models of Tomosyn-1 (middle) and Lgl-1 (right) docked with Sec4-GTP (grey). Structural models were built with MODELLER using the crystal structure of Sro7 as a template. The Tomosyn-1 model is similar to that shown by Williams *et al.* [103] except unstructured insertions were omitted from the structural models shown. The N-terminal propeller is blue, the C-terminal propeller is green and the regulatory tail is light pink. Ribbon diagrams of Sec4 are shown with the Switch I domain in yellow and the Switch II domain in cyan. Invariant residues were identified from 3 multiple sequence alignments. One alignment was of 16 Sro7 homologs from the Saccharomycetaceae family of budding yeast, a second of 47 Tomosyn-1 vertebrate homologs, and a third of 34 Lgl-1 vertebrate homologs. Sites of invariant conserved residues are indicated in pink on corresponding structures. Structures

flipped vertically 180 degrees were also slightly rotated horizontally 30 degrees to better view the binding pocket. Insets are enlargements of homologous Sro7-Sec4 binding site straight on. The Sro7 C-terminal tail and Sec9 N-terminus binding sites are indicated in the Sro7 crystal structure (top left). Conserved Sro7 residues involved in the Sro7-Sec4 interaction are indicated in the Sro7 inset (left inset). Invariant Tomosyn-1 residues that correspond with the Sro7-K395 site are indicated in the Tomosyn-1 model (middle inset). The aPKC phosphorylated residues on Lgl are within one of the omitted unstructured insertions. This region is indicated in the Lgl-1 structural model (middle right).

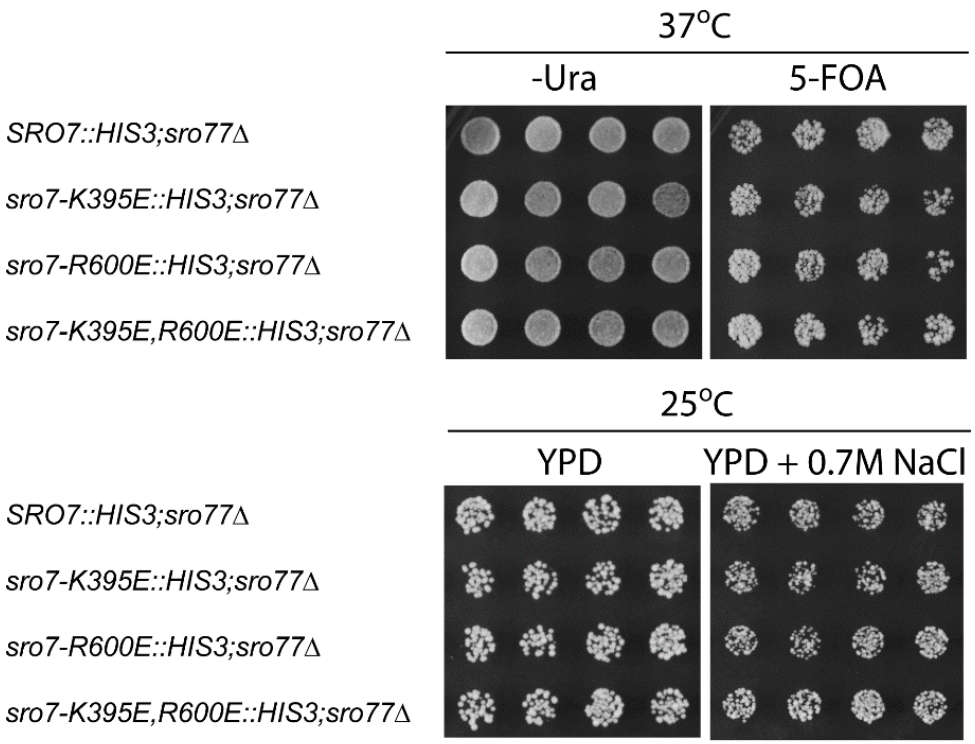

Figure 2.8 - *SRO7* alleles defective in binding to Sec4-GTP complement the salt sensitivity of *sro7Δ,sro77Δ* as **the sole source of *SRO7* in the cell**
Wildtype *SRO7, sro7-K395E, sro7-R600E* and *sro7-K395E,R600E* were integrated at the endogenous *SRO7* locus by gene replacement in the *sro7Δ ::LEU2 ;sro77Δ ::KANR* plasmid shuffle strain containing wildtype *SRO7* (*CEN, URA3*). Colonies containing the correct gene replacement (seen as His+, Leu- transformants) were transferred and grown on 5-FOA media at the permissive temperature (37°C) to select against the *SRO7* (*CEN, URA3*) plasmid. Four independent colonies were picked into microtiter wells and transferred to YPD or 0.7M NaCl at 25°C to determine growth defects.

	YPD		YPD+0.7M NaCl
	37°C	14°C	25°C
Vector (*CEN)*	+	-	-
SRO7	+	+	+
SRO7 K62E,K64E	+	+	+
SRO7 R118E	+	+	+
SRO7 K202E	+	+	+
SRO7 K246E	+	+	+
SRO7 K269E	+	+	+
SRO7 K395E	+	+	+
SRO7 K492E	+	+	+
SRO7 R599E,R600E	+	+	+
SRO7 R675E	+	+	+
SRO7 K792E	+	+	+
SRO7 K845E	+	+	+
SRO7 K859E	+	+	+
SRO7 D326R	+	+	+
SRO7 S327A,T329K	+	+	+
SRO7 D361K	+	+	+

Table 2.1 - Complementation of *sro7Δ,sro77Δ* by *SRO7* mutants used in this study
The *sro7Δ,sro77Δ* plasmid shuffle strain containing wildtype *SRO7* (*CEN, URA3*) was transformed with a plasmid (*CEN*, *HIS3*) expressing *SRO7*, *SRO7* mutants or vector only. Transformants were transferred and grown on 5-FOA media at the permissive temperature (37°C) to select against the *SRO7* (*CEN, URA3*) plasmid. Three independent transformants were then picked into microtiter wells and transferred to YPD or selective media at various temperatures to determine growth defects. Mutants were scored as (+) when growth was comparable to wildtype Sro7.

Strain	Genotype	Source
BY706	*sro7Δ::LEU2; his3-Δ200; leu2-3,112; ura3-52*	P. B. collection
BY1612	*sec15-1; his3-Δ200; ura3-52*	P. B. collection
BY2885	*sro7Δ::HIS3; pep4Δ::NAT^R; his3-Δ200; ura3-52*	P. B. collection
BY2906	*sro7Δ::HIS3; pep4Δ::NAT^R; his3-Δ200; ura3-52; SRO7* in pB966 (ProtA, 2μ, URA3)	P. B. collection
BY2971	*sro7Δ::HIS3; pep4Δ::NAT^R; his3-Δ200; ura3-52*; *SRO7-R118E* in pB966 (ProtA, 2μ, *URA3*)	This Study
BY2972	*sro7Δ::HIS3; pep4Δ::NAT^R; his3-Δ200; ura3-52*; SRO7-*K202E* in pB966 (ProtA, 2μ, *URA3)*	This Study
BY2973	*sro7Δ::HIS3; pep4Δ::NAT^R; his3-Δ200; ura3-52*; *SRO7-K246E* in pB966 (ProtA, 2μ, *URA3*)	This Study
BY2974	*sro7Δ::HIS3; pep4Δ::NAT^R; his3-Δ200; ura3-52*; *SRO7-R675E* in pB966 (ProtA, 2μ, *URA3*)	This Study
BY2998	*sro7Δ::HIS3; pep4Δ::NAT^R; his3-Δ200; ura3-52*; *SRO7-K62E,K64E* in pB966 (ProtA, 2μ, *URA3*)	This Study
BY2999	*sro7Δ::HIS3; pep4Δ::NAT^R; his3-Δ200; ura3-52*; *SRO7-K395E* in pB966 (ProtA, 2μ, *URA3*)	This Study
BY3000	*sro7Δ::HIS3; pep4Δ::NAT^R; his3-Δ200; ura3-52*; *SRO7-K859E* in pB966 (ProtA, 2μ, *URA3*)	This Study
BY3001	*sro7Δ::HIS3; pep4Δ::NAT^R; his3-Δ200; ura3-52*; *SRO7-K792E* in pB966 (ProtA, 2μ, *URA3*)	This Study
BY3012	*sro7Δ::HIS3; pep4Δ::NAT^R; his3-Δ200; ura3-52*; *SRO7-K269E* in pB966 (ProtA, 2μ, *URA3*)	This Study
BY3016	*sro7Δ::HIS3; pep4Δ::NAT^R; his3-Δ200; ura3-52*; *SRO7-K492E* in pB966 (ProtA, 2μ, *URA3*)	This Study
BY3018	*sro7Δ::HIS3; pep4Δ::NAT^R; his3-Δ200; ura3-52*; *SRO7-K845E* in pB966 (ProtA, 2μ, *URA3*)	This Study
BY3019	*sro7Δ::HIS3; pep4Δ::NAT^R; his3-Δ200; ura3-52*; *SRO7-R599E,R600E* in pB966 (ProtA, 2μ, *URA3*)	This Study
BY3061	*sec15-1; leu2-3,112; his3-Δ200; ura3-52*; *SRO7* in pRS316 (*CEN, URA3*)	This Study
BY3073	*sro7Δ::LEU2; his3-Δ200; leu2-3,112; ura3-52*	This Study
BY3090	*sro7Δ::LEU2; his3-Δ200; leu2-3,112; ura3-52; sec15-1*; *SRO7* in pRS316 (*CEN, URA3*)	This Study
BY3105	*sro7Δ::LEU2; sro77Δ::KAN^R; his3-Δ200; leu2-3,112; ura3-52*; *SRO7* in pRS316 (*CEN, URA3*)	This Study
BY3109	*sec4Δ::KAN^R; his3-Δ200; ura3-52; leu2-3,112; SEC4* in pRS316 (*CEN, URA3*)	This Study
BY3112	*sec4Δ::KAN^R; his3-Δ200; ura3-52; leu2-3,112*; pRS315 (*CEN, LEU2*)	This Study
BY3113	*sec4Δ::KAN^R; his3-Δ200; ura3-52; leu2-3,112*; *SEC4* in pRS315 (*CEN, LEU2*)	This Study
BY3114	*sec4Δ::KAN^R; his3-Δ200; ura3-52; leu2-3,112*; *SEC4-D56R* in pRS315 (*CEN, LEU2*)	This Study
BY3115	*sec4Δ::KAN^R; his3-Δ200; ura3-52; leu2-3,112*; *SEC4-E80K* in pRS315 (*CEN, LEU2*)	This Study
BY3116	*sec4Δ::KAN^R; his3-Δ200; ura3-52; leu2-3,112*; *SEC4-E120R* in pRS315 (*CEN, LEU2*)	This Study
BY3117	*sec4Δ::KAN^R; his3-Δ200; ura3-52; leu2-3,112*; *SEC4-D136R* in pRS315 (*CEN, LEU2*)	This Study
BY3124	*sro7Δ::HIS3; pep4Δ::NAT^R; ura3-52; his3-Δ200*; *SRO7-R600E* in pB966 (ProtA, 2μ, *URA3*)	This Study
BY3136	*sro7Δ::HIS3; pep4Δ::NAT^R; ura3-52; his3-Δ200*; *SRO7-R599E* in pB966 (ProtA, 2μ, *URA3*)	This Study
BY3138	*sro7Δ::HIS3; pep4Δ::NAT^R; ura3-52; his3-Δ200*; *SRO7-S327A,T329K* in pB966 (ProtA, 2μ, *URA3*)	This Study

BY3139	*sro7Δ::HIS3; pep4Δ::NAT^R; ura3-52; his3-Δ200*; *SRO7-D361K* in pB966 (ProtA, 2µ, *URA3*)	This Study
BY3140	*sro7Δ::HIS3; pep4Δ::NAT^R; ura3-52; his3-Δ200*; *SRO7-D326R* in pB966 (ProtA, 2µ, *URA3*)	This Study
BY3166	*sro7Δ::LEU2; sro77Δ::NAT^R*; *sec15-1; ura3-52; leu2-3,112; his3-Δ200*; *SRO7* (*CEN, URA3*)	This Study
BY3167	*sro7Δ::LEU2; sro77Δ::NAT^R*; *sec15-1; ura3-52; leu2-3,112; his3-Δ200*; *SRO7* (*CEN, HIS3*)	This Study
BY3168	*sro7Δ::LEU2; sro77Δ::NAT^R*; *sec15-1; ura3-52; leu2-3,112; his3-Δ200*; *SRO7-K395E* (*CEN, HIS3*)	This Study
BY3169	*sro7Δ::LEU2; sro77Δ::NAT^R*; *sec15-1; ura3-52; leu2-3,112; his3-Δ200*; *SRO7-R600E* (*CEN, HIS3*)	This Study
BY3178	*SRO7:: HIS3; sro77Δ:: KAN^R*; *ura3-52; his3-Δ200*	This Study
BY3179	*sro7-K395E:: HIS3; sro77Δ:: KAN^R*; *ura3-52; his3-Δ200*	This Study
BY3180	*sro7-R600E:: HIS3; sro77Δ:: KAN^R; ura3-52; his3-Δ200*	This Study
BY3181	*sro7-K395E,R600E:: HIS3; sro77Δ:: KAN^R*; *ura3-52; his3-Δ200*	This Study

Table 2.2 - Yeast strains used in this study.

Plasmid	Host	Description	Source
pB38	DH5α	*GAL1* Promoter in pRS313 (*CEN, HIS3)*	P.B. collection
pB39	DH5α	*GAL1* Promoter with *ADH1* Terminator in pRS313	P.B. collection
pB331	DH5α	pRS316 (*CEN, URA3)*	P.B. collection
pB844	DH5α	pRS315 (*CEN, LEU2)*	P.B. collection
pB966	DH5α	*ADH1* Promoter with ProtA-TEV tag in pRS426 (2μ, *URA3)*	P.B. collection
pB1331	DH5α	pRS313 (*CEN, HIS3)*	P.B. collection
pB1931	DH5α	*SEC4* in pB844 (*CEN, LEU2*)	P.B. collection
pB2042	DH5α	*YPT32* in pGEX6P-1	This Study
pB2043	DH5α	*YPT51* in pGEX6P-1	This Study
pB2044	DH5α	*YPT1* in pGEX6P-1	This Study
pB2045	BL21	*YPT32* in pGEX6P-1	This Study
pB2046	BL21	*YPT51* in pGEX6P-1	This Study
pB2047	BL21	*YPT1* in pGEX6P-1	This Study
pB2104	DH5α	*SRO7-K492E* in pB1331 (*CEN, HIS3*)	This Study
pB2105	DH5α	*SRO7-K845E* in pB1331 (*CEN, HIS3*)	This Study
pB2107	DH5α	*SRO7-R599E,R600E* in pB1331 (*CEN, HIS3*)	This Study
pB2108	DH5α	*SRO7-R118E* in pB1331 (*CEN, HIS3*)	This Study
pB2109	DH5α	*SRO7-R202E* in pB1331 (*CEN, HIS3*)	This Study
pB2110	DH5α	*SRO7-K246E* in pB1331 (*CEN, HIS3*)	This Study
pB2111	DH5α	*SRO7-R675E* in pB1331 (*CEN, HIS3*)	This Study
pB2112	DH5α	*SRO7-K62E,K64E* in pB1331 (*CEN, HIS3*)	This Study
pB2113	DH5α	*SRO7-K395E* in pB1331 (*CEN, HIS3*)	This Study
pB2114	DH5α	*SRO7-K801E* in pB1331 (*CEN, HIS3*)	This Study
pB2115	DH5α	*SRO7-K859E* in pB1331 (*CEN, HIS3*)	This Study
pB2116	DH5α	*SRO7-K792E* in pB1331 (*CEN, HIS3*)	This Study
pB2117	DH5α	*SRO7-K492E* in pB966	This Study
pB2118	DH5α	*SRO7-K845E* in pB966	This Study
pB2120	DH5α	*SRO7-R599E,R600E* in pB966	This Study
pB2121	DH5α	*SRO7-R118E* in pB966	This Study
pB2122	DH5α	*SRO7-K202E* in pB966	This Study

pB2123	DH5α	*SRO7-K246E* in pB966	This Study
pB2124	DH5α	*SRO7-R675E* in pB966	This Study
pB2125	DH5α	*SRO7-K62E,K64E* in pB966	This Study
pB2126	DH5α	*SRO7-K859E* in pB966	This Study
pB2127	DH5α	SRO7-K792E in pB966	This Study
pB2128	DH5α	*SRO7-K395E* in pB966	This Study
pB2129	DH5α	*SRO7* in pB1331 (*CEN, HIS3*)	This Study
pB2159	DH5α	*SEC4-D56R* in pGEX 6P-1	This Study
pB2161	DH5α	*SEC4-E80K* in pGEX 6P-1	This Study
pB2163	DH5α	*SEC4* in pGEX 6P-1	This Study
pB2167	DH5α	*SEC4-E80K* in pB844 (*CEN, LEU2*)	This Study
pB2169	DH5α	*SEC4-D56R* in pB844 (*CEN, LEU2*)	This Study
pB2175	BL21	*SEC4-D56R* in pGEX 6P-1	This Study
pB2177	BL21	*SEC4-E80K* in pGEX 6P-1	This Study
pB2187	DH5α	*SRO7-K269E* in pB1331 (*CEN, HIS3*)	This Study
pB2188	DH5α	*SRO7-K269E* in pB966	This Study
pB2195	DH5α	*SRO7* in pB331 (*CEN, URA3)* (No BamHI site)	This Study
pB2216	BL21	*SEC4-E120R* in pGEX 6P-1	This Study
pB2217	BL21	*SEC4-D136R* in pGEX 6P-1	This Study
pB2218	BL21	*SEC4-E138R* in pGEX 6P-1	This Study
pB2220	BL21	*SEC4-R83D* in pGEX 6P-1	This Study
pB2230	DH5α	*SRO7-R599E* in pB966	This Study
pB2231	DH5α	*SRO7-R600E* in pB966	This Study
pB2236	DH5α	*SRO7-D326R* in pB1331 (*CEN, HIS3*)	This Study
pB2237	DH5α	*SRO7- S327A,T329K* in pB1331 (*CEN, HIS3*)	This Study
pB2239	DH5α	*SRO7-D361K* in pB1331 (*CEN, HIS3*)	This Study
pB2240	DH5α	*SRO7-R599E* in pB1331 (*CEN, HIS3*)	This Study
pB2241	DH5α	*SRO7-R600E* in pB1331 (*CEN, HIS3*)	This Study

Table 2.3 - Plasmids used in this study.

CHAPTER 3

In Vitro Reconstitution of Rab GTPase-dependent Vesicle Clustering by the Yeast Lethal Giant Larvae/Tomosyn Homolog, Sro7[2]

3.1 Overview

Intracellular traffic in yeast between the Golgi and the cell surface is mediated by vesicular carriers that tether and fuse in a fashion that depends on the function of the Rab GTPase, Sec4. Overexpression of either of two Sec4 effectors, Sro7 or Sec15, results in the formation of a cluster of post-Golgi vesicles within the cell. Here, we describe a novel assay that recapitulates post-Golgi vesicle clustering *in vitro* utilizing purified Sro7 and vesicles isolated from late secretory mutants. We show clustering *in vitro* closely replicates the *in vivo* clustering process as it is highly dependent on both Sro7 and GTP-Sec4. We also make use of this assay to characterize a novel mutant form of Sro7 that results in a protein that is specifically defective in vesicle clustering both *in vivo* and *in vitro*. We show that this mutation acts by effecting a conformational change in Sro7 from the closed to a more open structure. Our analysis demonstrates that the N-terminal propeller needs to be able to engage the C-terminal tail for vesicle clustering to occur. Consistent with this, we show that occupancy of the N terminus of Sro7 by the t-SNARE Sec9, which results in the open conformation of Sro7, also acts to inhibit vesicle cluster formation by Sro7. This suggests a model by which a conformational switch in Sro7 acts to coordinate Rab-mediated vesicle tethering with SNARE assembly by requiring a single conformational state for both of these processes to occur.

[2] Reproduced from *The Journal of Biological Chemistry*, 2015 Jan 2; 290(1):612-24.

3.2 Introduction

We identified Sro7, the yeast member of the conserved family of Lgl proteins, in a screen for binding partners of the plasma membrane t-SNARE Sec9 [47]. Loss of Sro7 and its redundant paralog Sro77 results in both cold-sensitive growth and a severe secretory defect in post-Golgi vesicle tethering/fusion with the plasma membrane [47]. Importantly, Sro7 has been suggested to function as a direct effector of the GTPase Sec4 in a pathway that genetically appears to be parallel to that of the other effector of Sec4, the exocyst tethering complex [89]. Although Sro7 has been found to interact with several components of the exocytic tethering and fusion apparatus [47, 87, 113], the precise molecular mechanism by which it functions in this process remains elusive. Structural analysis has shown that Sro7 is composed of two interlocking β-propellers with a long C-terminal tail that binds back to the N-terminal propeller in an autoinhibitory mode. The region bound by the tail was shown to overlap with the binding site of the plasma membrane t-SNARE Sec9 in a way that suggested the possibility of a "triggered" release of the SNARE by Sro7 [48]. Although the Sec4 GTPase remained an attractive candidate triggering factor, its association with Sro7 had previously been shown to have no effect on Sro7's association with Sec9 [89]. Therefore, the precise role of Sro7 as an effector of the Rab GTPase Sec4 remains elusive.

Overexpression of Sro7 in the cell results in the accumulation of a large cluster of post-Golgi vesicles and cell lethality [113]. This observation was similar to that seen for another effector of the Sec4 GTPase, the Sec15 subunit of the exocyst tethering complex [114]. *In vivo* analysis of the vesicle clustering phenotype showed that clustering and cell lethality by both Sec15 and Sro7 depend on Sec4 function but are independent of the Sec9 t-SNARE [113-114].

In the case of Sro7, vesicle clustering also depends upon the interaction between Sro7 and the type V myosin Myo2[113].

In this study, we establish an *in vitro* assay that recapitulates the Sro7-mediated clustering we observed previously *in vivo*. Development of such an assay allows us to begin to biochemically dissect Rab GTPase and Rab effector function in parallel to our *in vivo* genetic analyses. We made use of this assay to analyze the effects of Sro7 mutants in which conserved charged patches on Sro7 were mutated to the reverse charge. We found that one of the charge reversal mutant proteins, Sro7-R189D,R222D, had a specific defect in clustering vesicles both *in vivo* and *in vitro*. Further analysis of this defect demonstrated a role for the "closed" conformation of the C-terminal autoinhibitory tail in vesicle clustering. This suggests a novel function for the conformational switch in Sro7 in coordinating Rab-dependent membrane tethering with regulation of SNARE assembly prior to membrane fusion.

3.3 Results

3.3.1 Sro7-dependent Vesicle Clustering *in Vitro* Requires Magnesium Chloride and Is Potentiated by GTPγS

We have previously shown that overexpression of *SRO7* behind a *GAL1/10* promoter results in a pronounced growth defect and the formation of a large cluster of post-Golgi vesicles within the cell [113]. Importantly, this clustering is dependent on GTP-Sec4 as mutations in *SEC4* and the gene encoding its exchange factor *SEC2* prevent clustering of vesicles when Sro7 is overexpressed [10, 113]. To further explore how Sro7 mediates vesicle clustering, we sought to determine whether we could recapitulate this process *in vitro* utilizing isolated post-Golgi vesicles and purified Sro7 protein. Sro7 was purified from yeast by a modification of a previous protocol used in the laboratory [89], and post-Golgi secretory vesicles were isolated from a *sec6*-

4 mutant strain that accumulates a large number of vesicles following a shift to the restricted temperature of 37 °C [1, 115]. To visualize vesicles in the assay, they were fluorescently labeled by two methods. In the first method, vesicles were labeled *in vivo* by expression of GFP-Sec4 in a *sec6-4* strain, and Sec4 is a well recognized marker of post-Golgi secretory vesicles [9]. In the second method, vesicles were labeled *in vitro* with the lipid dye FM4-64 during the vesicle isolation procedure. In both cases, post-Golgi vesicles were isolated by cell fractionation following a shift of the mutant *sec6-4* strain to the restrictive temperature.

To determine whether we could reconstitute Sro7-mediated vesicle clustering *in vitro*, fluorescently labeled vesicle fractions were incubated with increasing amounts of purified Sro7 under a number of different conditions. Following a 20-min incubation at room temperature, an aliquot of each condition was analyzed by fluorescence microscopy. Clustering appeared as the formation of fluorescently labeled puncta that were observed using either FITC (GFP-Sec4-labeled vesicles) or TRITC (for FM4-64 labeled vesicles) filter sets. Note individual post-Golgi vesicles (80–100 nm) were too small to be visualized by conventional fluorescence microscopy. When purified Sro7 was added to vesicles in buffer containing GTPγS and magnesium, large puncta formed that were visible by both FITC and TRITC channels (Figure 3.1A). The appearance of large puncta depended on the presence of Sro7, magnesium, and GTPγS. In the absence of either magnesium or Sro7, no puncta formed. Similarly, when BSA or IgG was added in place of Sro7 (at equivalent amounts), no clustering was observed (data not shown). When Sro7 and magnesium were present with GDP in place of GTPγS or no added nucleotide was present, then only small puncta formed (Figure 3.1A). Finally, we found that the clustering was dependent on both time and the dose of Sro7, as the size of puncta increased with time and with increasing amounts of Sro7 added (data not shown). Routine assays were done with the addition

of Sro7 to 1 μm incubated with vesicles for 20 min at 27 °C. Clustering activity was quantitated by counting the number of small (greater than 1 μm but less than 2 μm) and larger (>2 μm) clusters formed per 1 μl of assay mix (Figure 3.1B).

3.3.2 GTP-bound Sec4 Is Required for Sro7-mediated Vesicle Clustering *in Vitro*

To determine whether the *in vitro* clustering was also dependent on Sec4, we prepared FM4-64 labeled secretory vesicles from a number of late secretory mutants (*sec6-4*, *sec4-8*, *sec1-1*, and *sec9-4*) and examined the ability of purified Sro7 to induce vesicle clustering under the conditions described above. To ensure we had similar numbers of vesicles present from each mutant strain, we used immunoblots of the vesicle fractions used in this assay to monitor levels of three vesicle markers Sec4, the v-SNARE, Snc1/2, and the t-SNARE, Sso1/2 (which transits to the plasma membrane on post-Golgi vesicles). As expected, the vesicles from *sec4-8* have only a small amount of a form of Sec4 with altered mobility on SDS-PAGE [9] but have similar amounts of Snc1/2 and Sso1/2 when compared with the other three mutants (Figure 3.1D). When these four vesicle preparations were incubated with Sro7 under the conditions described above, robust clustering was observed for *sec6-4*, *sec1-1*, and *sec9-4* vesicle fractions, but only low levels of small puncta were observed for the *sec4-8* vesicle fraction (Figure 3.1C). The clustering activity of Sro7 was dose-dependent (Figure 3.1E). Therefore, similar to the *in vivo* clustering, the *in vitro* clustering reaction was dramatically impeded with otherwise equivalent vesicles isolated from a *sec4-8* mutant strain.

To further rule out a role for SNARE proteins in Sro7-mediated vesicle clustering, we prepared vesicles from strains deficient in either Snc1/2 or Sso1/2[25, 116]. Using post-Golgi vesicles isolated from a strain where the sole source of Snc1 was under control of the *GAL1/10* promoter, we found that clustering activity was unaffected, although the amounts of Snc1 on the

vesicles were virtually undetectable (Figure 3.2A). Likewise, when vesicles were isolated from the temperature-sensitive *sso1*Δ,*sso2-1* strain, we found Sro7-mediated clustering to be indistinguishable from that seen with vesicles from a *sec6-4* strain (Figure 3.2B). Taken together with the results from the *sec9-4* strain, it is clear that post-Golgi SNARE function was not required for Sro7-mediated vesicle clustering.

The assay described above makes use of a high speed pellet fraction produced from differential centrifugation as a highly enriched source of post-Golgi vesicles [115]. To determine whether purified post-Golgi vesicles are active in Sro7-mediated clustering, we subjected the FM4-64-labeled vesicle-enriched fraction to velocity sedimentation on sorbitol gradients [24]. Vesicle purification was performed in parallel on both *sec6-4* and *sec4-8* mutant strains and examined under conditions identical to those described above, except that clustering reactions were allowed to incubate for 60 rather than 20 min to achieve similar levels of clustering as monitored by fluorescence microscopy (Figure 3.3, A and B). The use of velocity gradient-purified vesicles of homogeneous size also allowed us to examine the clustering reactions by negative stain electron microscopy. The results, shown in Figure 3.3C, demonstrate that Sro7 induces clustering, but not fusion, of purified 80–100-nm post-Golgi vesicles and that this clustering depends on both GTPγS and Sec4 function. Both Western blot quantitation of Snc1/2 levels and negative stain analysis of the purified vesicles demonstrate that equivalent numbers of *sec6-4* and *sec4-8* vesicles were used in this analysis (Figure 3.3, C and D). Importantly, the quantification of vesicle clustering observed by electron microscopy is remarkably similar to the data obtained by quantification of the clustering reaction by fluorescence microscopy, indicating that both methods of visualizing clustering are indeed measuring the same event.

The Sec4 GTPase can cycle on and off membranes in a manner that is dependent on the nucleotide state of the Rab and its interaction with GDI [117]. To determine whether the absence of clustering seen with the *sec4-8* secretory vesicles correlated with a loss of Sec4 function and not with an indirect defect in the *sec4-8* mutation on the functionality of the vesicles, we made use of purified recombinant Rab GDI to extract Rab GTPases from the vesicles. Secretory vesicle-enriched fractions were generated from *sec6-4*, pretreated with GDP, and followed by either extraction with recombinant Rab GDI or mock-treated with buffer only before further purification on sorbitol gradients. Treatment with Rab GDI resulted in the removal of nearly ⅔ of the Sec4 from vesicles (Figure 3.4C). The vesicles were then used in the *in vitro* clustering assay with Sro7, magnesium chloride, and GTPγS. Although overall clustering was slightly reduced following the more extensive incubations necessary for GDI extraction (compare quantitation in Figure 3.3B to 3.4B), the observed clustering in the mock-treated vesicles was dependent on Sro7. Importantly, the results shown in Figure 3.4, *A* and *B*, demonstrate that GDI treatment of the secretory vesicles results in a dramatic loss of the clustering potential of the purified vesicles.

Rab GDI is known to have high specificity for Rab GTPases [118]; however, yeast post-Golgi vesicles are known to contain several other Rab GTPases, including Ypt31 and Ypt1, which could be responsible for the GDI-mediated inhibition in the assay [94, 119-120]. Therefore, to determine whether Sec4 is the relevant Rab in this assay, we made use of a monoclonal antibody specific to Sec4 [121] as a functional probe for Sec4 function *in vitro*. We treated *sec6-4* vesicles in a high speed pellet vesicle fraction with two different doses of either anti-Sec4 mAb or an identical amount of a control mAb. Both antibodies were purified and used at identical concentrations in the assay by preincubating them with vesicles for 1 h on ice prior to

use in the clustering assay. The results in Figure 3.4D show that vesicles treated with the anti-Sec4 monoclonal antibody, but not those treated with the control antibody, demonstrated a pronounced dose-dependent inhibition of clustering. Taken together with the data obtained with *sec4-8* vesicles and Rab GDI extraction studies, this result provides strong evidence that Sec4 on the surface of the post-Golgi vesicles is critical for Sro7-mediated vesicle clustering.

3.3.3 Novel Mutant, Sro7-R189D,R222D, Fails to Cluster Post-Golgi Vesicles *in Vivo* and *in Vitro*

To identify elements within Sro7 that are important for vesicle tethering, we carried out a small pilot screen of site-specific mutations in conserved surface patches and examined their effect on Sro7-mediated vesicle clustering *in vivo* and *in vitro*. Reverse charge mutagenesis of four conserved surface "patches" of charged amino acids resulted in four new mutants shown in Figure 3.5A. All four mutants were fully functional as the only copy of Sro7 in the cell when expressed behind the endogenous Sro7 promoter (data not shown). As a first attempt to determine whether any of these mutants affect post-Golgi vesicle clustering, we introduced each allele into a *GAL1/10* expression plasmid and examined the growth effects following induction on galactose-containing media. As we have previously shown, *GAL* overexpression of wild type *SRO7* results in a significant growth defect in wild type strains [113]. Although three of the four charge reversal mutants demonstrated pronounced growth defects, one of the mutants, *sro7-R189D,R222D* (abbreviated as *sro7-D189,D222*), did not cause cell lethality when overexpressed in wild type or a more sensitive *sec* mutant strain, *sec15-1,* in which exocyst function is compromised (Figure 3.5B). To understand the biological basis for the loss of growth inhibition, we determined the effect of the expression of this allele on post-Golgi vesicle clustering by immunofluorescence microscopy. As we have observed previously, *GAL* induction

of *SRO7* results in large puncta of Sec4- and Sro7-positive structures that correspond to clusters of 80–100-nm vesicles by thin section electron microscopy (Figure 3.5C) [113]. In contrast, when we induced expression of *sro7-D189,D222*, no puncta were observed by either Sec4 or Sro7 staining. Moreover, the normally highly polarized staining of Sec4 appeared to be replaced often by a much more diffuse staining pattern, although there is no effect on growth under these conditions (Figure 3.5C).

To compare the clustering activity of the *sro7-D189,D222* mutant *in vitro* to the *in vivo* results described above, we purified the mutant protein to homogeneity and examined its ability to promote clustering in our assay. Although the mutant protein shows no detectable effect on binding to GTP-Sec4 (Figure 3.6B), it completely fails to stimulate vesicle clustering of both FM4-64-labeled (Figure 3.6A) or GFP-Sec4-labeled vesicles (data not shown) isolated from *sec6-4* strains. Furthermore, the clustering defect cannot be ascribed to a defect in the interaction with Myo2 [74] or Exo84 [87] because we find binding of the purified Sro7-D189,D222 protein to recombinant forms of Myo2 and Exo84 is indistinguishable from that of the wild type Sro7 protein (Figure 3.6C).

Examination of the arginine residues at positions 189 and 222 in the Sro7 crystal structure indicates that these residues, which lie on the surface of the N-terminal β-propeller, play an important role in the interaction with the C-terminal autoinhibitory tail (Figure 3.5A). The autoinhibitory tail is thought to regulate interaction of Sro7 with the Qbc-SNARE domain of the plasma membrane t-SNARE, Sec9 [48]. To test the idea that the effect of the Asp-189 and Asp-222 mutations on clustering is through loss of the autoinhibitory interaction of the C-terminal domain with the propeller, we generated an additional set of mutations (N914K and S942F) in the C-terminal tail, which form strong hydrogen bond interactions with the two

arginine residues on the N-terminal propeller (Figure 3.7A). To test the structural prediction that the autoinhibitory tail would be in a more "open" conformation in both the Sro7-D189,D222 and Sro7-K914,F942 mutant proteins, we examined their ability to bind the Sec9-Qbc domain fused to GST. The results, shown in Figure 3.7B, demonstrate that both of these mutant proteins show significantly improved binding to GST-Sec9Qbc compared with equivalent quantities of wild type Sro7.

To determine whether the *sro7-K914,F942* mutant, like the *sro7-D189,D222* mutant, suppresses the vesicle clustering phenotype *in vivo*, we expressed this mutant behind the *GAL* promoter. The results in Figure 3.7C show that this new allele, like the *sro7-D189,D222*, prevents the galactose-dependent inhibition of growth. Importantly, we also find that *GAL* induction of this allele prevents formation of the large Sec4 positive vesicle clusters seen with wild type Sro7 (Figure 3.7D). Finally, we determined whether the purified Sro7-K914,F942 protein had reduced activity in the *in vitro* vesicle clustering assay by comparing it with the wild type Sro7 and the Sro7-D189,D222 mutant. The results in Figure 3.8A demonstrate that the two mutant forms of Sro7 are completely inactive for *in vitro* vesicle clustering, despite the fact they show normal binding to Myo2, Exo84, and enhanced binding to Sec9-Qbc.

These data strongly suggest that the closed form of Sro7, where the C-terminal autoinhibitory tail is engaged with the N-terminal propeller, is most active in Rab-dependent vesicle clustering. Because the closed conformation is mutually exclusive with binding of the Sec9-Qbc domain to Sro7, we asked whether prebinding of Sro7 to excess full-length Sec9 protein would affect the clustering activity of otherwise wild type Sro7. The results of this experiment, shown in Figure 3.8B, demonstrate that binding of Sec9 to Sro7 in the assay potently inhibited vesicle clustering by Sro7, exactly as predicted by this model. The inhibition by Sec9 is

dose-dependent (Figure 3.8D) and specific in that neither the cytoplasmic domain of Sso1 nor Snc1 showed any effect in the assay (Figure 3.8, B and C). Also consistent with the notion that Sec9 inhibition is through binding to Sro7, we find that eliminating the prebinding incubation step significantly reduced the inhibitory effect of Sec9 on Sro7-mediated clustering (data not shown). Taken together, we find that "opening" the autoinhibitory tail by three different means, propeller mutant, tail mutants, or Sec9 binding, all lead to inhibition of clustering activity. This suggests that the binding of the autoinhibitory tail acts as a "switch" to coordinate Sro7 function in Rab-dependent membrane tethering and SNARE assembly. Although the precise order of events necessary to turn this switch will need to be sorted out, one attractive model would be that closure of the autoinhibitory tail would act to temporally regulate Rab-mediated vesicle tethering with SNARE assembly necessary for subsequent fusion (Figure 3.8E).

3.4 Discussion

In this paper, we describe for the first time an *in vitro* system in which we recapitulate Rab-dependent post-Golgi vesicle/vesicle clustering induced by the yeast Lgl/tomosyn family member Sro7. We find that many of the features present in Sro7-mediated vesicle clustering *in vivo* and *in vitro* closely resemble vesicle tethering events that are thought to occur prior to fusion with the target membrane. The most important similarity is the requirement in both cases for GTP-bound Rab protein and a direct Rab effector in the formation of a close physical apposition of a vesicle with an opposing membrane. It has been previously suggested that this phenomenon might involve symmetric "pairing" of Rab-GTP molecules on both membranes, which may be stabilized by effector/Rab and effector/effector interactions [122]. Certainly the dependence of the clustering assay and post-Golgi transport on Sec4-GTP and Sro7 supports this

notion, although further biochemical dissection of this system will be required to distinguish the precise tethering mechanism involved.

Genetically and biochemically, Sro7 has features that suggest it likely functions parallel to the exocyst complex downstream of the Sec4 GTPase. Evidence for a parallel function to the exocyst complex includes direct GTP-dependent binding to Sec4 (like the Sec15 component) and dosage suppression of a number of exocyst mutants, including bypass suppression of *exo70*Δ, *sec5*Δ, and *sec3*Δ [47, 89]. However, because Sro7 also physically interacts with the Exo84 component of the exocyst complex, some aspects of its activity may be interdependent with the exocyst [90]. In the assay described in this paper, it is clear that the tethering/clustering activity we observe for Sro7 is almost certainly independent of the exocyst, as this complex does not stably associate with vesicles and is absent from post-Golgi vesicles following the size-dependent purification method used in this work [123].

Previous structural analyses of the Rab effector Sro7 [48] strongly suggest that binding of the C-terminal autoinhibitory tail of Sro7 to the N-terminal propeller represents a molecular switch in the function of this protein in vesicle transport. In this model, Sro7 would deliver the t-SNARE Sec9 to sites of fusion with the Sec9-Qbc domain bound to the N-terminal propeller and the autoinhibitory domain in the "open" conformation (see Figure 3.8E). When the appropriate signal or trigger is present, the autoinhibitory domain would bind back to the N-terminal propeller, resulting in the release of the Sec9-Qbc domain. This would then allow the Sec9-Qbc domain to be available for assembly into active t-SNARE and trans-SNARE complexes required for vesicle fusion. Here, using two sets of point mutations shown to destabilize the autoinhibitory tail, we demonstrate that the conformational status of the tail plays a critical role in determining the activity of Sro7 in Sec4-dependent vesicle clustering. Although both regulation of the tail of

Sro7 and the presence of Sec4-GTP are important for clustering *in vitro* and *in vivo*, Sec4 binding by itself does not appear to be the trigger for this conformational switch, because mutations that favor the open conformation show equivalent binding to Sec4-GTP.

Because Rab-dependent vesicle tethering to the appropriate membrane is thought to occur prior to the SNARE-mediated fusion, we expected that the open conformation of Sro7 would be most active in Rab-GTP-mediated vesicle clustering. The fact that we find exactly the opposite of this expectation, *i.e.* the open conformation is inactive, may be indicative of a quite different temporal relationship between Rab tethering and fusion. Instead of happening at quite discrete and sequential stages, these two events appear to be coincident in their regulation. This may help to ensure that neither Rab-mediated tethering nor SNARE-mediated fusion occur promiscuously with the wrong membrane by requiring an additional triggering interaction. We have previously described another "gating" interaction with the type V myosin Myo2, by which the interaction between Sro7 and Sec4 is regulated. Taken together, this suggests that Sro7 is well designed to orchestrate assembly and disassembly events on the surface of the post-Golgi vesicles that are critical for vesicle transport, tethering, and fusion. This may help to aid in increasing the overall spatial and temporal specificity of the transport events.

The development of the *in vitro* assay described here will be an important tool for further dissecting the mechanism by which Rab GTPases and their effectors function in transport. Further identification of protein/protein and protein/lipid interactions that are important for post-Golgi transport *in vivo* and vesicle clustering *in vitro* will allow specific models for the role of Sro7 in these processes to be tested.

3.5 Materials and Methods

3.5.1 Plasmids Used

Single copy plasmids expressing Sro7 or charge reversal point mutations were obtained by site-directed mutagenesis on pB741 (*SRO7*,*CEN*, and *HIS3*). All *GAL-SRO7* constructs, previously subcloned into the integrating vector pB24 (*LEU2*) as BamHI-HindIII fragments, were then subcloned as BamHI-ApaI inserts into pB38 (*GAL*, *CEN*, and *HIS3*). Protein A-tagged Sro7 constructs were generated as BamHI-HindIII fragments in pB966 (2μ, *URA3*, plasmid containing the *ADH1* promoter and a protein A tobacco etch virus tag). Full-length Sec9 with an N-terminal GST tag and a C-terminal His_6 tag was obtained as described previously [74]. Soluble GST-Snc1, GST-Sso1, and GST-Sso1(193–265) were obtained by standard glutathione elution of the fusion protein from glutathione-Sepharose beads following the manufacturer's directions (GE Healthcare). Plasmid for recombinant GDI [89] production, pGDI-CBD, was a gift of V. Starai and was used as described [124].

3.5.2 Protein Purification

Sro7 with an N-terminal Protein A tag was obtained from a modification of the purification protocol described previously [89]. Sro7 was expressed behind an *ADH1* promoter from a high copy plasmid in a yeast *pep4*Δ background strain. Approximately 5 liters of cells were grown overnight in synthetic media to an A_{599} of 3.0 and then shifted to YP + 2% glucose for one doubling time. Cells were then harvested and washed in 200 ml of ice-cold buffer containing 10 mm Tris, pH 7.8, 20 mm sodium azide, and 20 mm sodium fluoride to yield a final wet weight of ~50 g of cells. Cells were frozen on dry ice and stored at −80 °C. Lysis was obtained with a bead beater using ice-cold buffer containing 20 mm Tris, pH 7.8, 150 mm NaCl, 0.5% Tween 20, and 1 mm DTT, and protease inhibitors (2 μg/ml leupeptin, 2 μg/ml aprotinin, 2

μg/ml antipain, 14 μg/ml pepstatin A, and 1 mm phenylmethylsulfonyl fluoride). Five cycles of 1-min bead beating, followed by 2-min intervals on ice were used to lyse the cells. The lysate (60 ml) was then spun at 17,400 × *g* for 10 min at 4 °C in a JA 25.5 rotor before further dilution (120 ml) and ultracentrifugation at 140,000 × *g* for 30 min at 4 °C in a type 45Ti rotor to yield a final protein concentration of about 25 mg/ml. Binding to Sepharose CL-6B beads (1 ml of beads/45 ml of lysate) for 1 h at 4 °C was then used to preclear the lysate before binding to 1 ml of IgG-Sepharose beads for 2 h at 4 °C. Beads were then washed five times with lysis buffer, three times with lysis buffer containing 400 mm NaCl, and three times with ice-cold cleavage buffer containing 20 mm Tris, pH 7.8, 150 mm NaCl, 0.1 mm EDTA, and 1 mm DTT. Beads were then resuspended 1:1 in cleavage buffer, and cleavage was obtained with tobacco etch virus cleavage enzyme for 5 h at 17 °C (5000 units of tobacco etch virus/3-ml bed volume beads). Supernatant containing the cleaved protein was then collected and frozen at −80 °C.

3.5.3 Vesicle Enrichment

Yeast mutant cells grown overnight in YP + 2% glucose to an A_{599} of 0.6 were shifted to the restrictive temperature of 37 °C for 2 h. Sodium azide was then added (final 20 mm) to the culture, and 300 absorbance units were centrifuged, washed with 10 ml of 10 mm Tris, pH 7.5, 20 mm NaN_3, and spheroplasted in 10 ml of spheroplast buffer (0.1 m Tris, pH 7.5, 1.2 m sorbitol, 10 mm NaN_3, 21 mm β-mercaptoethanol, and 0.05 mg/ml Zymolyase 100T) for 30 min at 37 °C. Spheroplasts were then lysed in 4 ml of ice-cold lysis buffer (10 mm triethanolamine, pH 7.2, 0.8 m sorbitol) with protease inhibitors (2 μg/ml leupeptin, 2 μg/ml aprotinin, 2 μg/ml antipain, 14 μg/ml pepstatin A, and 1 mm phenylmethylsulfonyl fluoride). The yeast lysate was then centrifuged at 450 × *g* for 4 min at 4 °C to remove unbroken cells, and the remaining lysate was spun at 30,000 × *g* for 15 min at 4 °C in a Sorvall centrifuge to pre-clear larger membranes.

Approximately 2.5 ml of supernatant was then labeled with FM4-64 (1 μg/ml) for 10 min on ice. The labeled lysate was then layered over 2 ml of an ice-cold sorbitol cushion (20% w/v sorbitol in 10 mm triethanolamine, pH 7.2) and centrifuged at 100,000 × *g* for 1 h at 4 °C. After removal of the supernatant fraction, the pellet fraction was resuspended in 600 μl of lysis buffer and kept on ice for use in the clustering assay. When the *sec4-8* secretory mutant was used the following adjustments were made: 600 absorbance units were harvested and spheroplasted in 15 ml of spheroplast buffer. The final 100,000 × *g* pellet fraction was resuspended in 700 μl of lysis buffer. To obtain an enriched vesicle fraction from the *sec6-4* mutant expressing GFP-Sec4 (*CEN),* cells grown overnight in selective media were first shifted to YP + 2% glucose at 25 °C for 1 h before placing them at the restrictive temperature of 36 °C for 2 h. 350 absorbance units were spheroplasted with 10 ml of spheroplast buffer and treated as above except the 100,000 × *g* pellet was resuspended in 350 μl of lysis buffer. To obtain an enriched vesicle fraction from the *snc1*Δ;*snc2*Δ *GAL*-depletion strain, where the sole source of Snc1 is under the control of the *GAL1/10* promoter, cells were grown in YP + 2% glucose and then shifted to YP + 3% raffinose for 14 h before harvesting 700 absorbance units that were then spheroplasted, lysed, and subjected to centrifugation as described for the *sec6-4* mutant strain. The final high speed pellet fraction was resuspended in 160 μl of lysis buffer.

3.5.4 Vesicle Purification

To obtain a homogeneous population of post-Golgi vesicles, the 100,000 × *g* pellet, obtained as described above in the vesicle enrichment section, was subjected to a 20–40% sorbitol velocity gradient [24]. Adjustments to the above protocol included harvesting 700 absorbance units of cells and resuspending the 100,000 × *g* pellet in a final volume of 600 μl prior to loading at the top of 11 ml of linear sorbitol gradient prepared with 1.22-ml steps of 40,

37.5, 35, 32.5, 30, 27.5, 25, 22.5, and 20% sorbitol (w/v) in 10 mm triethanolamine acetate, pH 7.2. The gradient was centrifuged at 71,000 × *g* for 80 min at 4 °C and then fractionated into 0.72-µl fractions. Fractions 5–7 (pink color) containing the vesicle fractions were then pooled, diluted with 3 ml of lysis buffer, and centrifuged at 100,000 × *g* for 1 h. The pellet fraction containing the purified vesicles was resuspended in 200 µl of lysis buffer. For vesicle purification from the *sec4-8* mutant strain, the above protocol was adjusted by using 1000 absorbance units of mutant cells and spheroplasting with 25 ml of spheroplast buffer. The spheroplasts were then lysed with the same volume (9 ml) as the *sec6-4* mutant cells, and the 100,000 × *g* pellet was resuspended in 600 µl and loaded on a 20–40% sorbitol velocity gradient as described above. The sample was treated identically to the *sec6-4* mutant strain for the final concentration of the purified vesicle fraction.

3.5.5 GDI Extraction and Vesicle Purification

For the GDI-treated vesicles, the following modifications were made to the vesicle enrichment protocol described above: 1400 absorbance units of a *sec6-4* mutant strain were grown overnight and shifted to the restrictive temperature of 37 °C for 2 h. The final high speed pellet fraction was resuspended into 1 ml of lysis buffer and treated with 0.5 mm GDP and 3.6 mm $MgCl_2$ for 30 min on ice. The vesicles were then split into two 500-µl aliquots that were treated with 8 mm GDI or mock-treated with buffer only for 30 additional min on ice. Lysis buffer was then added to bring each volume to 600 µl before loading onto two separate but identical 20–40% sorbitol velocity gradients for vesicle purification. Vesicle-containing fractions from each gradient were then pooled, concentrated by a high speed centrifugation at 100,000 × *g* as described in the vesicle purification protocol, and resuspended in a final volume of 150 µl before using in the *in vitro* clustering assay.

3.5.6 Antibody Inhibition of Vesicle Clustering *in Vitro*

For the antibody inhibition studies, a, HSP fraction obtained from a *sec6-4* mutant strain was incubated with equal amounts of monoclonal anti-Sec4 or control monoclonal anti-Myc for 1 h on ice before treating with $MgCl_2$ (3 mm) and nucleotide (1 mm) for 30 additional min on ice. The vesicles were then incubated with Sro7 (1 μm) for 20 min at 27 °C.

3.5.7 Clustering Assay

Vesicle-enriched fraction or purified vesicles (10 μl) were preincubated with $MgCl_2$ (3 mm) and nucleotide (1 mm) for 30 min on ice prior to addition of Sro7 (1 μm) or mock buffer for 20 min at 27 °C.

3.5.8 Negative Staining

The carbon film grids were glow-discharged in a Harric Plasma Cleaner for 1.5 min. A drop of sample (10 μl) was placed onto a grid that was suspended in reverse forceps for 1 min. The sample was then washed off with 5 drops of 1% aqueous uranyl acetate. The stain was allowed to sit on the grid for 1 min. The grid was blotted on the tip of the forceps with filter paper before air drying and was examined by electron microscopy.

3.5.9 Immunofluorescence

Strains containing a *CEN* vector (pB38) expressing wild type *SRO7, sro7-R189D,R222D,* or *sro7-K914,F942* from a *GAL*-inducible promoter were grown overnight in synthetic media with raffinose (3%) to early log phase and then induced with 1% galactose for 6 h before fixing and processing as described previously [125].

3.5.10 Binding Assays

Bindings of wild type Sro7 or point mutant forms of Sro7 were set up as described previously [74] for Sec9-Qbc, Exo84-NT (amino acids 3–400), and Myo2-IQ (amino acids 782–

990). Bindings to GTP-Sec4 made use of procedures described in [89]. To compare wild type Sro7 to point mutant forms of Sro7, two different sets of soluble protein concentrations were used to ensure the binding response was in a linear range. Student's *t* test was done on three individual bindings for each protein concentration used.

3.6 Figures

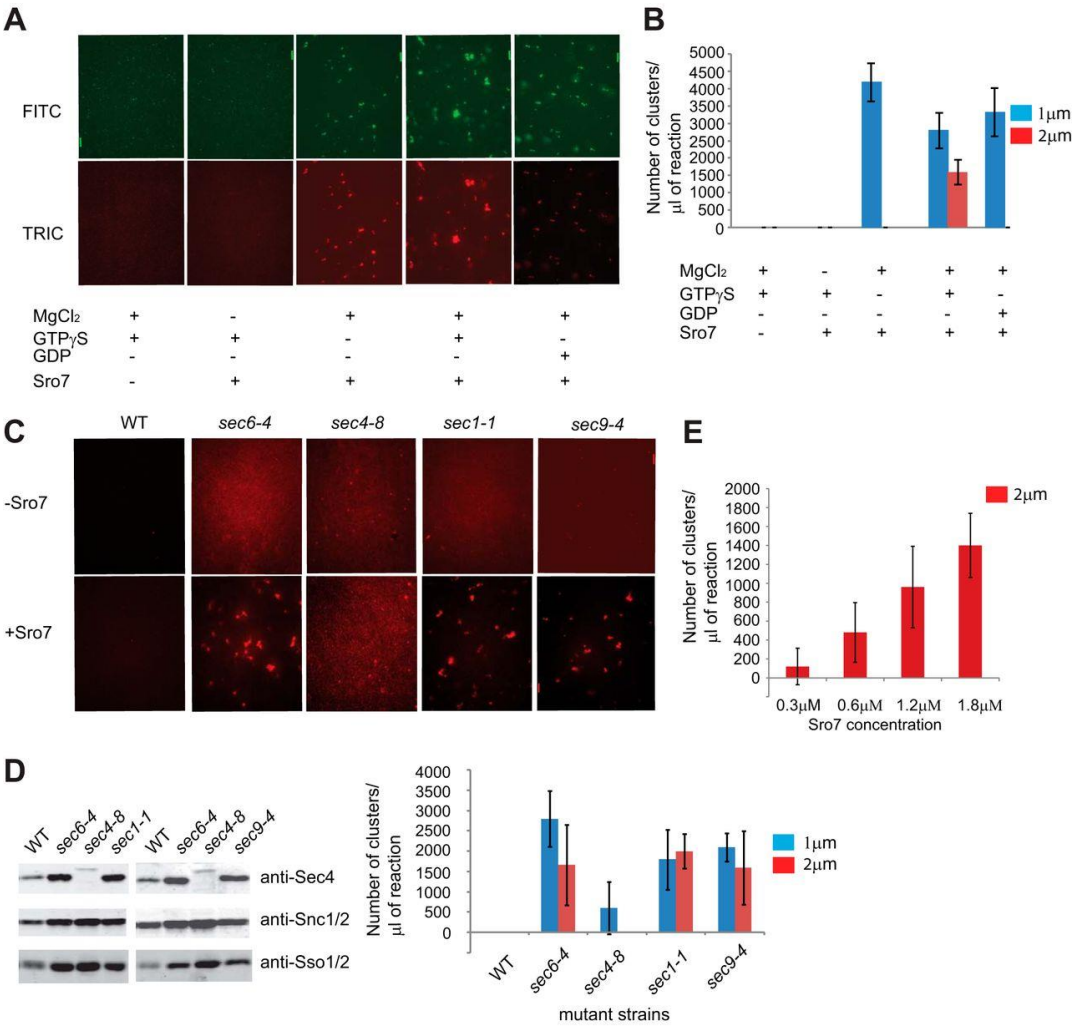

Figure 3.1 - In vitro system for clustering post-Golgi vesicles in the presence of Sro7, $MgCl_2$ and GTPγS.

A, *sec6-4* mutant strain expressing GFP-Sec4 (*CEN*) was shifted to the restrictive temperature of 37 °C to accumulate post-Golgi vesicles. The mutant cells were then spheroplasted, lysed, and spun at 30,000 × *g* to remove large membranes. The supernatant was then labeled with FM4-64 and spun at 100,000 × *g* over a sorbitol cushion to generate a concentrated HSP fraction enriched in post-Golgi secretory vesicles. The HSP fraction was then treated with or without $MgCl_2$ (3 mm), GTPγS, or GDP (1 mm) for 30 min on ice, and then Sro7 (1 µm) was added for 20 min at 27 °C. A 1-µl aliquot of the reaction mixture was analyzed by fluorescence microscopy, and quantitation of vesicle cluster formation (*B*) was based on counting 10 images at ×60 magnification and separating vesicle clusters by size. *Scale bar*, 2 µm. *C*, post-Golgi vesicle fractions (HSP) labeled with FM4-64 were obtained as above from WT, *sec6-4*, *sec4-8*, *sec1-1*, and *sec9-4* mutant strains. HSP fractions from the different strains were then treated with $MgCl_2$ (3 mm) and GTPγS (1 mm) for 30 min on ice and then with Sro7 (1 µm) for 20 min at 27 °C. *D*,

total vesicle material (HSP) was monitored by Western blot analysis with vesicle marker proteins (Sec4, Snc1/2, and Sso1/2), and quantitation of *in vitro* clustering was obtained as in *A. Scale bar*, 2 μm. *E*, vesicle clustering in a *sec6-4* HSP fraction labeled with FM4-64 increased with the concentration of Sro7 used in the assay.

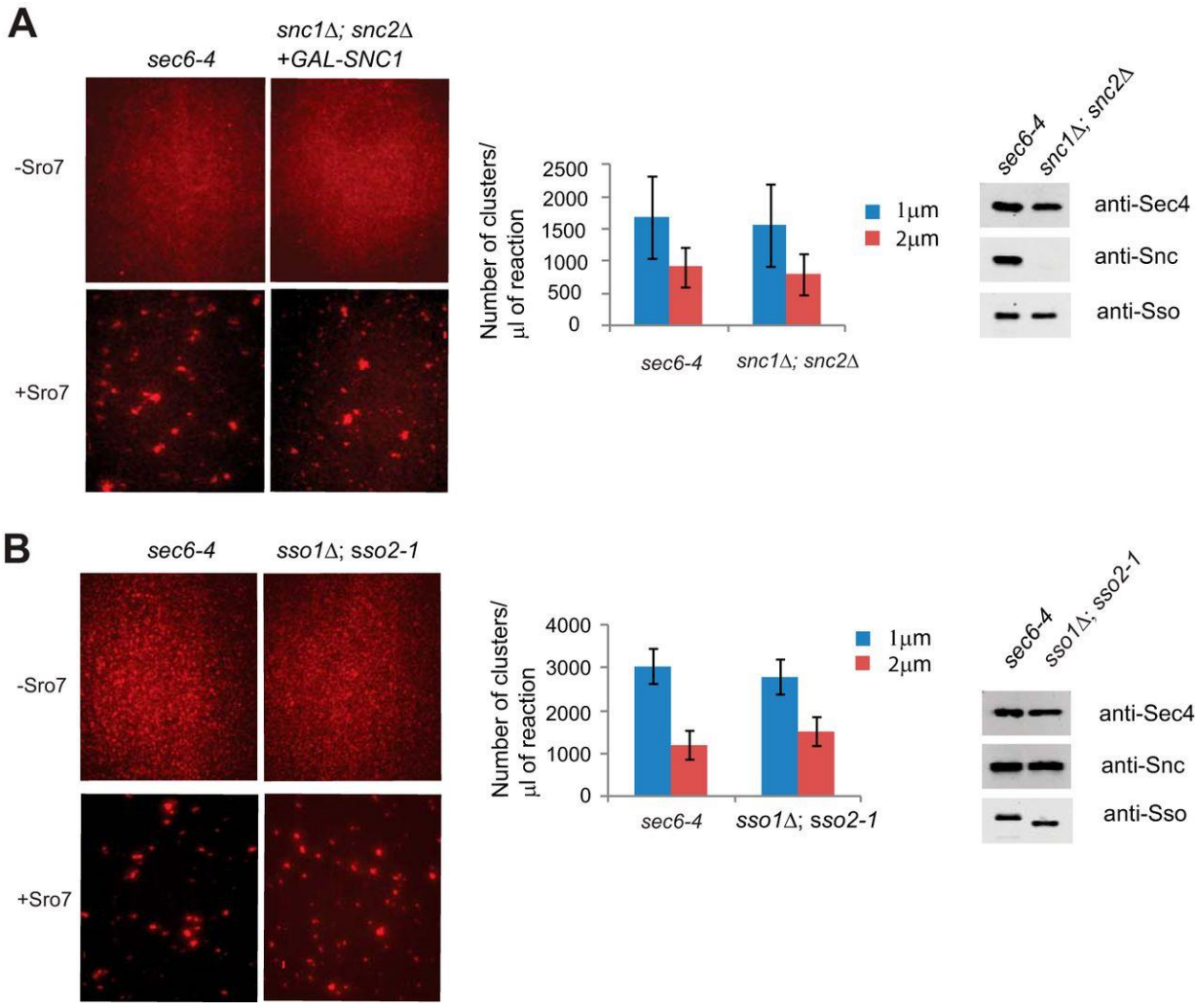

Figure 3.2 - Post-Golgi vesicles do not require functional SNARE proteins, Snc1/2 or Sso1/2, to cluster *in vitro* in the presence of Sro7, $MgCl_2$, and GTPγS.
A, *sec6-4* mutant strain was shifted to the restrictive temperature of 37 °C to accumulate post-Golgi secretory vesicles and then spheroplasted, lysed, and fractionated as described in Figure 3.1 to obtain an HSP fraction enriched in labeled post-Golgi vesicles for the clustering assay. Vesicles depleted of the v-SNARE Snc1/2 were generated by shifting a *snc1*Δ;*snc2*Δ strain expressing *GAL-SNC1* from YP + 2% glucose into YP + 3% raffinose for 14 h at room temperature before processing as seen for the *sec6-4* mutant strain. Vesicle amounts from the two strains were normalized by Western blot analysis of vesicle marker proteins (Sec4, Snc1/2, and Sso1/2). Vesicle fractions were incubated with $MgCl_2$ (3 mm) and GTPγS (1 mm) for 30 min on ice and then treated with Sro7 (1 µm) for 20 min at 27 °C before analysis by fluorescence microscopy as described in Figure 1. *B*, *sec6-4* and a *sso1*Δ;*sso2-1* secretory mutant strain were grown at room temperature and then shifted to 37 °C to accumulate post-Golgi vesicles. Strains were spheroplasted, lysed, and subjected to differential centrifugation to obtain an HSP fraction enriched in vesicles that were normalized using Western blot analysis of vesicle marker proteins. The *in vitro* assay was then conducted and quantitated as described in Figure 3.1. *Scale bar*, 2 µm.

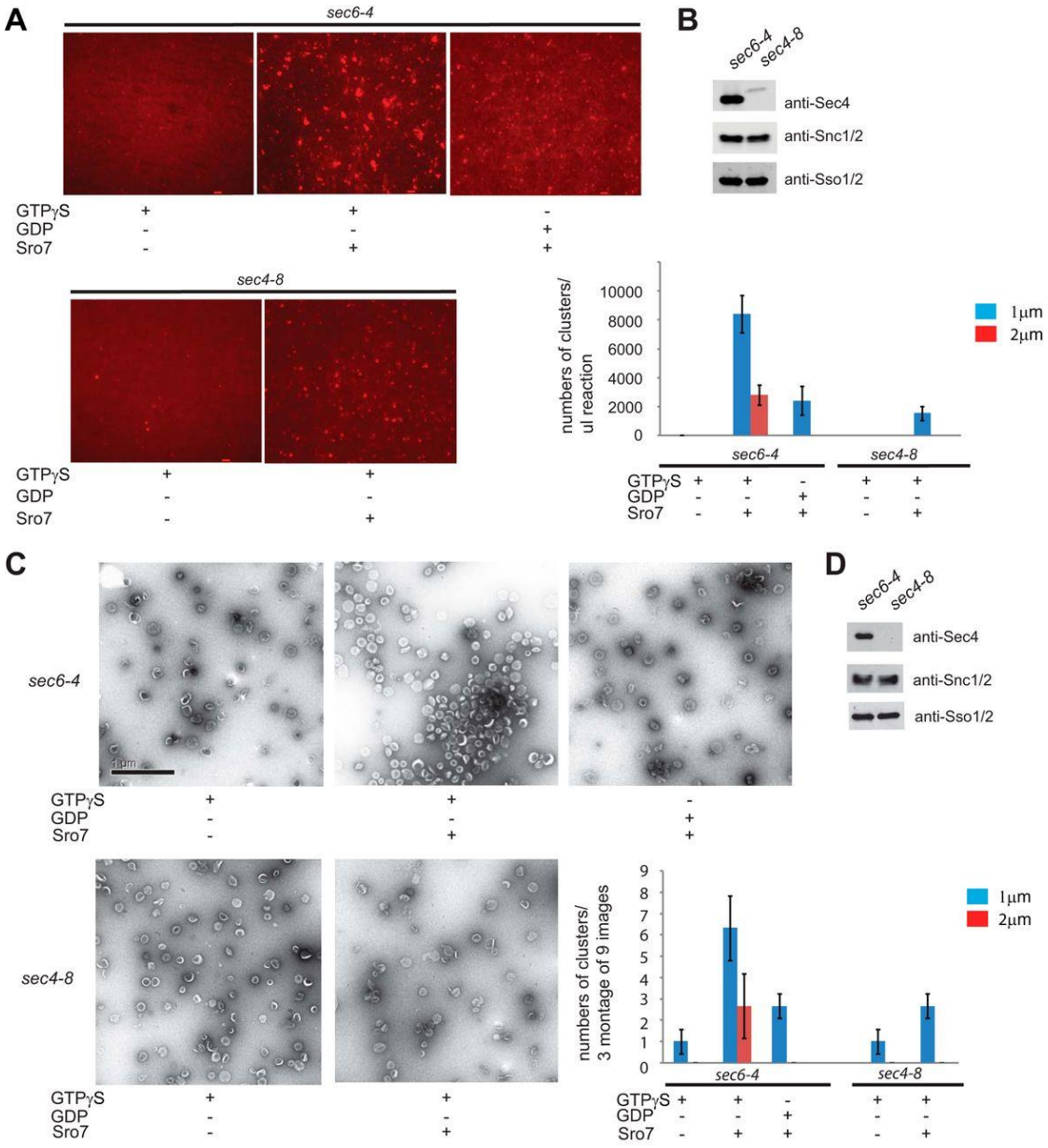

Figure 3.3 - Purified post-Golgi vesicles cluster *in vitro* in the presence of Sro7, $MgCl_2$, and GTPγS.

A, *sec6-4* and *sec4-8* mutant strains were shifted to the restrictive temperature of 37 °C to accumulate secretory vesicles. Cells were then spheroplasted, lysed, and subjected to a 30,000 × *g* spin to remove large membranes. The lysates were then treated with FM4-64 and spun through a sorbitol cushion at 100,000 × *g* to generate two HSP fractions that were then subjected to parallel 20–40% sorbitol velocity gradients. Vesicle-containing fractions were collected from each gradient and subjected to a second 100,000 × *g* centrifugation to generate a homogeneous fraction of *sec6-4* or *sec4-8* vesicles. These were then treated with $MgCl_2$ (3 mm) and GTPγS (1 mm) for 30 min on ice and then with Sro7 (1 μm) for 60 min at 27 °C. Clustering was analyzed both by fluorescence microscopy (*A*) and negative stain electron microscopy (*C*). HSP fractions

of purified vesicles were monitored by Western blot analysis (*B* and *D*), and quantitation of vesicle clustering for *A* was based on counting 10 images at ×60 magnification and separating vesicle clusters by size. *Scale bar,* 2 μm. Quantitation for *C* was based on counting three montages of nine frames each.

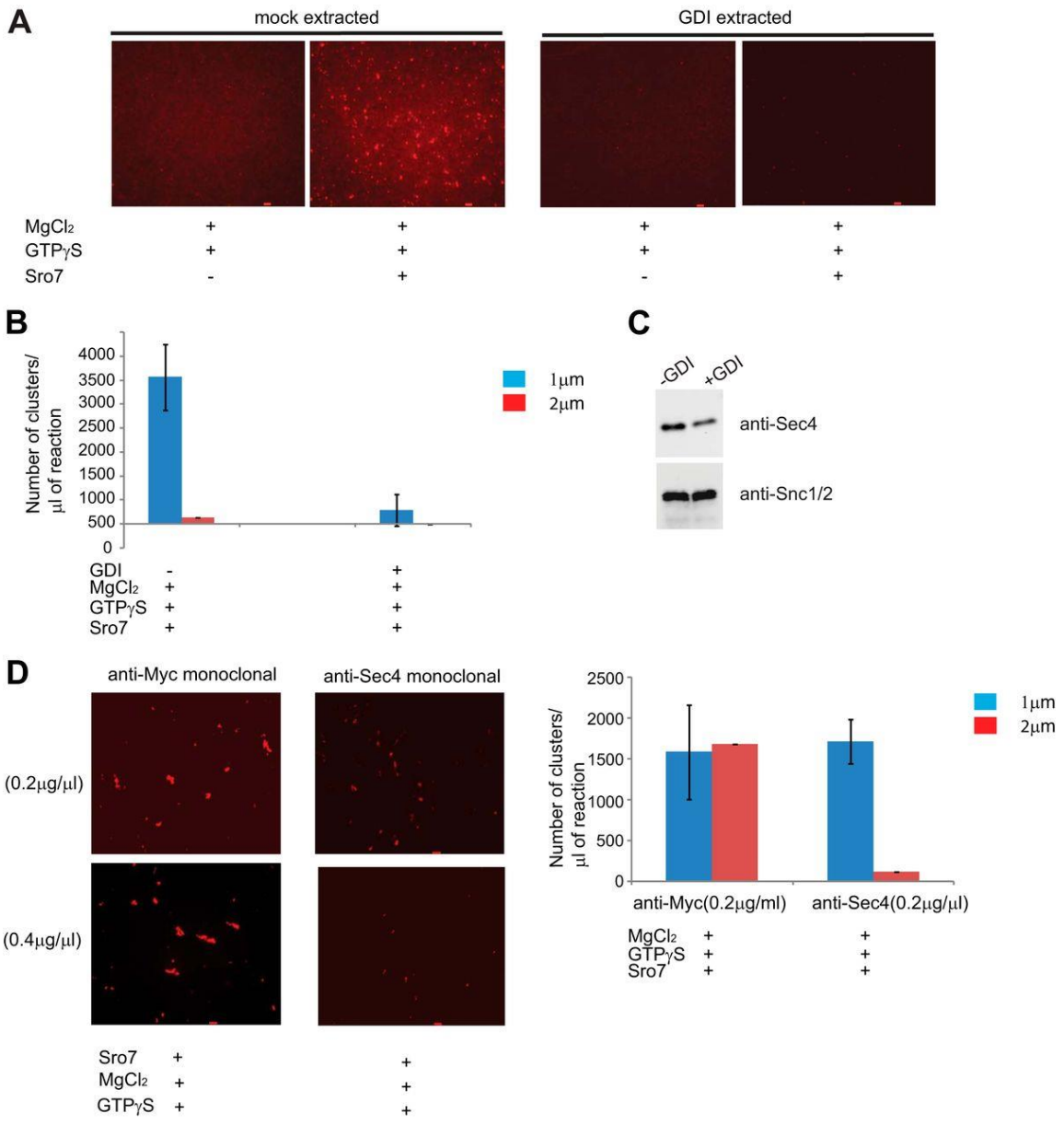

Figure 3.4 - *In vitro* post-Golgi vesicle clustering depends on the presence of GTP-Sec4 on vesicles.

A, HSP fraction obtained from a *sec6-4* mutant strain was treated with GDP (0.5 mm), $MgCl_2$ (3.6 mm, and GDI (8 mm) or a mock buffer for 30 min on ice. The vesicles were then purified on parallel 20–40% sorbitol velocity gradients. Vesicle-containing fractions from each column were subject to a second centrifugation to generate two concentrated vesicle fractions. GDI-treated and mock-treated samples were then incubated with $MgCl_2$ (3 mm) and GTPγS (1 mm) on ice for 30 min and then with Sro7 (1 µm) for 60 min at 27 °C. Results of the clustering assay were analyzed by fluorescence microscopy (*A*), and quantitation of clustering is shown in *B. Scale bar*, 2 µm. Vesicle amount used was monitored by Western blot analysis (*C*) using polyclonal antibody to vesicle markers Sec4 and Snc1/2. *D*, HSP fraction obtained from a *sec6-4* mutant

strain was incubated with equal amount of monoclonal anti-Sec4 or control monoclonal anti-Myc IgG for 1 h on ice before treating with $MgCl_2$ (3 mm) and GTPγS (1 mm) for 30 additional min on ice. The vesicles were then incubated with Sro7 (1 μm) for 20 min at 27 °C. The reaction was analyzed by fluorescence microscopy and quantitated as described previously. *Scale bar,* 2 μm.

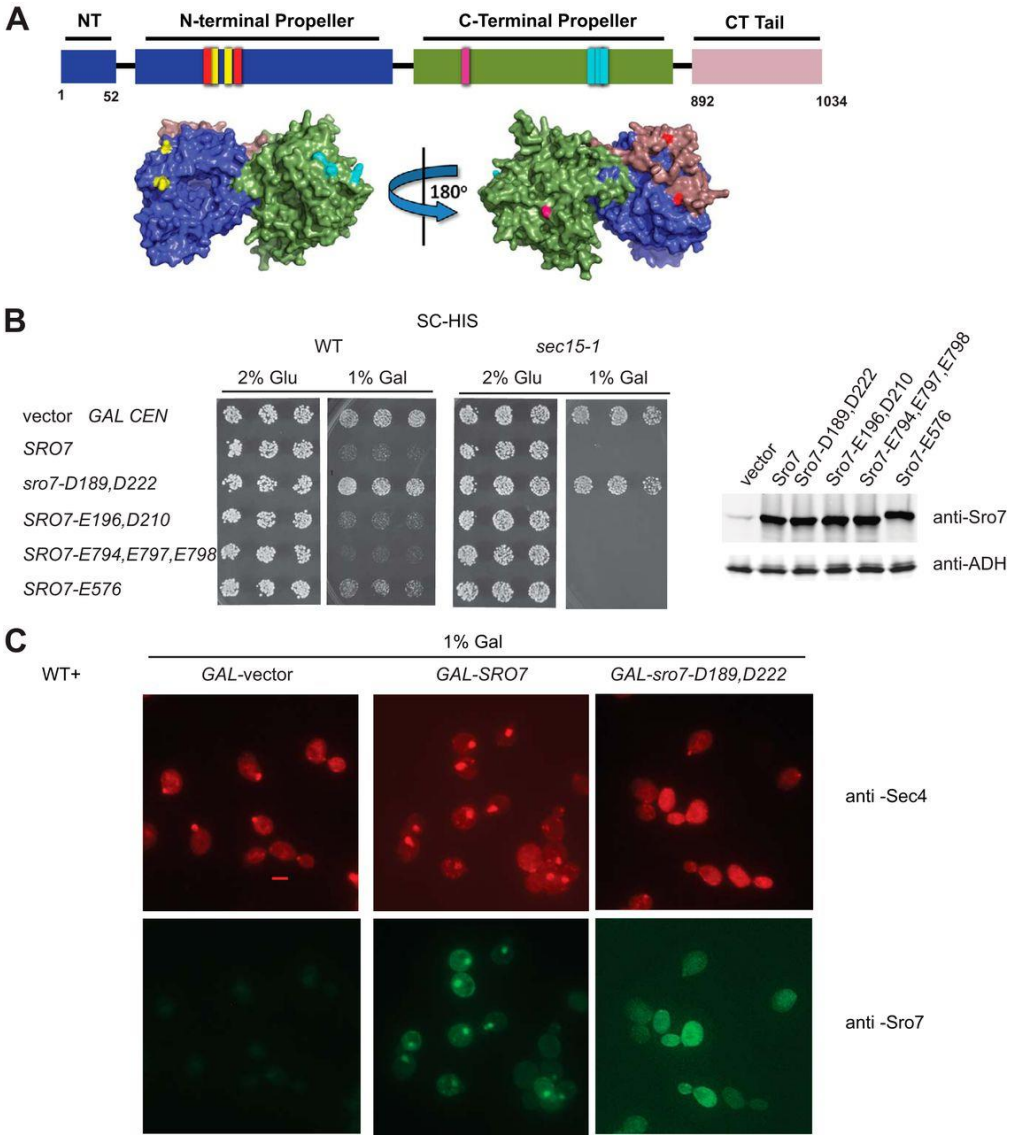

Figure 3.5 - Novel mutant of Sro7, *sro7-R189D,R222D* fails to induce clustering and cell lethality *in vivo*.

A, Schematic and surface-filling model show the four new, surface-exposed, conserved charge-reversal Sro7 mutants as follows: *red*, *Sro7-R189D,R222D*; *yellow*, *Sro7-K196E,R210D*; *light blue*, *Sro7-K794E,H797E,K798E*; *violet*, *Sro7-K576E*. *B*, wild type and *sec15-1* mutant strains were transformed with plasmids, (*CEN*) overexpressing Sro7, or the charge reversal mutants from a *GAL* promoter. Three individual colonies were picked and transferred to selective media in the presence of glucose or galactose. Equal absorbance units of the strains induced in galactose were harvested, washed in Tris (10 mm) and azide (20 mm), and lysed by glass bead lysis before subjecting to Western blot analysis. *C*, wild type cells containing plasmids expressing *SRO7* or *sro7-D189,D222* from a *GAL*-inducible promoter (*CEN*) or vector only were grown in selective media and induced for 6 h in galactose before fixing and processing for immunofluorescence analysis using monoclonal Sec4 and polyclonal Sro7 antibodies. *Scale bar*, 2 μm.

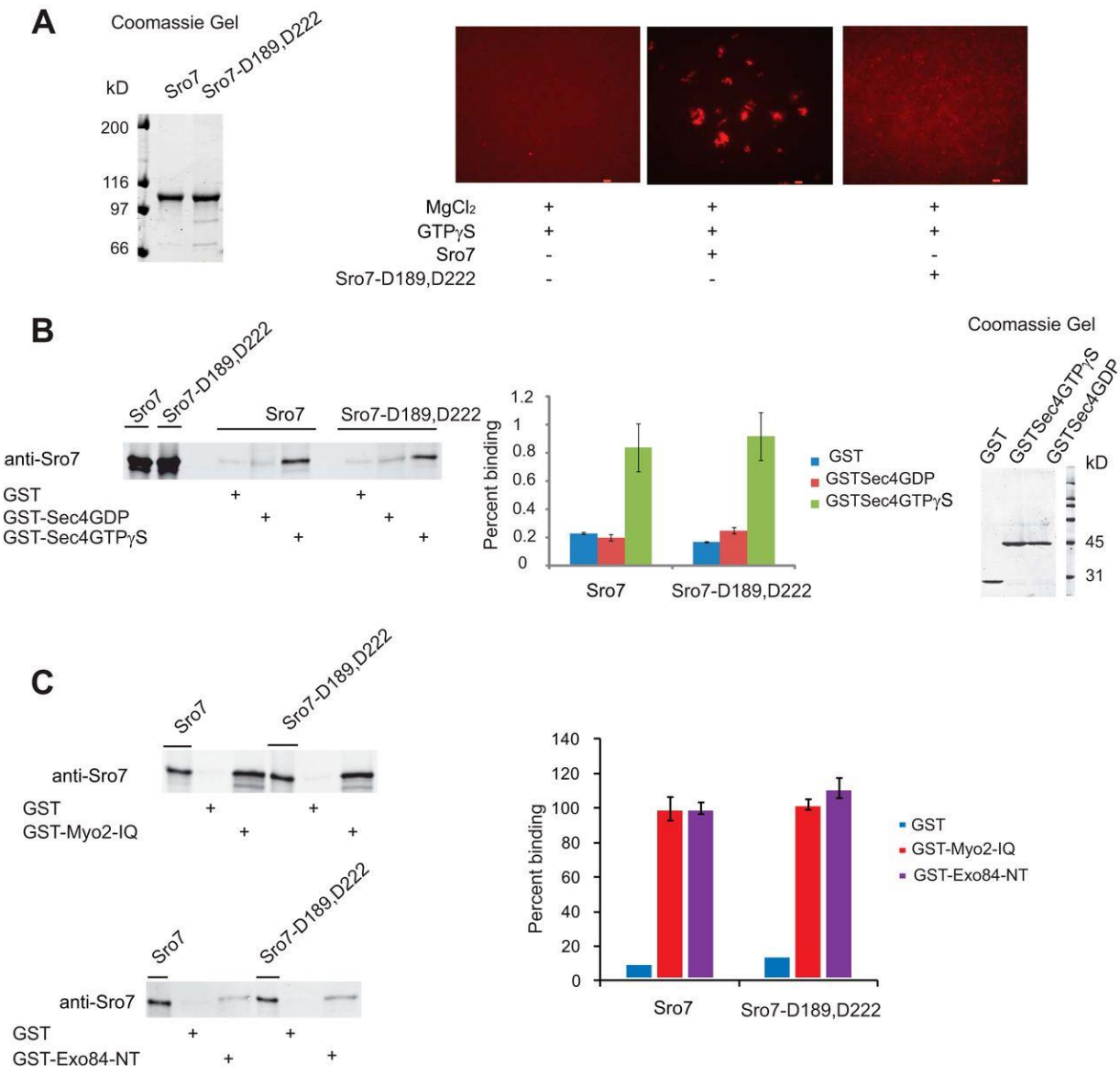

Figure 3.6 - Biochemical characterization of Sro7-D189,D222 shows that although the novel mutant cannot cluster vesicles in the *in vitro* clustering assay, it can still bind to Sec4-GTP, Myo2, and Exo84 in GST pulldown assays.

A, Sro7 and Sro7-D189,D222 were purified and analyzed at identical concentrations in the *in vitro* clustering assay. *Scale bar*, 2 μm. *B*, purified Sro7 and Sro7-D189,D222 also examined for binding to GST fusions of the Rab GTPase Sec4; *C*, IQ region of Myo2 (amino acids 782–990) and the N terminus of Exo84 (amino acids 3–400) by standard methods described previously. Percent binding in *C* was expressed using wild type Sro7 binding as 100%. All bindings represent the result of three independent experiments conducted with two different concentrations of GST fusion proteins on beads.

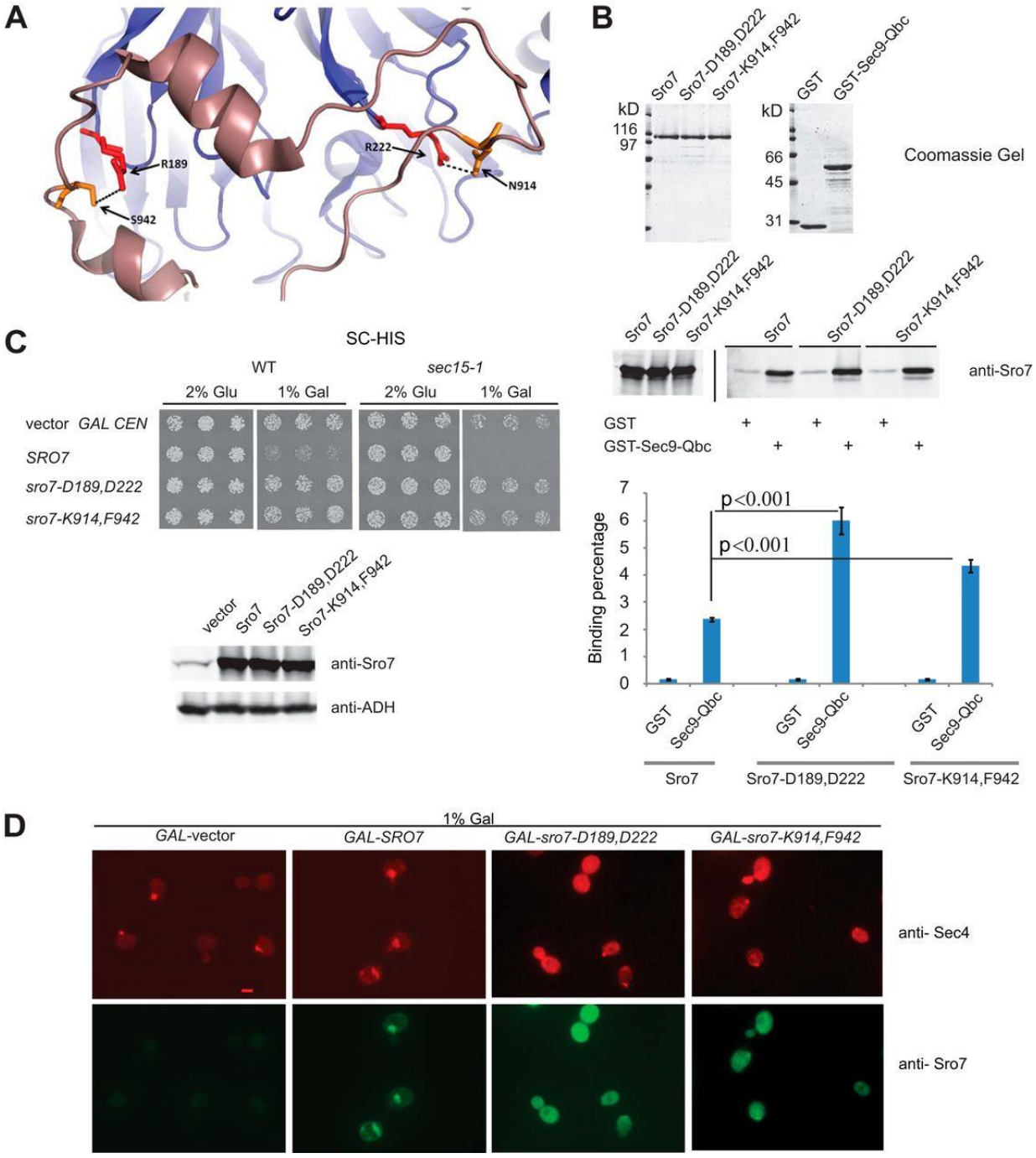

Figure 3.7 - Sro7-N914K,S942F behaves genetically and biochemically like Sro7-R189D,R222D.

A, schematic structure of Sro7 illustrating hydrogen bonds between R189,R222 on the N-terminal propeller of Sro7 and N914,S942 on the C-terminal tail. *B*, wild type and mutant Sro7 proteins were purified and analyzed for binding to the Sec9-Qbc domain as described previously. Standard Student's *t* test showed a *p* value of <0.001. *C*, wild type and *sec15-1* mutant strains were transformed with plasmids (*CEN*) overexpressing *SRO7*, *sro7-D189,D222* and *sro7-*

K914,F942 from a *GAL* promoter. Three individual colonies were picked and transferred to selective media in the presence of glucose or galactose. Equal absorbance units of the strains induced in galactose were harvested, washed in Tris (10 mm) and azide (20 mm), and lysed by glass bead lysis before subjecting to Western blot analysis. *D*, wild type cells containing plasmids expressing Sro7, or mutant proteins from a *GAL*-inducible promoter (*CEN*), or vector only were grown in selective media and induced for 6 h in galactose before fixing and processing for immunofluorescence analysis using monoclonal Sec4 and polyclonal Sro7 antibodies. *Scale bar,* 2 μm.

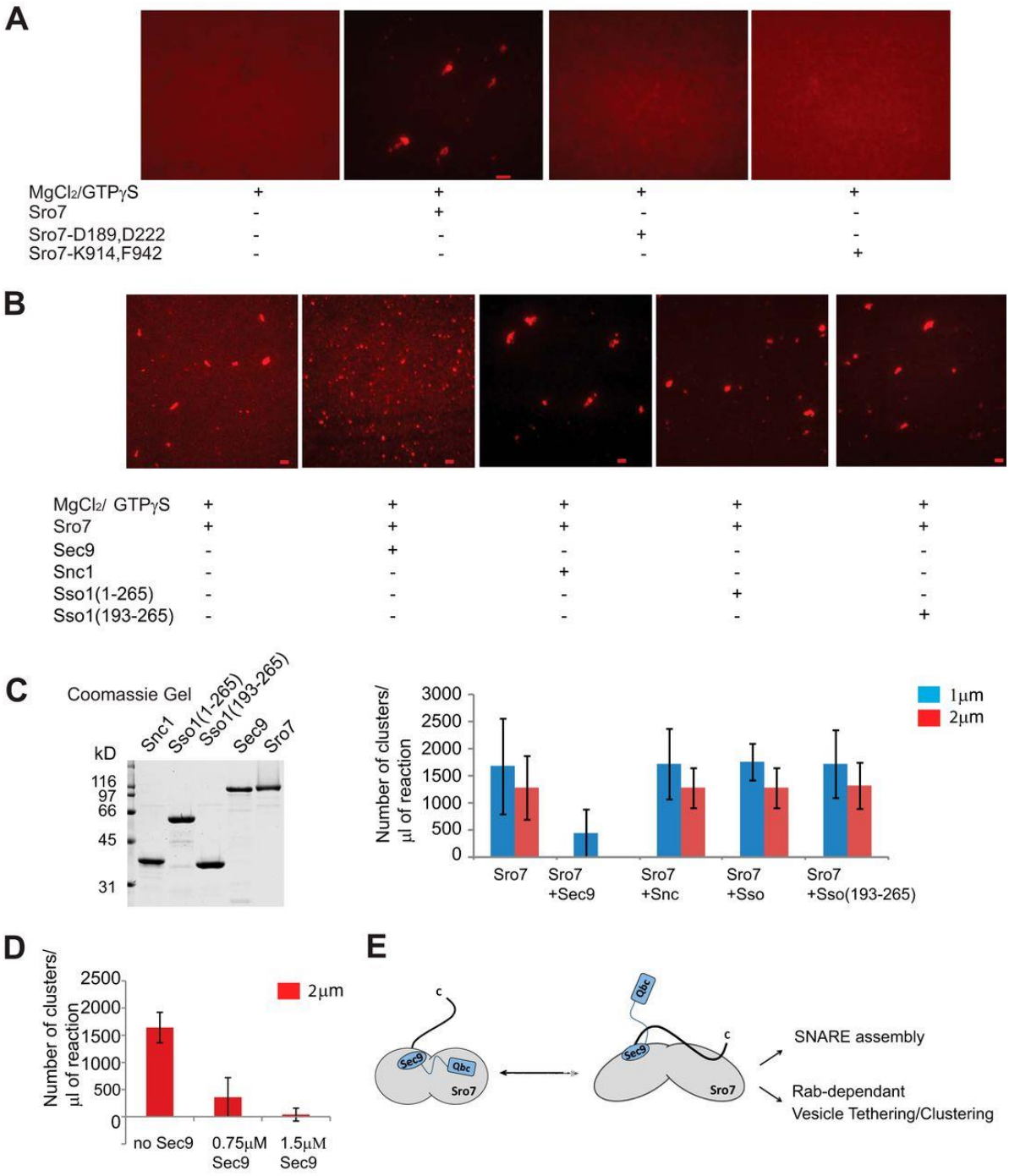

Figure 3.8 - Sro7 mutants that favor an open conformation inhibit Sro7-mediated vesicle clustering *in vitro*.

A, Sro7, Sro7-D189,D222 and Sro7-K914,F942 were purified and analyzed at identical concentrations in the *in vitro* clustering assay. *Scale bar*, 2 µm. *B*, *in vitro* clustering assay was performed with Sro7 (1.5 µm) or a mixture of Sro7 and Sec9 (1:1), Sro7 and GST-Snc (1:1), Sro7 and GST-Sso1 (1:1), or GST-Sso1 (amino acids 193–651) (1:1) previously incubated on ice for 60 min. The assay was analyzed and quantitated as described previously. Results of the

quantitation and Coomassie stain of the proteins used is shown in *C. D*, inhibitory effect of Sec9 on Sro7 is dose-dependent. *E,* model showing how the closed conformation of Sro7 allows release of the Sec9-Qbc domain and Rab-dependent vesicle clustering to occur simultaneously.

CHAPTER 4

Concluding Remarks

Polarized exocytosis is an elegantly designed process requiring the spatial and temporal coordination of numerous proteins functioning in vesicle transport at different stages of the secretory pathway. Although a near complete collection of genes critical for vesicle transport have been discovered, the mechanisms for how these proteins coordinate transport, docking and delivery of secretory vesicles is still mysterious. The goal of my thesis work was to tease out the molecular details and functional significance of the interaction between two of these proteins, Sro7 and the Rab GTPase Sec4.

In Chapter 2, studies were directed at understanding the structural details of the interaction between Sro7 and the Rab GTPase, Sec4. Genetic screens in yeast previously identified Sro7 to interact with the t-SNARE, Sec9 [47, 88]. More recently, Sro7 was also shown to bind *in vitro* preferentially to the GTP-locked form of Sec4 [89]. These results and genetic properties consistent with Sro7functioning downstream of Sec4 suggested that Sro7 is a direct effector of Sec4. We utilized the known crystal structure of Sro7 to identify conserved, charged residues on the surface of Sro7 and screened for their involvement in binding to Sec4. These biochemical results combined with *in vivo* suppression studies and computational modeling identified the Sro7-Sec4 docking interface. Specifically, we found that mutations in Sro7 which disrupt the Sro7-Sec4 interaction also demonstrate a clear deficiency *in vivo* to overcome defects in Exocyst complex function. Interestingly, our bioinformatics analysis of the sequence variation

within vertebrate members of the Tomosyn family revealed significant conservation within the region that corresponds with the Sec4-Sro7 binding interface on Sro7. Conversely, analysis of the sequence variation within vertebrate Lgl members revealed that the region corresponding to the Sec4-Sro7 binding pocket is significantly more variable than on Tomosyn. These results suggest a possible conserved Rab GTPase effector function in Tomosyn.

Chapter 3 describes a novel *in vitro* assay that recapitulates post-Golgi vesicle tethering by Sro7-induced clustering of vesicles. Our lab previously found that overexpression of Sro7 in cells results in the accumulation of large clusters of post-Golgi secretory vesicles in the cell and overall cell lethality [113]. Interestingly, this same phenotype is observed when overexpressing the Exocyst subunit, Sec15, another downstream effector of the Rab GTPase, Sec4 [114]. Vesicle clustering induced by both Sro7 and Sec15 depends on Sec4 function, but is independent of the t-SNARE, Sec9 [113, 114]. Studies in this chapter biochemically reconstruct the clustering phenotype as an *in vitro* assay. As demonstrated *in vivo*, the presence of the Rab GTPase Sec4 on the surface of post-Golgi vesicles is critical for vesicle clustering in the *in vitro* system as well. Additionally, Sro7 point mutations designed to destabilize the Sro7 C-terminal autoregulatory tail demonstrate that the conformational status of the tail plays an important role in regulating the activity of Sro7-induced vesicle clustering. The *in vitro* clustering assay provides a useful new method to analyze how post-Golgi vesicle transport and tethering is mediated by Rab GTPases and their effector proteins.

Our current hypothesis is that Sro7 may function as part of a partially redundant, parallel pathway with the Exocyst tethering complex, downstream of the Sec4 GTPase. As mentioned above, overexpression of either Sro7 or the Exocyst complex component, Sec15, results in a similar phenotype of Rab-dependent, SNARE-independent post-Golgi vesicle clusters in the cell.

Likewise, both Sro7 and Sec15 are direct effectors of Sec4-GTP and both bind to the t-SNARE, Sec9. Additionally, overexpression of Sro7 suppresses a number of Exocyst complex component mutations and deletions, including *exo70Δ*, *sec5Δ* and *sec3Δ*, and Sro7 has genetic properties consistent with a parallel function [47, 89].

Like *SRO7*, one additional copy of *SEC4* (on *CEN*) strongly suppresses the temperature sensitivity of the Exocyst mutant, *sec15-1* [98]. When we combine *sec15-1* with a *sro7*Δ, *sro77*Δ strain, Sec4 can no longer suppress this lethality, suggesting that functional Sro7 is required in order for Sec4 to bypass defects in the Exocyst complex [data not shown, K. Watson, unpublished]. Again, this view is consistent with our hypothesis that Sro7 functions in a parallel pathway to the Exocyst complex downstream of Sec4. To test if this function depends on the physical interaction between Sec4 and Sro7, we analyzed the ability of Sec4 to suppress *sec15-1* in cells where the only copy of *SRO7* is deficient in binding Sec4 (Mutants Sro7-K395E and Sro7-R600E, Chapter 2). In the absence of Sec4-Sro7 interaction, Sec4 fails to suppress *sec15-1* lethality, suggesting that this physical interaction is essential for Sec4 to bypass defects in the Exocyst complex [data not shown, K. Watson, unpublished]. We also examined the clustering activity of Sro7 mutants deficient in binding to Sec4 in the *in vitro* clustering assay [G. Rossi, unpublished]. Interestingly, both purified Sro7 mutants—Sro7-K395E and Sro7-R600E—failed to stimulate vesicle clustering when compared to Wildtype Sro7 [data not shown, G. Rossi, unpublished]. These data strongly suggest that the physical interaction between Sro7 and Sec4 is critical for its ability to cluster and perhaps tether post-Golgi vesicles in the absence of a functional Exocyst complex.

Despite the fact that structurally, Sro7 does not resemble a CATCHR family tethering complex, it likely has the same functional characteristics of this family, providing specificity to

vesicle transport as a Rab effector and coordinating vesicle docking with regulated SNARE complex assembly through interaction with SNARE proteins. Future studies will determine which aspects of the Sec4-mediated Sro7 pathway, such as vesicle tethering and SNARE complex assembly, function in parallel to those of the Exocyst complex and perhaps how Sro7 might function as a tethering agent to couple Rab-dependent vesicle tethering with SNARE complex assembly and vesicle fusion.

REFERENCES

1. Novick, P., C. Field, and R. Schekman, *Identification of 23 complementation groups required for post-translational events in the yeast secretory pathway.* Cell, 1980. **21**(1): p. 205-15.

2. Novick, P., S. Ferro, and R. Schekman, *Order of events in the yeast secretory pathway.* Cell, 1981. **25**(2): p. 461-9.

3. Wickner, W.T., *Profile of Thomas Sudhof, James Rothman, and Randy Schekman, 2013 Nobel Laureates in Physiology or Medicine*. Proc Natl Acad Sci U S A, 2013. **110**(46): p. 18349-50.

4. Botstein, D., S.A. Chervitz, and J.M. Cherry, *Yeast as a model organism.* Science, 1997. **277**(5330): p. 1259-60.

5. TerBush, D.R., and P. Novick, *Sec6, Sec8, and Sec15 are components of a multisubunit complex which localizes to small bud tips in Saccharomyces cerevisiae.* J Cell Biol, 1995. **130**(2): p. 299-312.

6. TerBush, D.R., T. Maurice, D. Roth, and P. Novick, *The Exocyst is a multiprotein complex required for exocytosis in Saccharomyces cerevisiae.* EMBO J, 1996. **15**(23): p. 6483-94.

7. Guo, W., D. Roth, C. Walch-Solimena, and P. Novick, *The exocyst is an effector for Sec4p, targeting secretory vesicles to sites of exocytosis.* EMBO J, 1999. **18**(4): p. 1071-80.

8. Pfeffer S.R., *Rab GTPases: master regulators of membrane trafficking.* Curr Opin Cell Biol., 1994. **6**(4): p. 522-6.

9. Goud, B., A. Salminen, N.C. Walworth, and P.J. Novick, *A GTP-binding protein required for secretion rapidly associates with secretory vesicles and the plasma membrane in yeast.* Cell, 1988. **53**(5): p. 753-68.

10. Walch-Solimena, C., R.N. Collins, and P.J. Novick, *Sec2p mediates nucleotide exchange on Sec4p and is involved in polarized delivery of post-Golgi vesicles.* J Cell Biol, 1997. **137**(7): p. 1495-509.

11. Sato, Y., et al., *Crystallization and crystallographic analysis of yeast Sec2p, a guanine nucleotide-exchange factor for the yeast Rab GTPase Sec4p.* Acta Crystallogr Sect F Struct Biol Cryst Commun. 2007. **63**(Pt7): p. 616-9.

12. Guo, W., A. Grant, and P. Novick, *Exo84p is an exocyst protein essential for secretion.* J Biol Chem, 1999. **274**(33): p. 23558-64.

13. Bennett, M.K., *SNAREs and the specificity of transport vesicle targeting.* Curr Opin Cell Biol., 1995. **7**(4): p. 581-6.

14. Brunger, A.T., *Structure of proteins involved in synaptic vesicle fusion in neurons*. Annu Rev Biophys Biomol Struct., 2001. **30**: 157-71

15. Rothman, J.E., and G. Warren, *Implications of the SNARE hypothesis for intracellular membrane topology and dynamics.* Curr Biol., 1994. **4**(3): p. 220-33.

16. Jahn, R, and R.H. Scheller, *SNAREs—engines for membrane fusion.* Nat Rev Mol Cell Biol., 2006. **7**(9): p. 631-43.

17. Scales, S.J., B.Y. Yoo, and R.H. Scheller, *The ionic layer is required for efficient dissociation of the SNARE complex by alpha-SNAP and NSF.* Proc Natl Acad Sci., 2001. **98**(25): p. 14262-7.

18. Fasshauer, D., R.B. Sutton, A.T. Brunger and R. Jahn, *Conserved structural features of the synaptic fusion complex: SNARE proteins reclassified as Q- and R-SNAREs.* Proc Natl Acad Sci., 1998. **95**(26): p. 15781-6.

19. Fasshauer, D., H. Otto, W.K. Eliason, R. Jahn, and A.T. Brunger, *Structural changes are associated with soluble N-ethylmaleimide-sensitive fusion protein attachment protein receptor complex formation.* J Biol Chem., 1997. **272**(44): p. 28036-41.

20. Sutton, R.B., D. Fasshauer, R. Jahn, and A.T. Brunger, *Crystal structure of a SNARE complex involved in synaptic exocytosis at 2.4 A resolution.* Nature., 1998. **395**(6700): p. 347-53.

21. Fasshauer, D., *Structural insights into the SNARE mechanism.* Biochim Biophys Acta., 2003. **164**(2-3): p. 87-97.

22. Katz, L., and P. Brennwald, *Testing the 3Q:1R "rule": mutational analysis of the ionic "zero" layer in the yeast exocytic SNARE complex reveals no requirement for arginine.* Mol Biol Cell., 2000. **11**(11): p. 3849-58.

23. Aalto, T.K., H. Ronne, and S. Keranen, *Yeast syntaxins Sso1p and Sso2p belong to a family of related membrane proteins that function in vesicular transport.* EMBO J., 1993. **12**(11): p. 4095-104.

24. Brennwald, P., B. Kearns, K. Champion, S. Keranen, V. Bankaitis, and P. Novick, *Sec9 is a SNAP-25-like component of a yeast SNARE complex that may be the effector of Sec4 function in exocytosis.* Cell, 1994. **79**(2): p. 245-58.

25. Protopopov, V., B. Govindan, P. Novick, and J.E. Gerst, *Homologs of the synaptobrevin/VAMP family of synaptic vesicle proteins function on the late secretory pathway in S. cerevisiae.* Cell., 1993. **74**(5): p. 855-61.

26. Katz, L., P.I. Hanson, J.E. Heuser, and P. Brennwald, *Genetic and morphological analyses reveal a critical interaction between the C-termini of two SNARE proteins and a parallel four helical arrangement for the exocytic SNARE complex.* EMBO J., 1998. **17**(21): p. 6200-9.

27. He, B., and W. Guo, *The exocyst complex in polarized exocytosis.* Curr Opin Cell Biol., 2009. **21**(4): p. 537-42.

28. Koumandou, V.L., J.B. Dacks, R.M. Coulson, and M.C. Field, *Control systems for membrane fusion in the ancestral eukaryote; evolution of tethering complexes and SM proteins.* BMC Evol Biol., 2007. **7**: p. 29.

29. Whyte, J.R. and S. Munro, *The Sec34/35 Golgi transport complex is related to the exocyst, defining a family of complexes involved in multiple steps of membrane traffic.* Dev Cell., 2001. **1**(4): p. 527-37.

30. Wu, S., et al., *Sec15 interacts with Rab11 via a novel domain and affects Rab11 localization in vivo.* Nat Struct Mol Biol, 2005. **12**: p. 879-85.

31. Zhang, X.M., et al., *Sec15 is an effector for the Rab11 GTPase in mammalian cells.* J Biol Chem, 2004. **279**: p. 43027-34.

32. Miller, V.J., et al., *Molecular insights into vesicle tethering at the Golgi by the conserved oligomeric Golgi (COG) complex and the golgin TATA element modulatory factor (TMF).* J Biol Chem, 2013. **288**: p. 4229-40.

33. Zolov, S.N., and W. Lupashin, *Cog3p depletion blocks vesicle-mediated Golgi retrograde trafficking in HeLa cells.* J Cell Biol, 2005. **168**(5): p. 747-59.

34. Pokrovskaya, I.D., et al., *Conserved oligomeric Golgi complex specifically regulates the maintenance of Golgi glycosylation machinery.* Glycobiology, 2011. **21**(12): p. 1544-69.

35. Shestakova, A., et al., *COG complex-mediated recycling of Golgi glycosyltransferases is essential for normal protein glycosylation.* Traffic, 2006. **7**(2): p. 191-204.

36. Suvorova, E.S., et al., *The Sec34/Sec35p complex, a Ypt1p effector required for retrograde intra-Golgi trafficking, interacts with Golgi SNAREs and COPI vesicle coat proteins.* J Cell Biol, 2002. **157**: p. 631-43.

37. Fukuda, M., et al., *Large scale screening for novel rab effectors reveals unexpected broad Rab binding specificity.* Mol Cell Proteomics, 2008. **7**: p. 1031-42.

38. Yu, E., et al., *Role of Rab27 in synaptic transmission at the squid giant synapse.* Proc Natl Acad Sci U S A, 2008. **105**: p. 16003-8.

39. Conibear, E., and T.H. Stevens., *Vps52p, Vps53p, and Vps54p form a novel multisubunit complex required for protein sorting at the yeast late Golgi.* Mol Biol Cell, 2000. **11**: p. 305-23.

40. Perez-Victoria, F.J., et al., *Requirement of the human GARP complex for mannose 6-phosphate-receptor-dependent sorting of cathepsin D to lysosomes.* Mol Biol Cell, 2008. **19**: p. 2350-62

41. Siniossoglou, S., and H.R. Pelham., *Vps51p links the VFT complex to the SNARE Tlg1p.* J Biol Chem, 2002. **277**: p. 48318-24.

42. Sivaram, M.V., et al., *Dimerization of the exocyst protein Sec6p and its interaction with the t-SNARE Sec9p.* Biochemistry, 2005. **44**: p. 6302-11.

43. Morgera, F., et al., *Regulation of exocytosis by the exocyst subunit Sec6 and the SM protein Sec1.* Mol Biol Cell, 2012. **23**: p. 337-46.

44. Arasaki, K., et al., *RINT-1 regulates the localization and entry of ZW10 to the syntaxin 18 complex.* Mol Biol Cell, 2006. **17**: p. 2780-8.

45. Hirose, H., et al., *Implication of ZW10 in membrane trafficking between the endoplasmic reticulum and Golgi.* EMBO J, 2004. **23**: p. 1267-78.

46. Laufman, O., et al., *The COG complex interacts with multiple Golgi SNAREs and enhances fusogenic assembly of SNARE complexes.* J Cell Sci, 2013. **126**: p. 1506-16.

47. Lehman, K., et al., *Yeast homologues of tomosyn and lethal giant larvae function in exocytosis and are associated with the plasma membrane SNARE, Sec9.* J Cell Biol, 1999. **146**: p. 125-40.

48. Hattendorf, D.A., et al., *Structure of the yeast polarity protein Sro7 reveals a SNARE regulatory mechanism.* Nature, 2007.**446**: p. 567-71.

49. Scharrer, B. and E. Hadorn, *The structure of the ring-gland (corpus allatum) in normal and lethal larvae of drosophila melanogaster.* Proc Natl Acad Sci U S A, 1938. **24**: p. 236-42.

50. De Lorenzo, C., et al., *What is Drosophila telling us about cancer?* Cancer Metastasis Rev, 1999. **18**: p. 295-311.

51. Manfruelli, P., et al., *The tumor suppressor gene, lethal(2)giant larvae (1(2)g1), is required for cell shape change of epithelial cells during Drosophila development.* Development, 2003. **122**: p. 2283-94.

52. Baek, K.H., *The first oncogene in Drosophila melanogaster.* Mutat Res, 1999. **436**: p. 131-6.

53. Bilder, D., *PDZ proteins and polarity: functions from the fly.* Trends Genet, 2001. **17**: p. 511-9.

54. Humbert, P., et al., *Dlg, Scribble and Lgl in cell polarity, cell proliferation and cancer.* Bioessays, 2003. **25**: p. 542-53.

55. Justice, N.J., and Y.N. Jan, *A lethal giant kinase in cell polarity.* Nat Cell Biol, 2003. **5**: p. 273-4.

56. Bilder, D., and N. Perrimon., *Localization of apical epithelial determinants by the basolateral PDZ protein Scribble.* Nature, 2000. **403**: p. 676-80.

57. Fang, C., et al., *Lethal (2) Giant Larvae: An indispensible regulator of cell polarity and cancer development.* Int J Biol Sci, 2015. **11**(4): p. 380-389.

58. Ohshiro, T., et al., *Role of cortical tumour-suppressor proteins in asymmetric division of Drosophila neuroblast.* Nature, 2000. **408**: p. 593-6.

59. Peng, C.Y., et al., *The tumour-suppressor genes lgl and dlg regulate basal protein targeting in Drosophila neuroblasts.* Nature, 2000. **408**: p. 596-600.

60. Albertson, R., and C.Q. Doe, *Dlg, Scrib and Lgl regulate neuroblast cell size and mitotic spindle asymmetry.* Nat Cell Biol, 2003. **5**: p. 166-70.

61. Betschinger, J., et al., *The Par complex directs asymmetric cell division by phosphorylating the cytoskeletal protein Lgl.* Nature, 2003. **422**: p. 326-30.

62. Tanentzapf, G., and Tepass, U., *Interactions between the crumbs, lethal giant larvae and bazooka pathways in epithelial polarization.* Nat Cell Biol, 2003. **5**: p. 46-52.

63. Musch, A., et al., *Mammalian homolog of Drosophila tumor suppressor lethal (2) giant larvae interacts with basolateral exocytic machinery in Madin-Darby canine kidney cells.* Mol Biol Cell, 2002. **13**: p. 158-68.

64. Plant, P.J., et al., *A polarity complex of mPar-6 and atypical PKC binds, phosphorylates and regulates mammalian Lgl.* Nat Cell Biol., 2003. **5**: p. 301-8.

65. Yamanaka, T., et al., *Mammalian Lgl forms a protein complex with PAR-6 and aPKC independently of PAR-3 to regulate epithelial cell polarity.* Curr Biol, 2003. **13**: p. 734-43.

66. Tian, A.G. and W.M. Deng, *Lgl and its phosphorylation by aPKC regulate oocyte polarity formation in Drosophila.* Development, 2008. **135**: p. 463-71.

67. Kalmes, A., et al., *A serine-kinase associated with the p127-l(2)gl tumour suppressor of Drosophila may regulate the binding of p127 to nonmuscle myosin II heavy chain and the attachment of p127 to the plasma membrane.* J Cell Science, 1996. **109**: p. 1359-68.

68. Grzeschik, N.A., et al., *Lgl, aPKC, and Crumbs regulate the Salvador/Warts/Hippo pathway through two distinct mechanisms.* Curr Biol, 2010. **20**: p. 573-81.

69. Strand, D., et al., *The Drosophila lethal(2)giant larvae tumor suppressor protein forms homo-oligomers and is associated with nonuscle myosin II heavy chain.* J Cell Biol, 1994. **127**: p. 1361-73.

70. Barros, C.S., et al., *Drosophila nonmuscle myosin II promotes the asymmetric segregation of cell fate determinants by cortical exclusion rather than active transport.* Dev Cell, 2003. **5**: p. 829-40.

71. Klezovitch, O., et al., *Loss of cell polarity causes severe brain dysplasia in Lgl1 knockout mice.* Genes Dev, 2004. **18**: p. 559-71.

72. Tullio, A.N., et al., *Structural abnormalities develop in the brain after ablation of the gene encoding nonmuscle myosin II-B heavy chain.* J Comp Neurol, 2001. **433**: p. 62-74.

73. Arquier, N., et al., *The Drosophila tumor suppressor gene lethal(2)giant larvae is required for the emission of the Decapentaplegic signal.* Development, 2001. **128**: p. 2209-20.

74. Gangar, A., et al., *Structurally conserved interaction of Lgl family with SNAREs is critical to their cellular function.* Curr. Biol., 2005. **15**: p. 1136-1142.

75. Wang, T., et al., *Lgl1 activation of rab10 promotes axonal membrane trafficking underlying neuronal polarization.* Dev Cell., 2011. **21**: p. 431-44.

76. Fujita, Y., et al., *Tomosyn: a syntaxin-1-binding protein that forms a novel complex in the neurotransmitter release process.* Neuron, 1998. **20**: p. 905-15.

77. Yokoyama, S., et al., *Three splicing variants of tomosyn and identification of their syntaxin-binding region.* Biochem Biophys Res Commun., 1999. **256**: p. 218-22.

78. Groffen, A.J., et al., *Two distinct genes drive expression of seven tomosyn isoforms in the mammalian brain, sharing a conserved structure with a unique variable domain.* J Neurochem, 2005. **92**: p. 554-68.

79. Masuda, E.S., et al., *Tomosyn binds t-SNARE proteins via a VAMP-like coiled coil.* Neuron, 1998. **21**: p. 479-80

80. Hatsuzawa, K., et al., *The R-SNARE motif of tomosyn forms SNARE core complexes with syntaxin 1 and SNAP-25 and down-regulates exocytosis.* J Biol Chem, 2003. **278**(33): p. 31159-66.

81. Ashery, U., et al., *Friends and foes in synaptic transmission: the role of tomosyn in vesicle priming.* Trends Neurosci, 2009. **32**: p. 275-82.

82. Yizhar, O., et al., *Tomosyn inhibits priming of large dense-core vesicles in a calcium-dependent manner.* Proc Natl Acad Sci U S A, 2004. **101**(8): p. 2578-83.

83. Baba, T., et al., *PKA-catalyzed phosphorylation of tomosyn and its implication in Ca2+-dependent exocytosis of neurotransmitter.* J Cell Biol, 2005. **170**: p. 1113-25.

84. Gladycheva, S.E., et al., *Receptor-mediated regulation of tomosyn-syntaxin 1A interactions in bovine adrenal chromaffin cells.* J Biol Chem, 2007. **282**: p. 22887-99.

85. Constable, J.R., et al., *Amisyn regulates exocytosis and fusion pore stability by both syntaxin-dependent and syntaxin-independent mechanisms.* J Biol Chem, 2005. **280**: p. 31615-23.

86. Widberg, C.H., et al., *Tomosyn interacts with the t-SNAREs syntaxin4 and SNAP23 and plays a role in insulin-stimulated GLUT4 translocation.* J Biol Chem, 2003. **278**: p. 35093-101.

87. Zhang, X., et al., *Lethal giant larvae proteins interact with the exocyst complex and are involved in polarized exocytosis.* J. Cell Biol., 2005. **170**: p. 273-83.

88. Kagami, M., et al., *Sro7p, a Saccharomyces cerevisiae counterpart of the tumor suppressor l(2)gl protein, is related to myosins in function.* Genetics, 1998. **149**: p. 1717-27..

89. Grosshans, B.L., et al., *The yeast lgl family member Sro7 is an effector of the secretory Rab GTPase Sec4p.* J Cell Biol., 2006. **172**: p. 55-66.

90. Vasioukhin, V., *Lethal giant puzzle of Lgl.* Dev. Neurosci., 2006. **28**: p. 13-24.

91. Hutterer, A., et al., *Sequential roles of Cdc42, Par-6, aPKC, and Lgl in the establishment of epithelial polarity during Drosophila embryogenesis.* Dev Cell, 2004. **6**: p. 845-54.

92. Lazar, T., et al., *Vesicular transport: how many Ypt/Rab-GTPases make a eukaryotic cell?.* Trends Biochem Sci., 1997. **22**: p. 468-72.

93. Buvelot Frei, S., et al., *Bioinformatic and comparative localization of Rab proteins reveals functional insights into the uncharacterized GTPases Ypt10p and Ypt11p.* Mol Cell Biol, 2006. **26**: p. 7299-317.

94. Lipatova, Z., et al., *Ypt/Rab GTPases: Principles learned from yeast.* Crit Rev Biochem Mol Bio, 2015. **23**: p. 1-9.

95. Rossi, G., et al., *In vitro reconstitution of Rab GTPase-dependent vesicle clustering by the yeast lethal giant larvae/tomosyn homolog Sro7.* J Biol Chem, 2015. **290**: p. 612-24.

96. Wadskog, I., et al., *Yeast lacking the SRO7/SOP1-encoded tumor suppressor homologue show increased susceptibility to apoptosis-like cell death on exposure to NaCl stress.* Mol. Biol. Cell, 2004. **15:** p. 1436-44.

97. Stroupe, C., and A.T. Brunger, *Crystal structures of a Rab protein in its inactive and active conformations.* J. Mol Biol., 2000. **304**: p. 585-98.

98. Salminen, A., and P.J. Novick., *A ras-like protein is required for a post-Golgi event in yeast secretion.* Cell, 1987. **49**: p. 527-38.

99. Vetter, J.R., and A. Wittinghoffer, *The guanine nucleotide-binding switch in three dimensions.* Science, 2001. **294**: p. 1299-304.

100. Levin, K.B., et al., *Following evolutionary paths to protein-protein interactions with high affinity and selectivity.* Nat. Struct. Mol. Biol., 2009. **16**: p. 1049-55.

101. Dey, S., et al., *The subunit interfaces of weakly associated homodimeric proteins.* J Mol Biol, 2010. **398**: p. 146-60.

102. Sakisaka, T., et al., *Regulation of SNAREs by tomosyn and ROCK: implication in extension and retraction of neurites.* J. Cell. Biol., 2004. **166**: p. 17-25.

103. Williams, A.L., et al., *Structural and functional analysis of tomosyn identifies domains important in exocytic regulation.* J. Biol. Chem., 2011. **286**: p. 14542-53.

104. Fasshauer, D. and R. Jahn, *Budding insights on cell polarity.* Nat. Struct. Mol. Biol, 2007. **5**: p. 360-2.

105. Kloepper, T.H., et al., *SNAREing the basis of multicellularity: consequences of protein family expansion during evolution.* Mol. Biol. Evol., 2008. **9**: p. 2055-68.

106. Heider, M.R. and M. Munson, *Exorcising the exocyst complex.* Traffic, 2012. **13**: p. 898-907.

107. Moerschell, R.P., et al., *Transformation of yeast directly with synthetic oligonucleotides.* Methods Enzymol, 1991. **194**: p. 362-9.

108. Comeau, S.R., et al., *ClusPro: a fully automated algorithm for protein-protein docking.* Nucleic Acids Research, 2004. **32**: p. W96-9

109. Eswar, N., et al., *Comparative protein structure modeling using MODELLER.* In: Curr Protoc Bioinformatics, ed. John Wiley & Sons, Inc., Supplement 15, 5.6.1-5.6.30.

110. Altschul, S.F., et al., *Basic local alignment search tool.* J. Mol. Biol., 1990. **215**: p. 403-10.

111. Higgins, D.G., and P.M. Sharp., *CLUSTAL: a package for performing multiple sequence alignment on a microcomputer.* Gene, 1988. **73**: p. 237-44.

112. Thompson, J.D., et al., *The CLUSTAL_X windows interface: flexible strategies for multiple sequence alignment aided by quality analysis tools.* Nucleic Acids Res, 1997. **25**: p. 4876-82.

113. Rossi, G., and Brennwald, P., *Yeast homologues of lethal giant larvae and type V myosin cooperate in the regulation of Rab-dependent vesicle clustering and polarized exocytosis.* Mol. Biol. Cell., 2011. **22**: p. 842-857.

114. Salminen, A. and Novick, P.J., *The Sec15protein responds to the function of the GTP binding protein, Sec4, to control vesicular traffic in yeast* . J Cell Biol., 1989. **109**: p. 1023-1036.

115. Walworth, N.C. and Novick, P.J., *Purification and characterization of constitutive secretory vesicles from yeast* . J Cell Biol., 1987. **105**: p. 163-174

116. Jantti, J., et al., *Characterization of temperature-sensitive mutations in the syntaxin 1 homologues Sso1p and Sso2p, and evidence of a distinct function for Sso1p in sporulation.* J Cell Sci., 2002. **115**: p. 409-420

117. Garrett, M.D., et al., *GDI encodes a GDP dissociation inhibitor that plays an essential role in the yeast secretory pathway.* EMBO J., 1994. **13**: p. 1718-1728

118. Ullrich, O., et al., *Rab GDP dissociation inhibitor as a general regulator for the membrane association of Rab proteins.* J Biol. Chem., 1993. **268**: p. 18143-18150

119. Forsmark, A., et al., *Quantitative proteomics of yeast post-Golgi vesicles reveals a discriminating role for Sro7p in protein secretion.* Traffic., 2011. **12**: p. 740-753

120. Mulholland, J., et al., *Yeast actin cytoskeleton mutants accumulate a new class of Golgi-derived secretory vesicle.* Mol Biol. Cell., 1997. **8**: p. 1481-1499

121. Novick, P. and P. Brennwald., *Friends and family: the role of the Rab GTPases in vesicular traffic.* Cell., 1993. **75**: p. 597-601

122. Lo, S.Y., et al., *Intrinsic tethering activity of endosomal Rab proteins.* Nat. Struct. Mol. Biol., 2012. **19**: p. 40-47

123. Bowser, R. and P. Novick, *Sec15p, an essential component of the exocytic apparatus, is associated wih the plasma membrane and with a soluble 19.5 S particle.* J. Cell. Biol., 1991. **112**: p. 1117-1131

124. Starai, V.J., et al., *Excess vacuolar SNAREs drive lysis and Rab bypass fusion.* Proc. Natl. Acad. Sci. U S A., 2007. **104**: p. 13551-13558

125. Adamo, J.E., et al., *The Rho GTPase, Rho3 has a direct role in exocytosis that is distinct from its role in actin polarity.* Mol. Biol. Cell., 1999. **10**: p. 4121-4133